

Patterns of Flavour Violation in the Presence of a Fourth Generation of Quarks and Leptons

Andrzej J. Buras^{a,b}, Björn Duling^a, Thorsten Feldmann^a,
Tillmann Heidsieck^a, Christoph Promberger^a, Stefan Recksiegel^a

^a*Physik Department, Technische Universität München, James-Frank-Straße,
D-85748 Garching, Germany*

^b*TUM Institute for Advanced Study, Technische Universität München, Arcisstr. 21,
D-80333 München, Germany*

Abstract

We calculate a number of observables related to particle-antiparticle mixing and the branching ratios for the most interesting rare and CP-violating K and B decays in the Standard Model (SM3) extended by a fourth generation of quarks and leptons (SM4). A model-independent parametrisation of these observables in terms of gauge-independent functions is adopted, which is useful for studying the breaking of the universality between K , B_d and B_s systems through non-minimal flavour violating interactions. We calculate first the mass differences ΔM_i in the neutral K and B systems, the mixing-induced CP asymmetries $S_{\psi K_S}$, $S_{\psi\phi}$, $S_{\phi K_S}$, $S_{\eta' K_S}$ and ε_K . Subsequently, a detailed analysis of $K^+ \rightarrow \pi^+ \nu \bar{\nu}$, $K_L \rightarrow \pi^0 \nu \bar{\nu}$, $B_{s,d} \rightarrow \mu^+ \mu^-$, $B \rightarrow X_{s,d} \nu \bar{\nu}$, $K_L \rightarrow \pi^0 \ell^+ \ell^-$, $B \rightarrow X_s \gamma$ and $B \rightarrow X_{s,d} \ell^+ \ell^-$ is presented, and also ε'/ε is considered. For some of these observables the departures from SM3 predictions can still be spectacular.

We discuss how the new mixing parameters (3 angles, 2 CP phases) can be determined using the flavour observables in question. We identify the different hierarchical structures in the SM4 flavour mixing matrix, allowed by phenomenological and theoretical constraints, and define the corresponding generalised Wolfenstein expansion. Most importantly, we show how the characteristic patterns of correlations among the considered flavour observables allow to distinguish this New Physics scenario from supersymmetric flavour models, the Littlest Higgs model with T-parity and the Randall-Sundrum model with custodial protection. Of particular importance are the correlations involving $S_{\psi\phi}$, $S_{\phi K_S}$, $\text{Br}(K^+ \rightarrow \pi^+ \nu \bar{\nu})$, $\text{Br}(K_L \rightarrow \pi^0 \nu \bar{\nu})$ and $\text{Br}(B_{s,d} \rightarrow \mu^+ \mu^-)$, which could in principle rule out the SM4. Interestingly ε'/ε turns out to be suppressed below the data for large positive values of $S_{\psi\phi}$ unless the relevant hadronic matrix elements differ strongly from the large N results. The important role of ε'/ε in bounding large enhancements of rare K decay branching ratios is emphasised. We also show how the existing anomalies in the unitarity triangle fits as well as in $S_{\psi\phi}$ and $S_{\phi K_S}$ can be simultaneously explained in the SM4 scenario.

1 Introduction

One of the simplest extensions of the Standard Model (hereafter referred to as SM3) is the addition of a sequential fourth generation (4G) of quarks and leptons [1] (hereafter referred to as SM4). While the setup we are considering here (e.g. perturbative Yukawa couplings) does not address any of the known hierarchy and naturalness problems, if present in nature, a 4G is likely to have a number of profound implications that makes it interesting to consider. These are:

1. While being consistent with electroweak precision data (EWPT) [2–7], a 4G can remove the tension between the SM3 fit and the lower bound on the Higgs mass m_H from LEP II. Indeed, as pointed out in [3, 5, 8], a heavy Higgs boson does not contradict EWPT as soon as the 4G exists.
2. $SU(5)$ gauge coupling unification could in principle be achieved without supersymmetry [9], although the present lower bound on the masses of 4G quarks and the appearance of Landau poles in Yukawa couplings well below the GUT scales practically excludes this possibility if one wants to stay within a perturbative framework at short-distance (SD) scales.
3. Electroweak baryogenesis might be viable [10–12].
4. Most importantly, from the point of view of the present paper, certain anomalies present in flavour-changing processes could in principle be resolved [13–15].
5. The structure of the lepton sector in the SM4 can be interesting as shown recently in [16]: a heavy (mostly Dirac) 4G neutrino in addition to very light (mostly Majorana) neutrinos can be obtained in a setup with electroweak symmetry breaking in warped extra dimensions.

On the other hand there are scenarios where a fourth generation might trigger dynamical breaking of electroweak symmetry [17–23]. However since it is in the very nature of non-perturbative Yukawa couplings to defy direct calculations there is until now no explicit model for this scenario.

There is a rich literature on the implications and phenomenology of the SM4. Reviews and summary statements can be found in [1, 24]. In particular during the last years, a number of analyses were published with the goal to investigate the impact of the existence of a 4G on Higgs physics [5], electroweak precision tests [4–7] and flavour physics [13–15, 25–28]. In this context, Bobrowski et al. [27] have studied the constraint on the mixing between the fourth and third generation by using FCNC processes, and

Chanowitz [6] by using global fits to EWPT. Interesting bounds on this mixing could be derived in this manner. We will address these bounds in the course of our analysis.

Detailed analyses of supersymmetry in the presence of a 4G have recently been performed in [29, 30]. These analyses show that the marriage of SUSY with the SM4 is rather challenging because of Landau poles in Yukawa couplings present at relatively low scales. The last paper contains a good up to date collection of references to papers on the SM4.

In the present paper we will take a different strategy by considering, in addition to $\Delta F = 2$ transitions and $B \rightarrow X_s \gamma$ and $B \rightarrow X_s \ell^+ \ell^-$ decays as done in [15, 27], also rare K and B decays, as considered in [13], on which new data will be available in the coming decade. In particular,

- i) We will establish a number of correlations between various observables that should allow us to distinguish this NP scenario from the Littlest Higgs model with T-parity (LHT), the Randall-Sundrum model with custodial protection (RSc) and supersymmetric flavour models that have been analysed in [31–36] recently. We will also carefully study how these correlations depend on the size of the 4G mixing angles and phases.
- ii) For the most interesting observables, we will investigate the departures from models with (constrained) minimal flavour violation ((C)MFV), taking into account all existing constraints.
- iii) We will demonstrate transparently how certain anomalies observed in the unitarity triangle fits and in the CP asymmetries $S_{\psi\phi}$ and $S_{\phi K_S}$ can be resolved simultaneously and how these solutions affect other observables.
- iv) We will address the question how the additional five parameters of the 4×4 quark mixing matrix, θ_{14} , θ_{24} , θ_{34} , δ_{14} and δ_{24} , could — in principle — be determined by means of the mixing-induced CP asymmetries $S_{\psi\phi}$ and $S_{\psi K_S}$, the $B_{d,s}^0 - \bar{B}_{d,s}^0$ mixing mass differences $\Delta M_{d,s}$, ϵ_K and the branching ratios for the rare decays $K^+ \rightarrow \pi^+ \nu \bar{\nu}$, $K_L \rightarrow \pi^0 \nu \bar{\nu}$, $B_{s,d} \rightarrow \mu^+ \mu^-$, $B \rightarrow X_s \nu \bar{\nu}$.
- v) On the theoretical side, we will discuss how the SM4 can be understood as a particular realisation of a next-to-minimal flavour violation scenario. This introduces certain consistency conditions between the SM3 and SM4 mixing angles which can be used to eliminate “fine-tuned” values in parameter space. The remaining cases can be classified according to the scaling of the 4G mixing angles with the Cabibbo angle, and for each individual case an SM4 generalisation of the Wolfenstein parametrisation can be constructed.

Our paper is organised as follows: In Section 2, we discuss the flavour symmetries in the SM4, provide the 4×4 quark mixing matrix and address the question of possible hierarchies between the 4G mixing angles. In Section 3, we generalise the effective weak Hamiltonians to the SM4. In Section 4, we compile basic formulae for FCNC processes considered in our paper. As the SM4 goes beyond MFV, but the operator structure of the SM3 effective Hamiltonian remains intact, it is very efficient to introduce – as done in the LHT model [31–33] – generalised complex master functions $S_i, X_i, Y_i, Z_i, D'_i, E'_i, E_i, (i = K, d, s)$, that enter the expressions for various observables. On the one hand, in the absence of the 4G, these functions reduce to the SM3 flavour-universal functions $S_0, X_0, Y_0, Z_0, D'_0, E'_0$ and E_0 . On the other hand, using these functions, non-MFV effects in this model can be very transparently compared to those found in the LHT model.

In Section 5, we summarise the insights gained by other authors, who studied in particular the impact of the 4G on the electroweak precision observables. In Section 6, we will summarise our strategy for the phenomenological analysis of the SM4. In Section 7, we present a detailed global numerical analysis, using the formulae of previous sections. In particular, we identify a number of correlations between various observables, and we estimate approximate upper bounds on several CP asymmetries and branching ratios. In Section 8, we study the anatomy of flavour effects in the SM4 scenario. In this context, we address the most important phenomenological anomalies found in the present flavour data.

In Section 9, we outline an efficient procedure how to constrain the new mixing angles $\theta_{14}, \theta_{24}, \theta_{34}$ and the new phases δ_{14} and δ_{24} from

$$S_{\psi\phi}, \quad S_{\psi K_S}, \quad \Delta M_{d,s}, \quad \epsilon_K, \\ \text{Br}(K^+ \rightarrow \pi^+ \nu \bar{\nu}), \quad \text{Br}(K_L \rightarrow \pi^0 \nu \bar{\nu}), \quad \text{Br}(B_{s,d} \rightarrow \mu^+ \mu^-), \quad \text{Br}(B \rightarrow X_{s,d} \nu \bar{\nu}). \quad (1.1)$$

For this purpose, we will provide a classification of the 4G mixing parameters which allows us to connect the different patterns found in flavour observables to particular properties of the 4G mixing angles and CP phases. Finally, in Section 10, we summarise our main findings. Here we will also compare the patterns of flavour violation in the SM4 with those found in supersymmetric flavour models, the LHT model and the RSc model. An appendix collects the one-loop functions used in our paper.

2 The 4×4 Mixing Matrix V_{SM4}

2.1 Yukawa Couplings and (Approximate) Flavour Symmetries

The SM4 quark Yukawa sector involves two 4×4 Yukawa matrices,

$$-\mathcal{L}_{\text{Yuk}} = \bar{Q}_L Y_U^{\text{SM4}} \tilde{H} U_R + \bar{Q}_L Y_D^{\text{SM4}} H D_R + \text{h.c.} . \quad (2.1)$$

Following [37], we identify the Yukawa couplings as spurions, being the (only) sources for the breaking of the flavour symmetry in the SM4,

$$G_F^{\text{SM4}} = SU(4)_{Q_L} \times SU(4)_{U_R} \times SU(4)_{D_R} \times U(1)_{U_R} \times U(1)_{D_R} , \quad (2.2)$$

where we have divided out one $U(1)$ factor corresponding to the conserved baryon number. Under the flavour symmetry, the Yukawa spurions transform as

$$Y_U^{\text{SM4}} \sim (4, \bar{4}, 1)_{1,0} , \quad Y_D^{\text{SM4}} \sim (4, 1, \bar{4})_{0,1} . \quad (2.3)$$

As in the SM3 case (see also [38–40]), the counting of symmetry generators (related to 18 angles + 29 phases) vs. complex Yukawa entries ($32 + 32$) gives the number of physical parameters

$$14 + 3 = 8 \text{ masses} + 6 \text{ angles} + 3 \text{ phases} ,$$

i.e. 2 additional masses, 3 additional angles and 2 additional phases compared to the SM3 case.

Alternatively, we can consider the flavour symmetries from the SM3 point of view: Taking only the large t' and b' Yukawa couplings into account, the effective flavour symmetry is

$$G_{\text{eff}}^{\text{SM3}} = SU(3)_{Q_L} \times SU(3)_{U_R} \times SU(3)_{D_R} \times U(1)_{U_R} \times U(1)_{D_R} \times U(1)_{Q'} , \quad (2.4)$$

which, compared to the SM3 case, involves an additional $U(1)_{Q'}$ symmetry, since – without mixings involving the first three generations – the 4G quark number is approximately conserved. The mixings between the fourth and the first three generations can be parametrised by an $SU(3)_{Q_L}$ triplet which is charged under the $U(1)_{Q'}$,

$$\chi_L \sim (3, 1, 1)_{0,0,1} . \quad (2.5)$$

Of the six independent entries of χ_L , one phase is unobservable due to the $U(1)_{Q'}$ symmetry, leaving exactly the additional 3 mixing angles and 2 CP-violating phases of the SM4. The remaining parameters for the first three generations are contained in SM3 Yukawa matrices

$$Y_U^{\text{SM3}} \sim (3, \bar{3}, 1)_{1,0,0} , \quad Y_D^{\text{SM3}} \sim (3, 1, \bar{3})_{0,1,0} . \quad (2.6)$$

The so-defined SM4 thus provides a particular example of the next-to-minimal flavour violating construction discussed in [41], with new non-minimal flavour structures generated by means of the χ_L spurion. Using a non-linear parametrisation (as it has been used for the SM3 case in [42, 43]),

$$Y_U^{\text{SM4}} = \xi_L^\dagger \begin{pmatrix} 0 \\ Y_U^{\text{SM3}} & 0 \\ 0 \\ 0 & 0 & 0 & y_{t'} \end{pmatrix}, \quad Y_D^{\text{SM4}} = \xi_L \begin{pmatrix} 0 \\ Y_D^{\text{SM3}} & 0 \\ 0 \\ 0 & 0 & 0 & y_{b'} \end{pmatrix}, \quad (2.7)$$

we introduce the 4×4 matrix

$$\xi_L = \exp \left[i \begin{pmatrix} 0 & 0 & 0 \\ 0 & 0 & 0 & \chi_L \\ 0 & 0 & 0 \\ \chi_L^\dagger & 0 \end{pmatrix} \right]. \quad (2.8)$$

It transforms as $V_{Q_L} \xi_L V_{Q_L}^\dagger$ where V_{Q_L} contains an $SU(3)_{Q_L}$ block matrix for the SM3 generations, while the 4G fields remain constant. The consistency conditions discussed in [41] translate into

$$\begin{aligned} |(\chi_L)_i| |(\chi_L)_j| &\lesssim \theta_{ij}, & (i, j = 1 \dots 3) \\ \Leftrightarrow \quad \theta_{ik} \theta_{jk} &\lesssim \theta_{ij} & (i, j, k = 1 \dots 4) \end{aligned} \quad (2.9)$$

where no summation over "k" is understood. Here $\theta_{12} \sim \lambda$, $\theta_{23} \sim \lambda^2$, $\theta_{13} \sim \lambda^3$ are the SM3 mixing angles and θ_{i4} the 4G mixing angles (see below). Notice that for the SM3 case, one has one of the inequalities (2.9) saturated,

$$\theta_{12} \theta_{23} \sim \theta_{13}, \quad \text{but} \quad \theta_{12} \theta_{13} \ll \theta_{23}, \quad \theta_{13} \theta_{23} \ll \theta_{12}. \quad (2.10)$$

A particular way to realise the constraints (2.9) is to consider a simple Froggatt-Nielsen (FN) setup [44], where the scaling of the mixing angles is controlled by different $U(1)$ charge factors b_i for the left-handed doublets of different generations, leading to

$$\theta_{ij} \sim \lambda^{|b_i - b_j|}. \quad (2.11)$$

Here λ is given by the VEV of some $U(1)$ -breaking scalar field divided by a large UV-scale. The triangle inequalities for $|b_i - b_k| + |b_k - b_j|$ then guarantee that (2.9) always holds. Since (2.11) only involves charge *differences*, we may set $b_4 \equiv 0$, while the charges b_{1-3} and the related 4G mixing angles are not completely fixed. However, we can identify certain benchmark cases which may later be compared with the phenomenological constraints from EWPT, tree-level decays and rare decays of SM3 quarks: Scenarios with

some 4G mixing angles being of order $\mathcal{O}(1)$ are already ruled out by EWPT [4, 6] and tree-level quark decays (see below). Among the interesting scenarios with sufficiently small mixing angles, we identify:

$$(a) \quad b_3 = 1, b_2 = 3, b_1 = 4: \quad \Rightarrow \quad V_{\text{SM4}} \sim \begin{pmatrix} 1 & \lambda & \lambda^3 & \lambda^4 \\ \lambda & 1 & \lambda^2 & \lambda^3 \\ \lambda^3 & \lambda^2 & 1 & \lambda \\ \lambda^4 & \lambda^3 & \lambda & 1 \end{pmatrix}, \quad (2.12)$$

which yields a very symmetric scaling pattern for the 4G mixing matrix, and shares the feature of the SM3 CKM matrix that more off-diagonal elements get smaller. Notice that of the 9 inequalities in (2.9) involving the 4G mixing angles, 3 are saturated, namely

$$(a) \quad \theta_{12}\theta_{24} \sim \theta_{13}\theta_{34} \sim \theta_{14}, \quad \theta_{24} \sim \theta_{23}\theta_{34}. \quad (2.13)$$

Scenarios with even smaller mixing angles ($\theta_{i4} \rightarrow \lambda^n \theta_{i4}$) can simply be obtained from (2.12) by increasing $b_{1-3} \rightarrow b_{1-3} + n$. An FN example for a scenario with (relatively) large 4G mixing angles is given by

$$(b) \quad b_3 = 1, b_2 = -1, b_1 = -2: \quad \Rightarrow \quad V_{\text{SM4}} \sim \begin{pmatrix} 1 & \lambda & \lambda^3 & \lambda^2 \\ \lambda & 1 & \lambda^2 & \lambda \\ \lambda^3 & \lambda^2 & 1 & \lambda \\ \lambda^2 & \lambda & \lambda & 1 \end{pmatrix}, \quad (2.14)$$

In this case, the saturated inequalities are

$$(b) \quad \theta_{14}\theta_{34} \sim \theta_{13}, \quad \theta_{24}\theta_{34} \sim \theta_{23}, \quad \theta_{12}\theta_{24} \sim \theta_{14}. \quad (2.15)$$

For later use, we further identify two interesting non-FN scenarios. The first one is given by

$$(c) \quad V_{\text{SM4}} \sim \begin{pmatrix} 1 & \lambda & \lambda^3 & \lambda^2 \\ \lambda & 1 & \lambda^2 & \lambda^3 \\ \lambda^3 & \lambda^2 & 1 & \lambda \\ \lambda^2 & \lambda^3 & \lambda & 1 \end{pmatrix} \quad \text{with} \quad \theta_{14}\theta_{34} \sim \theta_{13}, \quad \theta_{12}\theta_{14} \sim \theta_{23}\theta_{34} \sim \theta_{24}. \quad (2.16)$$

In this case, the SM4 mixing matrix takes a very symmetric form, where the mixing angle θ_{14} between the fourth and first generation is larger than θ_{24} . Finally, for

$$(d) \quad V_{\text{SM4}} \sim \begin{pmatrix} 1 & \lambda & \lambda^3 & \lambda^3 \\ \lambda & 1 & \lambda^2 & \lambda^2 \\ \lambda^3 & \lambda^2 & 1 & \lambda \\ \lambda^3 & \lambda^2 & \lambda & 1 \end{pmatrix} \quad \text{with} \quad \theta_{12}\theta_{24} \sim \theta_{14} \quad (2.17)$$

we encounter the situation that the mixing of the fourth and third generation with the first and second one is similar in size, $\theta_{13} \sim \theta_{14}$, $\theta_{23} \sim \theta_{24}$.

Depending on which of the inequalities (2.9) are saturated, the effects of the 4G on CP-violating observables can be quite different. The different scaling of the 4G mixing angles will thus provide a useful tool to classify different scenarios in the anatomy for flavour observables, which will be further discussed in Section 9.3.

2.2 Parametrisation of V_{SM4}

We will use a standard parametrisation of the SM4 mixing matrix from [45, 46], which has also been used in [27]. Defining

$$s_{ij} = \sin \theta_{ij}, \quad c_{ij} = \cos \theta_{ij}, \quad (2.18)$$

we have for the generalised 4×4 mixing matrix V_{SM4} :

$$\begin{pmatrix} c_{12}c_{13}c_{14} & c_{13}c_{14}s_{12} & c_{14}s_{13}e^{-i\delta_{13}} & s_{14}e^{-i\delta_{14}} \\ -c_{23}c_{24}s_{12} - c_{12}c_{24}s_{13}s_{23}e^{i\delta_{13}} & c_{12}c_{23}c_{24} - c_{24}s_{12}s_{13}s_{23}e^{i\delta_{13}} & c_{13}c_{24}s_{23} & c_{14}s_{24}e^{-i\delta_{24}} \\ -c_{12}c_{13}s_{14}s_{24}e^{i(\delta_{14}-\delta_{24})} & -c_{13}s_{12}s_{14}s_{24}e^{i(\delta_{14}-\delta_{24})} & -s_{13}s_{14}s_{24}e^{-i(\delta_{13}+\delta_{24}-\delta_{14})} & \\ -c_{12}c_{23}c_{34}s_{13}e^{i\delta_{13}} + c_{34}s_{12}s_{23} & -c_{12}c_{34}s_{23} - c_{23}c_{34}s_{12}s_{13}e^{i\delta_{13}} & c_{13}c_{23}c_{34} & c_{14}c_{24}s_{34} \\ -c_{12}c_{13}c_{24}s_{14}s_{34}e^{i\delta_{14}} & -c_{12}c_{23}s_{24}s_{34}e^{i\delta_{24}} & -c_{13}s_{23}s_{24}s_{34}e^{i\delta_{24}} & \\ +c_{23}s_{12}s_{24}s_{34}e^{i\delta_{24}} & -c_{13}c_{24}s_{12}s_{14}s_{34}e^{i\delta_{14}} & -c_{24}s_{13}s_{14}s_{34}e^{i(\delta_{14}-\delta_{13})} & \\ +c_{12}s_{13}s_{23}s_{24}s_{34}e^{i(\delta_{13}+\delta_{24})} & +s_{12}s_{13}s_{23}s_{24}s_{34}e^{i(\delta_{13}+\delta_{24})} & & \\ -c_{12}c_{13}c_{24}c_{34}s_{14}e^{i\delta_{14}} & -c_{12}c_{23}c_{34}s_{24}e^{i\delta_{24}} + c_{12}s_{23}s_{34} & -c_{13}c_{23}s_{34} & c_{14}c_{24}c_{34} \\ +c_{12}c_{23}s_{13}s_{34}e^{i\delta_{13}} & -c_{13}c_{24}c_{34}s_{12}s_{14}e^{i\delta_{14}} & -c_{13}c_{34}s_{23}s_{24}e^{i\delta_{24}} & \\ +c_{23}c_{34}s_{12}s_{24}e^{i\delta_{24}} - s_{12}s_{23}s_{34} & +c_{23}s_{12}s_{13}s_{34}e^{i\delta_{13}} & -c_{24}c_{34}s_{13}s_{14}e^{i(\delta_{14}-\delta_{13})} & \\ +c_{12}c_{34}s_{13}s_{23}s_{24}e^{i(\delta_{13}+\delta_{24})} & +c_{34}s_{12}s_{13}s_{23}s_{24}e^{i(\delta_{13}+\delta_{24})} & & \end{pmatrix}. \quad (2.19)$$

In the limiting case of vanishing mixing with the 4G quarks, the standard parametrisation of the CKM matrix is recovered. Note that in (2.19), just as in the SM3 case, all angles θ_{ij} can be chosen to lie in the interval $[0, \pi/2]$. This can be shown in the following way [47]: In the above parametrisation, V_{SM4} is a product of six matrices $V_{ij} \in SU(2)$, $i, j = 1, \dots, 4$, consecutively mixing the different quark generations. The phases of each of these matrices can be factored out via

$$\begin{aligned} V_{ij} &= I_i(\alpha)\bar{V}_{ij}I_i(\beta)I_j(\gamma) = I_j(\alpha')\bar{V}_{ij}I_i(\beta')I_j(\gamma') \\ &= I_i(\alpha'')I_j(\beta'')\bar{V}_{ij}I_i(\gamma'') = I_i(\alpha''')I_j(\beta''')\bar{V}_{ij}I_j(\gamma'''), \end{aligned} \quad (2.20)$$

where

$$[I_i(\alpha)]_{jk} = \delta_{j,k}e^{i\alpha\delta_{i,j}} \quad (2.21)$$

are phase operators and \bar{V}_{ij} are $SO(2)$ rotation matrices with angles θ_{ij} in the interval $[0, \pi/2]$. Each of the four sets of angles in (2.20) obeys one relation $\alpha + \beta + \gamma = 0$ etc., such that each V_{ij} has three parameters. Clearly, with 6×3 parameters V_{SM4} must have 9 redundant phases. However, these unphysical phases will either cancel or be rotated away by quark field redefinitions. To see this, write V_{SM4} as

$$V_{\text{SM4}} = V_{34}V_{24}V_{14}V_{23}V_{13}V_{12}, \quad (2.22)$$

factor out the phases as done in (2.20), and re-arrange the phase operators in that expression, repeatedly using $[I_i(\alpha), I_j(\beta)] = 0$ and (2.20). In doing so, all but three of those operators can be moved to the extreme left or right of V_{SM4} , where they can be absorbed into phase redefinitions of the quark fields, such that one ends up with the standard parametrisation

$$V_{\text{SM4}} = \bar{V}_{34}I_4(\delta_{24})\bar{V}_{24}I_4(-\delta_{24})I_4(\delta_{14})\bar{V}_{14}I_4(-\delta_{14})\bar{V}_{23}I_3(\delta_{13})\bar{V}_{13}I_3(-\delta_{13})\bar{V}_{12}, \quad (2.23)$$

with all angles θ_{ij} in $[0, \pi/2]$ and phases δ_{ij} in $[0, 2\pi]$.

While it is advisable to use this exact parametrisation in numerical calculations, its structure turns out to be much simpler than its appearance in (2.19). Indeed, from the tree level measurements of $|V_{ud}|$, $|V_{us}|$, $|V_{ub}|$, $|V_{cd}|$, $|V_{cs}|$ and the unitarity of V_{SM4} , we know already that $c_{ij} \approx 1$ and that s_{14} and s_{24} are not larger than s_{12} [5]. On the other hand, from the global fits of the precision electroweak data one finds $s_{34} \leq 0.35$ [4, 6]. Our refined analysis of the implications of tree level measurements and of V_{SM4} unitarity in Section 7 combined with the results of [6] leads to the upper bounds

$$s_{14} \leq 0.04, \quad s_{24} \leq 0.17, \quad s_{34} \leq \frac{M_W}{m_{t'}} \leq 0.27, \quad (2.24)$$

that we will adopt in our paper. This particularly implies a decrease of the upper bound on s_{34} with increasing $m_{t'}$ [6]. The maximal value of s_{34} in (2.24) corresponds to $m_{t'} = 300 \text{ GeV}$. In order to be consistent with EWPT, one should choose the b' mass to be [5]

$$m_{b'} \approx m_{t'} - 55 \text{ GeV}. \quad (2.25)$$

However, $m_{b'}$ will not enter B and K observables and therefore is not crucial for our analysis.

In the limit $c_{ij} \approx 1$, as indicated above, the six mixing angles are directly determined by the moduli of the off-diagonal elements in the upper right corner of V_{SM4} :

$$\begin{aligned} s_{12} &\simeq |V_{us}|, & s_{13} &\simeq |V_{ub}|, & s_{23} &\simeq |V_{cb}|, \\ s_{14} &\simeq |V_{ub'}|, & s_{24} &\simeq |V_{cb'}|, & s_{34} &\simeq |V_{tb'}|. \end{aligned} \quad (2.26)$$

For a given scaling of the 4G mixing angles — like in our benchmark scenarios (2.12)–(2.17) — the subleading terms of V_{SM4} can then be characterised in terms of a generalised Wolfenstein expansion [48, 49].

$$\lambda \equiv s_{12}, \quad s_{23} \equiv A\lambda^2, \quad s_{13}e^{i\delta_{13}} \equiv A\lambda^3(\rho + i\eta) \equiv A\lambda^3 z_\rho \quad (2.27)$$

for the SM3 parameters, and

$$s_{14}e^{i\delta_{14}} = \lambda^{n_1} z_\tau, \quad s_{24}e^{i\delta_{24}} = \lambda^{n_2} z_\sigma, \quad s_{34} = \lambda^{n_3} B, \quad (2.28)$$

where A , B , z_i , z_i^* are coefficients of order one, and the exponents n_i depend on the scaling of the 4G mixing angles.

- For instance, in the case (2.12) we obtain the expansion of V_{SM4} as

$$\begin{aligned} & \begin{pmatrix} 1 - \frac{\lambda^2}{2} & \lambda & \lambda^3 A z_\rho^* & 0 \\ -\lambda & 1 - \frac{\lambda^2}{2} & \lambda^2 A & \lambda^3 z_\sigma^* \\ \lambda^3 A(1 - z_\rho) & -\lambda^2 A & 1 - \frac{\lambda^2}{2} B^2 & \lambda B \\ 0 & \lambda^3 (AB - z_\sigma) & -\lambda B & 1 - \frac{\lambda^2}{2} B^2 \end{pmatrix} \\ & + \lambda^4 \begin{pmatrix} -\frac{1}{8} & 0 & 0 & z_\tau^* \\ 0 & -\frac{1}{8}(1 + 4A^2) & 0 & 0 \\ 0 & (\frac{1}{2}A(1 + B^2 - 2z_\rho) - Bz_\sigma) & -\frac{1}{8}(4A^2 + B^4) & 0 \\ (AB(z_\rho - 1) + z_\sigma - z_\tau) & 0 & 0 & -\frac{B^4}{8} \end{pmatrix} + \mathcal{O}(\lambda^5). \end{aligned} \quad (2.29)$$

Here, we included terms up to order λ^4 , where V_{ts} receives an additional imaginary part from the 4G parameter z_σ , while the other off-diagonal elements of the effective 3×3 CKM sub-matrix keep their SM3 expansion at this order.

- On the other hand, in the case of (2.14), we obtain the expansion

$$\begin{aligned} & \begin{pmatrix} 1 - \frac{\lambda^2}{2} & \lambda & \lambda^3 A z_\rho^* & \lambda^2 z_\tau^* \\ -\lambda & 1 - \frac{\lambda^2}{2}(1 + |z_\sigma|^2) & \lambda^2 A & \lambda z_\sigma^* \\ \lambda^3 A(1 - z_\rho) & -\lambda^2(A + Bz_\sigma) & 1 - \frac{\lambda^2}{2} B^2 & \lambda B \\ \lambda^2(-z_\tau + z_\sigma) & -\lambda z_\sigma & -\lambda B & 1 - \frac{\lambda^2}{2}(|z_\sigma|^2 + B^2) \end{pmatrix} \\ & + \lambda^3 \begin{pmatrix} 0 & 0 & 0 & 0 \\ \frac{1}{2}(-2z_\tau z_\sigma^* + |z_\sigma|^2) & 0 & 0 & 0 \\ B(-z_\tau + z_\sigma) & 0 & 0 & -\frac{1}{2}B|z_\sigma|^2 \\ 0 & \frac{1}{2}(z_\sigma(1 + B^2) + 2AB - 2z_\tau) & -Az_\sigma & 0 \end{pmatrix} + \mathcal{O}(\lambda^4) \end{aligned} \quad (2.30)$$

This reveals that, in this case, V_{ts} and V_{td} receive order-one CP-violating phases from z_σ and $(z_\sigma - z_\tau)$, respectively. The associated CP-violating observables will thus strongly constrain the magnitude of δ_{14} and δ_{24} in a correlated way, which we will verify numerically in Section 9.3.

- Similarly, for (2.16), the generalised Wolfenstein expansion reads

$$\begin{pmatrix} 1 - \frac{\lambda^2}{2} & \lambda & \lambda^3 A z_\rho^* & \lambda^2 z_\tau^* \\ -\lambda & 1 - \frac{\lambda^2}{2} & \lambda^2 A & \lambda^3 z_\sigma^* \\ \lambda^3 (A(1 - z_\rho) - B z_\tau) & -\lambda^2 A & 1 - \frac{\lambda^2}{2} B^2 & \lambda B \\ -\lambda^2 z_\tau & \lambda^3 (AB - z_\tau - z_\sigma) & -\lambda B & 1 - \frac{\lambda^2}{2} B^2 \end{pmatrix} + \mathcal{O}(\lambda^4) \quad (2.31)$$

In this case, V_{td} receives a new phase from z_τ at leading order.

- Finally, for (2.17), the SM4 mixing matrix is approximated as

$$\begin{pmatrix} 1 - \frac{\lambda^2}{2} & \lambda & \lambda^3 A z_\rho^* & \lambda^3 z_\tau^* \\ -\lambda & 1 - \frac{\lambda^2}{2} & \lambda^2 A & \lambda^2 z_\sigma^* \\ \lambda^3 A(1 - z_\rho) & -\lambda^2 (A + B \lambda z_\sigma) & 1 - \frac{\lambda^2}{2} B^2 & \lambda B \\ \lambda^3 (z_\sigma - z_\tau) & \lambda^2 (\lambda AB - z_\sigma) & -\lambda B & 1 - \frac{\lambda^2}{2} B^2 \end{pmatrix} + \mathcal{O}(\lambda^4) \quad (2.32)$$

In this case, the new contributions to the phases of V_{td} and V_{ts} , compared to the SM3 parametrisation, are suppressed by an additional power of the Wolfenstein parameter λ .

While approximations like (2.29–2.32) will not be used in our actual numerical calculations, they reveal the different potential for new CP-violating effects as discussed below.

Finally, it should be remarked that other parameterisations of V_{SM4} can be found in the literature. One of them is the parameterisation in [50] in which the 4th row, i.e. $V_{t'd}$, $V_{t's}$ and $V_{t'b}$, are identified with the 3 new rotation angles and two new phases. While such a choice is certainly valid, we follow other recent studies and use the parameterisation presented above, which has the benefit of keeping the first row simple.

2.3 Unitarity

In writing the formulae for the observables of interest, it is useful to use the unitarity of the matrix V_{SM4} . To this end, we define the factors ($i = u, c, t, t'$)

$$\lambda_i^{(K)} = V_{is}^* V_{id}, \quad \lambda_i^{(d)} = V_{ib}^* V_{id}, \quad \lambda_i^{(s)} = V_{ib}^* V_{is}. \quad (2.33)$$

The unitarity relations are then written as

$$\lambda_u^{(K)} + \lambda_c^{(K)} + \lambda_t^{(K)} + \lambda_{t'}^{(K)} = 0, \quad (2.34)$$

with analogous expressions for the B_d and B_s system. Relation (2.34) allows to eliminate $\lambda_u^{(K)}$ so that only $\lambda_c^{(K)}$, $\lambda_t^{(K)}$ and $\lambda_{t'}^{(K)}$ enter the final expressions. We summarise the scaling of $\lambda_i^{K,d,s}$ compared to the SM3 expressions for our four benchmark scenarios in

Scenario $n_1 n_2 n_3$			(a) 431	(b) 211	(c) 231	(d) 321
Im	$\lambda_t^{(d)}/\lambda_t^{(d)} _{\text{SM}}$	$\simeq -\text{Im} \left[\lambda_{t'}^{(d)}/\lambda_t^{(d)} _{\text{SM}} \right]$	$\mathcal{O}(\lambda^2)$	$\mathcal{O}(1)$	$\mathcal{O}(1)$	$\mathcal{O}(\lambda)$
Im	$\lambda_t^{(s)}/\lambda_t^{(s)} _{\text{SM}}$	$\simeq -\text{Im} \left[\lambda_{t'}^{(s)}/\lambda_t^{(s)} _{\text{SM}} \right]$	$\mathcal{O}(\lambda^2)$	$\mathcal{O}(1)$	$\mathcal{O}(\lambda^2)$	$\mathcal{O}(\lambda)$
Im	$\lambda_t^{(K)}/\lambda_t^{(K)} _{\text{SM}}$		$\mathcal{O}(\lambda^2)$	$\mathcal{O}(1)$	$\mathcal{O}(1)$	$\mathcal{O}(\lambda)$
Im	$\lambda_{t'}^{(K)}/\lambda_t^{(K)} _{\text{SM}}$		$\mathcal{O}(\lambda^2)$	$\mathcal{O}(\lambda^{-2})$	$\mathcal{O}(1)$	$\mathcal{O}(1)$
Im	$\lambda_c^{(d)}/\lambda_c^{(d)} _{\text{SM}}$	$\simeq \text{Im} \left[\lambda_c^{(K)}/\lambda_c^{(K)} _{\text{SM}} \right]$	$\mathcal{O}(\lambda^6)$	$\mathcal{O}(\lambda^2)$	$\mathcal{O}(\lambda^4)$	$\mathcal{O}(\lambda^4)$
Im	$\lambda_c^{(s)}/\lambda_c^{(s)} _{\text{SM}}$		$\mathcal{O}(\lambda^8)$	$\mathcal{O}(\lambda^4)$	$\mathcal{O}(\lambda^6)$	$\mathcal{O}(\lambda^6)$

Table 1: Scaling of new 4G-induced flavour coefficients in CP-violating observables for different benchmark scenarios.

Table 1. As a general feature, we observe the approximate relations between the 4G contributions to the flavour coefficients with t and t' ,

$$\text{Im} \left[\lambda_t^{(d)}/\lambda_t^{(d)}|_{\text{SM}} \right] \simeq -\text{Im} \left[\lambda_{t'}^{(d)}/\lambda_t^{(d)}|_{\text{SM}} \right] , \quad (2.35)$$

$$\text{Im} \left[\lambda_t^{(s)}/\lambda_t^{(s)}|_{\text{SM}} \right] \simeq -\text{Im} \left[\lambda_{t'}^{(s)}/\lambda_t^{(s)}|_{\text{SM}} \right] . \quad (2.36)$$

Furthermore, the 4G effects on the light-quark coefficients $\lambda_c^{(d,s,K)}$ are always strongly suppressed.

Depending on the respective scenario, this has a different impact on CP-violating observables, for instance for the mixing-induced CP asymmetries $S_{\psi K_S}$ and $S_{\psi\phi}$:

- (a) For the scenario (2.12), the 4G contributions in Table 1 are suppressed by at least order λ^2 . Therefore, the mixing-induced asymmetry $S_{\psi K_S}$ will be dominated by the argument of $\lambda_t^{(d)}$, and similarly $S_{\psi\phi}$ will be dominated by $\arg(\lambda_t^{(s)})$, allowing only for small deviations compared to the SM3 analysis.
- (b) The situation is completely different in the case (2.14), where the modifications from 4G to $\lambda_{t,t'}^{(d,s)}$ and $\lambda_t^{(K)}$ are generically of $\mathcal{O}(1)$, and to $\lambda_{t'}^{(K)}$ even of order λ^{-2} . For $\lambda_{t'}^{(s)}/\lambda_t^{(s)} \sim \mathcal{O}(1)$, one might be worried about sizable corrections to $S_{\psi K_S}$ from t' -penguin pollution, because, in contrast to the SM3, the interference effects from weak phases in the $b \rightarrow s$ transition are no longer Cabibbo-suppressed. In spite of the fact that the new contributions are GIM-suppressed, without further hadronic input, we cannot exclude corrections as large as 10% to $S_{\psi K_S}$. In this case, the experimental bound from $S_{\psi K_S}$ will be a bit softer.

The constraints from $S_{\psi K_S}$ and ϵ_K then favour solutions of

$$\text{Im} \left[\lambda_{t,t'}^{(d)}/\lambda_t^{(d)}|_{\text{SM}} \right] \approx \lambda^2 \text{Im} \left[\lambda_{t'}^{(K)}/\lambda_t^{(K)}|_{\text{SM}} \right] \approx 0 , \quad (2.37)$$

which translates into strong correlations for the 4G mixing parameters, implying

$$(b) \quad \Rightarrow \quad s_{14} \approx s_{12}s_{24}, \quad \delta_{14} \approx \delta_{24},$$

$$\left| \text{Im} \left[\lambda_{t,t'}^{(s)} / \lambda_t^{(s)} |_{\text{SM}} \right] \right| \approx \left| \text{Im} \left[\lambda_t^{(K)} / \lambda_t^{(K)} |_{\text{SM}} \right] \right| \approx \frac{s_{24}s_{34} |\sin \delta_{14}|}{s_{23}}. \quad (2.38)$$

The last relation will lead to strong correlations between $b \rightarrow s$ and rare kaon decay observables.

- (c) For (2.16), only the phase of V_{td} is affected by leading-order 4G modifications, and therefore the $b \rightarrow s$ observables are not very much affected, while the modifications in $b \rightarrow d$ and $s \rightarrow d$ CP observables are constraining the two independent quantities

$$\text{Im} \left[\lambda_{t'}^{(K)} / \lambda_t^{(K)} |_{\text{SM}} \right] \quad \text{and} \quad \text{Im} \left[\lambda_{t,t'}^{(d)} / \lambda_t^{(d)} |_{\text{SM}} \right] \approx \text{Im} \left[\lambda_t^{(K)} / \lambda_t^{(K)} |_{\text{SM}} \right] \quad (2.39)$$

- (d) Finally, in the case (2.17), the modifications from 4G to $\lambda_{t,t'}^{(d,s)}$ and $\lambda_t^{(K)}$ are of $\mathcal{O}(\lambda)$, and to $\lambda_{t'}^{(K)}$ of $\mathcal{O}(1)$. On the one hand — compared to (b) — this leads to somewhat relaxed correlations between the 4G mixing parameters. On the other hand, it leaves room for moderate deviations from SM3 predictions.

These general type of observations will be verified numerically in Section 9.3.

2.4 CP-violating Invariants

The amount of CP violation in the quark Yukawa sector — which is relevant for the discussion of the baryon-antibaryon asymmetry [10] — can be quantified by studying appropriate basis-independent invariants built from the Yukawa matrices. The generalisation of the well-known Jarlskog determinant [51, 52] to the SM4 case has, for instance, been discussed in [53]. In the limit $m_{u,d,s,c}^2 \ll m_b^2 \ll m_{t,b',t'}^2$, and restricting ourselves to scenarios that fulfil the inequalities (2.9), the invariants reduce to one new CP-violating quantity,

$$I_1 = \text{Im tr} \left[(Y_U Y_U^\dagger)^2 (Y_D Y_D^\dagger) (Y_U Y_U^\dagger) (Y_D Y_D^\dagger)^2 \right]$$

$$\simeq -m_b^2 m_t^2 m_b^4 m_{t'}^2 (m_{t'}^2 - m_t^2) (F_{2323} + F_{1313} + F_{2313} + F_{1323})$$

$$\simeq m_b^2 m_t^2 m_b^4 m_{t'}^2 (m_{t'}^2 - m_t^2) \left\{ \begin{array}{l} -s_{23}s_{24}s_{34} \sin \delta_{24}, \\ s_{34} (s_{13}s_{14} \sin(\delta_{13} - \delta_{14}) - s_{23}s_{24} \sin \delta_{24}) \end{array} \right., \quad (2.40)$$

which can be related to the area of a quadrangle in the complex plane, described by the functions

$$F_{ijkl} = \text{Im} (V_{ik} V_{jk}^* V_{il}^* V_{jl}) .$$

The first line in (2.40) refers to scenarios with $s_{24} \gtrsim s_{14}$, like (2.12,2.14,2.17). The second line is valid for $s_{24} \sim \lambda s_{14}$, like in case of (2.16). It has been stressed in [10] that the quark mass-dependent prefactor in (2.40) can lead to an enhancement of several orders of magnitude compared to the SM3 analogue.

The overall scaling with the Wolfenstein parameter λ is given by $I_1 \sim \lambda^{2+n_2+n_3}$, which can be as large as λ^4 for scenario (2.14). For the benchmark scenario (2.17) one obtains $I_1 \sim \lambda^5$, whereas (2.12,2.16) would lead to $I_1 \sim \lambda^6$. As we will illustrate in the numerical section below, the dependence of I_1 on the SM4 mixing parameters is directly correlated with the size of $S_{\psi\phi}$.

3 Effective Hamiltonians in the SM4

3.1 Effective Hamiltonians for $\Delta F = 2$ Transitions

The effective Hamiltonian for $\Delta S = 2$ transitions can be written as

$$\begin{aligned} \mathcal{H}_{\text{eff}}^{\Delta S=2} = & \frac{G_F^2}{16\pi^2} M_W^2 \left[\lambda_c^{2(K)} \eta_{cc}^{(K)} S_0(x_c) + \lambda_t^{2(K)} \eta_{tt}^{(K)} S_0(x_t) + \lambda_{t'}^{2(K)} \eta_{t't'}^{(K)} S_0(x_{t'}) \right. \\ & + 2\lambda_t^{(K)} \lambda_c^{(K)} \eta_{ct}^{(K)} S_0(x_t, x_c) + 2\lambda_{t'}^{(K)} \lambda_c^{(K)} \eta_{ct'}^{(K)} S_0(x_{t'}, x_c) \\ & \left. + 2\lambda_t^{(K)} \lambda_{t'}^{(K)} \eta_{tt'}^{(K)} S_0(x_{t'}, x_t) \right] \times \\ & \times (\alpha_s^{(3)}(\mu))^{-2/9} \left[1 + \frac{\alpha_s^{(3)}(\mu)}{4\pi} J_3 \right] Q(\Delta S = 2), \end{aligned} \quad (3.1)$$

where the functions $\eta_{ij}^{(K)}$ and explicit factors of α_s arise from QCD corrections. The operator $Q(\Delta S = 2)$ is defined in (4.13) below. Absorbing the contributions of the 4G quarks into a redefinition of the loop function $S_0(x_t)$, we can bring this Hamiltonian into a form as in the SM3,

$$\begin{aligned} \mathcal{H}_{\text{eff}}^{\Delta S=2} = & \frac{G_F^2}{16\pi^2} M_W^2 \left[\lambda_c^{2(K)} \eta_{cc}^{(K)} S_0(x_c) + \lambda_t^{2(K)} \eta_{tt}^{(K)} S_K + 2\lambda_t^{(K)} \lambda_c^{(K)} \eta_{ct}^{(K)} S_0(x_t, x_c) \right] \times \\ & \times (\alpha_s(\mu))^{-2/9} \left[1 + \frac{\alpha_s(\mu)}{4\pi} J_3 \right] Q(\Delta S = 2), \end{aligned} \quad (3.2)$$

where

$$\begin{aligned} S_K = & S_0(x_t) + \frac{\eta_{t't'}^{(K)}}{\eta_{tt}^{(K)}} \left(\frac{\lambda_{t'}^{(K)}}{\lambda_t^{(K)}} \right)^2 S_0(x_{t'}) + 2 \frac{\eta_{tt'}^{(K)}}{\eta_{tt}^{(K)}} \left(\frac{\lambda_{t'}^{(K)}}{\lambda_t^{(K)}} \right) S_0(x_t, x_{t'}) \\ & + 2 \frac{\eta_{ct'}^{(K)}}{\eta_{tt}^{(K)}} \left(\frac{\lambda_c^{(K)} \lambda_{t'}^{(K)}}{\lambda_t^{(K)2}} \right) S_0(x_{t'}, x_c). \end{aligned} \quad (3.3)$$

The standard loop functions $S_0(x)$ and $S_0(x_i, x_j)$ are given in Appendix A.

In principle, (3.2) can be directly generalised to the B_d, B_s systems. In practise, only the analogue of the S_K term is relevant, and consequently ($q = d, s$)

$$\mathcal{H}_{\text{eff}}^{(q)} = \frac{G_F^2}{16\pi^2} M_W^2 \eta_B \left(\lambda_t^{(q)} \right)^2 S_q \left[\alpha_s^{(5)} \right]^{-6/23} \left[1 + \frac{\alpha_s^{(5)}}{4\pi} J_5 \right] Q^q(\Delta B = 2), \quad (3.4)$$

$$\begin{aligned} S_q = S_0(x_t) &+ \frac{\eta_{t't'}^{(q)}}{\eta_{tt}^{(q)}} \left(\frac{\lambda_{t'}^{(q)}}{\lambda_t^{(q)}} \right)^2 S_0(x_{t'}) + 2 \frac{\eta_{tt'}^{(q)}}{\eta_{tt}^{(q)}} \left(\frac{\lambda_{t'}^{(q)}}{\lambda_t^{(q)}} \right) S_0(x_t, x_{t'}) \\ &+ 2 \frac{\eta_{ct'}^{(q)}}{\eta_{tt}^{(q)}} \left(\frac{\lambda_c^{(q)} \lambda_{t'}^{(q)}}{\lambda_t^{(q)2}} \right) S_0(x_{t'}, x_c). \end{aligned} \quad (3.5)$$

In contrast to the last term in (3.3), that can be relevant for certain values of the parameters involved, the last term in (3.5) turns out to be negligibly small.

3.2 Effective Hamiltonians for $K_L \rightarrow \mu^+ \mu^-$ and $B_{d,s} \rightarrow \mu^+ \mu^-$

As for the rare leptonic decays, we first consider $K_L \rightarrow \mu^+ \mu^-$, where we also have to address the charm contribution. For pedagogical reasons, we will neglect QCD corrections for a moment (they will be discussed subsequently). The effective Hamiltonian for the SD part of $K_L \rightarrow \mu^+ \mu^-$ is given in the SM3 as follows [54],

$$\mathcal{H}_{\text{eff}} = -\frac{G_F}{\sqrt{2}} \frac{\alpha}{2\pi \sin^2 \theta_W} \left(\lambda_c^{(K)} Y_0(x_c) + \lambda_t^{(K)} Y_0(x_t) \right) (\bar{s}d)_{V-A} (\bar{\mu}\mu)_{V-A}, \quad (3.6)$$

with the function $Y_0(x)$ given in Appendix A. This Hamiltonian can be generalised in a straightforward manner by

- including the effects of the heavy t' and the heavy 4G neutrino, with the latter exchanged only in the box diagram and the former in both, the Z^0 penguin and box diagrams;
- including the mixing in the lepton sector, parametrised by a 4×4 matrix with the elements denoted by W_{ij} . Here, the first index applies to neutrinos, the second to charged leptons.

Neglecting the masses of the lightest neutrinos and of the up-quark, and using the unitarity of the SM4 quark and lepton mixing matrices, we find – not unexpectedly – that the final result can be written in terms of the function Y_0 and the box function

$$\begin{aligned} F^{\mu\bar{\mu}}(x_i, y_4) &= B^{\mu\bar{\mu}}(x_i, 0) + B^{\mu\bar{\mu}}(0, y_4) - B^{\mu\bar{\mu}}(0, 0) - B^{\mu\bar{\mu}}(x_i, y_4) \\ &= -S_0(x_i, y_4), \end{aligned} \quad (3.7)$$

where

$$x_i = \frac{m_i^2}{M_W^2}, \quad y_4 = \frac{(m_4^\nu)^2}{M_W^2}. \quad (3.8)$$

The functions $B^{\mu\bar{\mu}}$ and S_0 are given in Appendix A.

The generalisation of (3.6) to include the 4G quarks and the mixing in the 4G lepton sector is then given as follows:

$$\lambda_c^{(K)} Y_0(x_c) \rightarrow \lambda_c^{(K)} (Y_0(x_c) + |W_{4\mu}|^2 F^{\mu\bar{\mu}}(x_c, y_4)) , \quad (3.9)$$

$$\begin{aligned} \lambda_t^{(K)} Y_0(x_t) &\rightarrow \lambda_t^{(K)} (Y_0(x_t) + |W_{4\mu}|^2 F^{\mu\bar{\mu}}(x_t, y_4)) \\ &+ \lambda_{t'}^{(K)} (Y_0(x_{t'}) + |W_{4\mu}|^2 F^{\mu\bar{\mu}}(x_{t'}, y_4)) . \end{aligned} \quad (3.10)$$

Concerning QCD corrections, they have been found to be very small in the case of the top quark part within the SM3 [55, 56], and we will neglect them for the t and t' contributions in the SM4. In the case of the charm part, QCD corrections are significant and have to be included [55, 57]. As seen in (3.9) in the absence of mixing with the heavy new charged lepton, the charm contribution remains intact including QCD corrections. If significant mixing is present, the charm contribution is modified and also the corresponding QCD corrections should be reconsidered. Although this would be straightforward, we do not expect these effects to be important, in particular in comparison with the 4G effects in the top sector. Therefore we postpone their inclusion until after the discovery of the 4G.

Clearly the terms involving $|W_{4\mu}|^2$ are only relevant if $|W_{4\mu}|^2$ is substantial. We will comment on the size of these terms in the next section.

The generalisation to $B_{d,s} \rightarrow \mu^+ \mu^-$ is straightforward. First we can drop the charm contribution, as it is negligibly small relative to the t and t' contributions. Second, $\lambda_t^{(K)}$ and $\lambda_{t'}^{(K)}$ should be replaced by $\lambda_t^{(d,s)}$ and $\lambda_{t'}^{(d,s)}$, respectively.

3.3 Effective Hamiltonian for $K \rightarrow \pi \nu \bar{\nu}$ and $B \rightarrow X_{d,s} \nu \bar{\nu}$

We begin with $K^+ \rightarrow \pi^+ \nu \bar{\nu}$. The effective Hamiltonian for this decay within the SM3, neglecting QCD corrections, is given by [54]

$$\mathcal{H}_{\text{eff}} = \frac{G_F}{\sqrt{2}} \frac{\alpha}{2\pi \sin^2 \theta_W} \sum_{\ell=e,\mu,\tau} \left(\lambda_c^{(K)} X_0(x_c, z_\ell) + \lambda_t^{(K)} X_0(x_t) \right) (\bar{s}d)_{V-A} (\bar{\nu}_\ell \nu_\ell)_{V-A}, \quad (3.11)$$

where

$$X_0(x_c, 0) = X_0(x_c), \quad z_e = z_\mu \simeq 0, \quad z_\tau = \frac{m_\tau^2}{M_W^2}. \quad (3.12)$$

The τ -lepton mass dependence in the top-contribution can be neglected, but not in the case of the charm contribution. We want to generalise this Hamiltonian to include the

effects of the heavy t' and the heavy charged lepton, as well as the effect of the mixing in the lepton sector described by the W_{ij} elements of the 4×4 lepton-mixing matrix.

A small complication, relative to the $\mu^+\mu^-$ case, arises from the summation over three light neutrino species that — being mass eigenstates — will be denoted by ν_1, ν_2, ν_3 , with ν_4 denoting the heavy neutrino which is exchanged in the box diagram for the $K_L \rightarrow \mu^+\mu^-$ decay. Here the 4G heavy charged lepton that enters the box diagrams in $K^+ \rightarrow \pi^+\nu\bar{\nu}$ will be represented by $z_4 = m_4^{\ell 2}/M_W^2$. The final result can be written in terms of the function X_0 and the box function

$$F^{\nu\bar{\nu}}(x_i, z_4) \equiv B^{\nu\bar{\nu}}(x_i, 0) + B^{\nu\bar{\nu}}(0, z_4) - B^{\nu\bar{\nu}}(0, 0) - B^{\nu\bar{\nu}}(x_i, z_4), \quad (3.13)$$

with X_0 and $B^{\nu\bar{\nu}}$ given in Appendix A.

The generalisation of (3.11) to include the 4G quarks and the mixing in the 4G lepton sector is given for the ℓ -th neutrino ν_ℓ in the final state as follows

$$\lambda_c^{(K)} X_0(x_c, z_\ell) \rightarrow \lambda_c^{(K)} (X_0(x_c) + 4|W_{\ell\tau}|^2 F^{\nu\bar{\nu}}(x_c, z_\tau) + 4|W_{\ell 4}|^2 F^{\nu\bar{\nu}}(x_c, z_4)) , \quad (3.14)$$

$$\begin{aligned} \lambda_t^{(K)} X_0(x_t) &\rightarrow \lambda_t^{(K)} (X_0(x_t) + 4|W_{\ell 4}|^2 F^{\nu\bar{\nu}}(x_t, z_4)) \\ &+ \lambda_{t'}^{(K)} (X_0(x_{t'}) + 4|W_{\ell 4}|^2 F^{\nu\bar{\nu}}(x_{t'}, z_4)) . \end{aligned} \quad (3.15)$$

Concerning QCD corrections the same comments apply as after (3.10).

The generalisation to $K_L \rightarrow \pi^0\nu\bar{\nu}$ and $B \rightarrow X_{d,s}\nu\bar{\nu}$ is straightforward: the charm contribution can be neglected and in the case of $B \rightarrow X_{d,s}\nu\bar{\nu}$, $\lambda_t^{(K)}$ and $\lambda_{t'}^{(K)}$ should be replaced by $\lambda_t^{(d,s)}$ and $\lambda_{t'}^{(d,s)}$, respectively.

3.4 Other Hamiltonians

The examples of effective Hamiltonians presented above make it clear how to find the corresponding Hamiltonians for $B \rightarrow X_s\gamma$, $B \rightarrow X_s\ell^+\ell^-$, $K_L \rightarrow \pi^0\ell^+\ell^-$, non-leptonic two-body decays and ε'/ε . Therefore for these cases we will only present and/or discuss the final formulae for branching ratios and CP asymmetries.

4 Master Formulae in the SM4

4.1 Preliminaries

The generalisation of the known SM3 formulae for FCNC observables in the quark sector [54] to the SM4 is straightforward. One just extends the summation over flavours to the 4G quarks and uses the unitarity relation of V_{SM4} , like the one in (2.34), in order to eliminate $\lambda_u^{(K)}$, $\lambda_u^{(d)}$ and $\lambda_u^{(s)}$ from the final expressions. As discussed in the previous

section, the only complication arises from the effects of the 4G heavy leptons in box diagrams, contributing to semi-leptonic and leptonic decays if their mixing with SM3 leptons is non-vanishing. In the SM3, this effect can be neglected in view of the smallness of the SM3 lepton masses, but in the presence of 4G heavy leptons it could, in principle, be non-negligible.

In fact, the numerical analysis of these effects shows that, for $|W_{\ell 4}|$ and $|W_{4\mu}|$ of $\mathcal{O}(1)$, the impact of these additional contributions cannot be neglected. In our numerical analysis we will however assume that $|W_{\ell 4}|$ are at most $\mathcal{O}(\lambda)$, and consequently these effects can be neglected. This will avoid any detailed assumptions about the heavy lepton masses and about their mixing with three SM3 lepton generations. However, in order to be complete, we will present the formulae for the branching ratios taking this mixing into account.

Next, it is useful, as in the case of the LHT model [32], to generalise the real and universal Inami-Lim functions in the SM3, as introduced in [58], to complex and non-universal functions ($i = K, d, s$)

$$S_i \equiv |S_i| e^{i\theta_S^i}, \quad X_i^\ell \equiv |X_i^\ell| e^{i\theta_X^{\ell}}, \quad Y_i \equiv |Y_i| e^{i\theta_Y^i}, \quad Z_i \equiv |Z_i| e^{i\theta_Z^i}, \quad (4.1)$$

which govern particle-antiparticle mixing and rare K and B decays. In the limit of three generations, S_i, X_i^ℓ, Y_i, Z_i reduce to the flavour universal functions S_0, X_0, Y_0, Z_0 that are real. This formulation allows a transparent comparison of our results with those obtained for particle-antiparticle mixing and rare decays in the LHT model [31–33]. The index “ ℓ ” in the case of X_i^ℓ distinguishes between different neutrinos in the final state. This distinction is only necessary in the presence of $\mathcal{O}(1)$ elements $|W_{\ell 4}|$.

In the case of $B \rightarrow X_{s,d}\gamma$ and $B \rightarrow X_{s,d}\ell^+\ell^-$, one has to introduce new functions representing the contributions of dipole operators. For the magnetic photon and gluon penguin, we have respectively ($i = s, d$)

$$D'_i \equiv |D'_i| e^{i\theta_{D'}^i}, \quad E'_i \equiv |E'_i| e^{i\theta_{E'}^i}. \quad (4.2)$$

For the electromagnetic and chromomagnetic penguins, the corresponding functions are

$$D_i \equiv |D_i| e^{i\theta_D^i}, \quad E_i \equiv |E_i| e^{i\theta_E^i}. \quad (4.3)$$

D_i is gauge dependent and enters the gauge-independent function Z_i through

$$Z_i = C_i + \frac{1}{4}D_i, \quad C_i \equiv |C_i| e^{i\theta_C^i}, \quad (4.4)$$

with C_i being the Z -penguin function. In the SM3, the functions $D'_i, E'_i, D_i, E_i, C_i$ reduce to the known real and flavour-universal functions $D'_0, E'_0, D_0, E_0, C_0$ [54].

Thus, our next step is to find the expressions for the master functions of (4.1)–(4.4) in the SM4.

4.2 Master Functions

As discussed, the master functions of the SM4 can be expressed in terms of the functions known from the SM3 and the elements of V_{SM4} . No new loop calculations are necessary, except for those involving heavy leptons, which have been performed in the previous section. We expect these contributions to be small, but for completeness we include them in the formulae below.

Starting with the effective Hamiltonian for $\Delta F = 2$ transitions given in the previous section and proceeding as explicitly shown there, one can absorb the effects of t' into the master functions S_i . We then find for the $\Delta F = 2$ transitions ($q = d, s$)

$$S_q = S_0(x_t) + \left(\frac{\lambda_{t'}^{(q)}}{\lambda_t^{(q)}} \right)^2 S_0(x_{t'}) + 2 \frac{\lambda_{t'}^{(q)}}{\lambda_t^{(q)}} S_0(x_t, x_{t'}), \quad (4.5)$$

where $x_i = m_i^2/M_W^2$. In the K system, we also have to keep the last term in (3.3), such that

$$S_K = S_0(x_t) + \left(\frac{\lambda_{t'}^{(K)}}{\lambda_t^{(K)}} \right)^2 S_0(x_{t'}) + 2 \frac{\lambda_{t'}^{(K)}}{\lambda_t^{(K)}} S_0(x_t, x_{t'}) + 2 \frac{\eta_{ct}^{(K)}}{\eta_{tt}^{(K)}} \frac{\lambda_c^{(K)} \lambda_{t'}^{(K)}}{\lambda_t^{(K)2}} S_0(x_c, x_{t'}). \quad (4.6)$$

In writing these expressions, we have assumed the following approximate relations for the QCD corrections,

$$\eta_{tt}^{(i)} = \eta_{tt'}^{(i)} = \eta_{t't'}^{(i)}, \quad \eta_{ct}^{(i)} = \eta_{ct'}^{(i)}. \quad (4.7)$$

This approximation is justified as $m_{t'}$ is only by a factor of 2–3 larger than m_t , the anomalous dimension of the involved $(V-A) \otimes (V-A)$ operator is small, and the QCD corrections only very weakly depend on the actual value of $m_{t'}$ (where the t' -mass is defined as $m_{t'}(m_{t'})$).

Proceeding in an analogous manner, we obtain

$$X_i^\ell = X_0(x_t) + \frac{\lambda_{t'}^{(i)}}{\lambda_t^{(i)}} X_0(x_{t'}) + \Delta_X^{\ell i}, \quad (4.8)$$

$$Y_i = Y_0(x_t) + \frac{\lambda_{t'}^{(i)}}{\lambda_t^{(i)}} Y_0(x_{t'}) + \Delta_Y^i, \quad (4.9)$$

as well as

$$Z_i = Z_0(x_t) + \frac{\lambda_{t'}^{(i)}}{\lambda_t^{(i)}} Z_0(x_{t'}), \quad E_i = X_0(x_t) + \frac{\lambda_{t'}^{(i)}}{\lambda_t^{(i)}} E_0(x_{t'}), \quad (4.10)$$

$$D'_i = D'_0(x_t) + \frac{\lambda_{t'}^{(i)}}{\lambda_t^{(i)}} D'_0(x_{t'}), \quad E'_i = E'_0(x_t) + \frac{\lambda_{t'}^{(i)}}{\lambda_t^{(i)}} E'_0(x_{t'}). \quad (4.11)$$

A similar expression exists for D_i , but we do not need it as D_i is absorbed in Z_i . The heavy-lepton corrections $\Delta_X^{\ell i}$ and Δ_Y^i can be extracted from (3.15) and (3.10), respectively.

This completes the presentation of the master functions. The SM3 functions $S_0(x_t)$, $S_0(x_c, x_t)$, $X_0(x_t)$, $Y_0(x_t)$, $Z_0(x_t)$, $D'_0(x_t)$, $E'_0(x_t)$, $E_0(x_t)$ and those relevant for the evaluation of $\Delta_X^{\ell i}$ and Δ_Y^i are given in Appendix A. We should emphasise that the approximate formula for $S_0(x_c, x_t)$, valid only for $m_c \ll m_t$ and used in the literature, cannot be used for $S_0(x_{t'}, x_t)$. The exact expression [59] is given in Appendix A.

4.3 $\Delta F = 2$ Observables

We recall that the off-diagonal element in the dispersive part of the amplitude for $K^0 - \bar{K}^0$ mixing is given by

$$2m_K (M_{12}^K)^* = \langle \bar{K}^0 | H_{\text{eff}}^{\Delta S=2} | K^0 \rangle, \quad (4.12)$$

with analogous expressions for the B_d and B_s systems. Our conventions follow [60]. In particular, the operators being involved are ($q = d, s$)

$$Q(\Delta S = 2) = (\bar{s}d)_{V-A}(\bar{s}d)_{V-A}, \quad Q^q(\Delta B = 2) = (\bar{b}q)_{V-A}(\bar{b}q)_{V-A}. \quad (4.13)$$

The usual procedure [60] then gives

$$M_{12}^K = \frac{G_F^2}{12\pi^2} F_K^2 \hat{B}_K m_K M_W^2 \overline{M}_{12}^K, \quad (4.14)$$

where

$$\overline{M}_{12}^K = \lambda_c^{*(K)^2} \eta_{cc} S_0(x_c) + \lambda_t^{*(K)^2} \eta_{tt}^{(K)} S_K^* + 2\eta_{ct}^{(K)} \lambda_t^{*(K)} \lambda_c^{*(K)} S_0(x_t, x_c), \quad (4.15)$$

and we used the fact that $S_0(x_c)$ and $S_0(x_t, x_c)$ are real-valued functions. Then

$$\Delta M_K = 2\text{Re} (M_{12}^K), \quad (4.16)$$

$$\varepsilon_K = \frac{\kappa_\varepsilon e^{i\varphi_\varepsilon}}{\sqrt{2}(\Delta M_K)_{\text{exp}}} \text{Im} (M_{12}^K), \quad (4.17)$$

where the parameters $\varphi_\varepsilon = (43.51 \pm 0.05)^\circ$ and $\kappa_\varepsilon = 0.92 \pm 0.02$ [61] take into account that $\varphi_\varepsilon \neq \pi/4$ and include an additional effect from $\text{Im}(A_0)$, the imaginary part of the isospin-0 amplitude in $K \rightarrow \pi\pi$. The result for κ_ε has been recently confirmed in [62]¹. For M_{12}^q , describing the $B_q - \bar{B}_q$ mixing, we then have ($q = d, s$)

$$M_{12}^q = \frac{G_F^2}{12\pi^2} F_{B_q}^2 \hat{B}_{B_q} m_{B_q} M_W^2 \overline{M}_{12}^q, \quad (4.18)$$

¹The recent inclusion of additional long distance contributions modifies κ_ε to 0.94 ± 0.02 [63] without any visible impact on our numerical results.

where

$$\overline{M}_{12}^q = \left(\lambda_t^{*(q)} \right)^2 \eta_B S_q^* . \quad (4.19)$$

The contributions involving charm can be neglected.

For the mass differences in the $B_{d,s}^0 - \bar{B}_{d,s}^0$ systems we have

$$\Delta M_q = 2 |M_{12}^q| . \quad (4.20)$$

Defining

$$M_{12}^q = |M_{12}^q| e^{2i\varphi_{B_q}^{\text{tot}}} , \quad (4.21)$$

the mixing-induced CP asymmetries $S_{\psi K_S}$ and $S_{\psi\phi}$ are simply given as follows,

$$S_{\psi K_S} = \sin 2\varphi_{B_d}^{\text{tot}} , \quad S_{\psi\phi} = -\sin 2\varphi_{B_s}^{\text{tot}} . \quad (4.22)$$

The latter two observables are the coefficients of $\sin(\Delta M_d t)$ and $\sin(\Delta M_s t)$ in the time-dependent CP asymmetries in $B_d^0 \rightarrow \psi K_S$ and $B_s^0 \rightarrow \psi\phi$, respectively. We also have

$$2\varphi_{B_d}^{\text{tot}} = 2\bar{\beta} - \theta_S^d , \quad 2\varphi_{B_s}^{\text{tot}} = 2\bar{\beta}_s - \theta_S^s , \quad (4.23)$$

where the phases $\bar{\beta}$ and $\bar{\beta}_s$ are defined as follows,

$$V_{td} = |V_{td}| e^{-i\bar{\beta}} , \quad V_{ts} = -|V_{ts}| e^{-i\bar{\beta}_s} . \quad (4.24)$$

Similarly, the phase $2\varphi_K$ of the leading S_K^* term in (4.15) is given by

$$2\varphi_K = 2\bar{\beta} - 2\bar{\beta}_s - \theta_S^K . \quad (4.25)$$

It should be emphasised that $\bar{\beta}$ and $\bar{\beta}_s$ differ from $\beta \approx 21^\circ$ and $\beta_s \approx -1^\circ$, familiar from the SM3 and unitarity triangle (UT) analyses. Indeed, the expressions for V_{td} and V_{ts} as seen in (2.19) differ from the ones in the CKM matrix. In the SM3 $\bar{\beta}$ and $\bar{\beta}_s$ reduce to β and β_s , respectively. Moreover, the contributions of the t' quark are absent, and the two asymmetries in question are given as follows,

$$(S_{\psi K_S})_{\text{SM}} = \sin 2\beta , \quad (S_{\psi\phi})_{\text{SM}} = -\sin 2\beta_s . \quad (4.26)$$

In the presence of contributions from the 4G quarks, these two asymmetries do not measure β and β_s , not even $\bar{\beta}$ and $\bar{\beta}_s$, but determine $\varphi_{B_q}^{\text{tot}}$ that includes also the contributions from the t' quark. As we will see, $\varphi_{B_d}^{\text{tot}}$ will only slightly differ from β because of the experimental constraint² on $S_{\psi K_S}$. On the other hand, $\varphi_{B_s}^{\text{tot}}$ must be very different from

² Concerning the suppression of t' -penguin pollution in the determination of β , the comment before Eq. (2.37) applies.

β_s , in order to reproduce the data on $S_{\psi\phi}$ from CDF [64] and D0 [65]. HFAG [66] gives the following values for $\varphi_{B_s}^{\text{tot}}$

$$\varphi_{B_s}^{\text{tot}} = -(0.39_{-0.14}^{+0.18}) \left[-(1.18_{-0.18}^{+0.14}) \right]. \quad (4.27)$$

As we will see in Section 7, the present tensions in the SM3 UT fits favour $\theta_S^d > 0$ and $\theta_S^K < 0$, while the enhanced value of $S_{\psi\phi}$ at Tevatron favours $\theta_S^s > 0$. In the case of the ε_K anomaly, also an enhanced value of $|S_K|$ would help. As we discussed already in Section 2.2, and as we will numerically confirm later in Section 9, a big $S_{\psi\phi}$ will strongly correlate δ_{14} and δ_{24} as well as s_{14} and s_{24} .

Finally, it should also be emphasised that in the SM4 the ratio $\Delta M_d/\Delta M_s$ does not determine directly the side R_t in the UT, as now the UT does not close, and there are non-MFV contributions. Therefore, the determination of the ratio $|V_{td}|/|V_{ts}|$ by means of

$$\frac{\Delta M_d}{\Delta M_s} = \frac{m_{B_d} \hat{B}_{B_d} F_{B_d}^2}{m_{B_s} \hat{B}_{B_s} F_{B_s}^2} \left| \frac{V_{td}}{V_{ts}} \right|^2 \frac{|S_d|}{|S_s|}, \quad (4.28)$$

will clearly be affected since the last ratio is now generally different from unity.

4.4 $B_{s,d} \rightarrow \mu^+ \mu^-$

One of the main targets of flavour physics in the coming years will be the measurement of the branching ratio for the highly suppressed decay $B_s \rightarrow \mu^+ \mu^-$. Hopefully, the even more suppressed decay $B_d \rightarrow \mu^+ \mu^-$ will be discovered as well. These two decays are helicity suppressed in the SM3 and CMFV models. Their branching ratios are proportional to the squares of the corresponding weak decay constants that still suffer from sizable uncertainties. However, using simultaneously the SM3 expressions for the very well measured mass differences $\Delta M_{s,d}$, this uncertainty can be eliminated [67], leaving the uncertainties in the hadronic parameters \hat{B}_{B_s} and \hat{B}_{B_d} as the only theoretical uncertainty in $\text{Br}(B_{s,d} \rightarrow \mu^+ \mu^-)$. As seen in Table 3, these parameters are already known from lattice calculations with 5 – 10% precision, and they enter the branching ratios linearly.

Generalising this idea to the SM4, we find

$$\text{Br}(B_q \rightarrow \mu^+ \mu^-) = C \frac{\tau(B_q)}{\hat{B}_{B_q}} \frac{|Y_q|^2}{|S_q|} \Delta M_q, \quad (q = s, d), \quad (4.29)$$

where ΔM_q is supposed to be taken from experiment, and the prefactor C is defined as

$$C = 6\pi \frac{\eta_Y^2}{\eta_B} \left(\frac{\alpha}{4\pi \sin^2 \theta_W} \right)^2 \frac{m_\mu^2}{M_W^2} = 4.39 \cdot 10^{-10}. \quad (4.30)$$

Consequently, the golden relation between $\text{Br}(B_{d,s} \rightarrow \mu^+\mu^-)$ and $\Delta M_d/\Delta M_s$, valid in CMFV models [67], gets modified as follows:

$$\frac{\text{Br}(B_s \rightarrow \mu^+\mu^-)}{\text{Br}(B_d \rightarrow \mu^+\mu^-)} = \frac{\hat{B}_{B_d} \tau(B_s) \Delta M_s}{\hat{B}_{B_s} \tau(B_d) \Delta M_d} r, \quad r = \left| \frac{Y_s}{Y_d} \right|^2 \frac{|S_d|}{|S_s|}, \quad (4.31)$$

with r being generally different from unity.

Using these expressions, one finds in the SM3 the rather precise predictions

$$\text{Br}(B_s \rightarrow \mu^+\mu^-) = (3.2 \pm 0.2) \cdot 10^{-9}, \quad \text{Br}(B_d \rightarrow \mu^+\mu^-) = (1.0 \pm 0.1) \cdot 10^{-10}, \quad (4.32)$$

where the updated value of $\text{Br}(B_s \rightarrow \mu^+\mu^-)$ has already been reported in [68].

These predictions should be compared to the 95% C.L. upper limits from CDF [69] and D0 [70] (in parentheses)

$$\text{Br}(B_s \rightarrow \mu^+\mu^-) \leq 3.3 \text{ (5.3)} \cdot 10^{-8}, \quad \text{Br}(B_d \rightarrow \mu^+\mu^-) \leq 1 \cdot 10^{-8}. \quad (4.33)$$

The numbers given above are updates presented at the EPS-HEP09 conference. More information is given by Punzi [71]. It is clear from (4.32) and (4.33) that a lot of room is still left for NP contributions.

4.5 $K_L \rightarrow \mu^+\mu^-$

The discussion of the NP contributions to this decay is analogous to $B_{d,s} \rightarrow \mu^+\mu^-$. Again, only the SM3 operator $(V-A) \otimes (V-A)$ contributes, and the real function $Y_0(x_t)$ is replaced by the complex function Y_K defined in (4.9).

In contrast to $B_{s,d} \rightarrow \mu^+\mu^-$, the SD contribution calculated here is only one part of a dispersive contribution to $K_L \rightarrow \mu^+\mu^-$ that is by far dominated by the absorptive contribution with two internal photon exchanges. Consequently, the SD contribution constitutes only a small fraction of the branching ratio. Moreover, because of long-distance (LD) contributions to the dispersive part of $K_L \rightarrow \mu^+\mu^-$, the extraction of the SD part from the data is subject to considerable uncertainties. The most recent estimate gives [72]

$$\text{Br}(K_L \rightarrow \mu^+\mu^-)_{\text{SD}} \leq 2.5 \cdot 10^{-9}, \quad (4.34)$$

to be compared with $(0.8 \pm 0.1) \cdot 10^{-9}$ in the SM3 [57]. In the SM4, we have

$$\text{Br}(K_L \rightarrow \mu^+\mu^-)_{\text{SD}} = 2.08 \cdot 10^{-9} \left(\frac{\text{Re}\lambda_c^{(K)}}{|V_{us}|} P_c(Y_K) + \frac{\text{Re}(\lambda_t^{(K)} Y_K)}{|V_{us}|^5} \right)^2, \quad (4.35)$$

where $P_c(Y_K) = 0.113 \pm 0.017$ [57]. The numerical results are discussed in Section 7.

4.6 $B \rightarrow X_{s,d}\nu\bar{\nu}$

Also B decays with $\nu\bar{\nu}$ in the final state provide a very good test of modified Z -penguin contributions [73, 74], but their measurements appear to be even harder than those of the rare K decays discussed subsequently. Recent analyses of these decays within the SM3 and several NP scenarios can be found in [75, 76]. The experimental prospects for these decays at future Super-B machines are summarised in [77].

Here we will concentrate on the theoretical clean decays $B \rightarrow X_{s,d}\nu\bar{\nu}$. The recently improved SM3 prediction for $B \rightarrow X_s\nu\bar{\nu}$ reads [75]

$$\text{Br}(B \rightarrow X_s\nu\bar{\nu})_{\text{SM}} = (2.7 \pm 0.2) \cdot 10^{-5}. \quad (4.36)$$

As the refinements related to this result apply also to the SM4, we will only consider the ratios

$$\frac{\text{Br}(B \rightarrow X_s\nu\bar{\nu})}{\text{Br}(B \rightarrow X_s\nu\bar{\nu})_{\text{SM}}} = \frac{1}{3} \frac{\sum_{\ell=1,2,3} |X_s^\ell|^2}{|X_0(x_t)|^2} r_s, \quad r_s = \frac{|V_{ts}|^2}{|V_{ts}|_{\text{SM}}^2}, \quad (4.37)$$

$$\frac{\text{Br}(B \rightarrow X_d\nu\bar{\nu})}{\text{Br}(B \rightarrow X_d\nu\bar{\nu})_{\text{SM}}} = \frac{1}{3} \frac{\sum_{\ell=1,2,3} |X_d^\ell|^2}{|X_0(x_t)|^2} r_d, \quad r_d = \frac{|V_{td}|^2}{|V_{td}|_{\text{SM}}^2}, \quad (4.38)$$

$$\frac{\text{Br}(B \rightarrow X_d\nu\bar{\nu})}{\text{Br}(B \rightarrow X_s\nu\bar{\nu})} = \frac{\sum_{\ell=1,2,3} |X_d^\ell|^2}{\sum_{\ell=1,2,3} |X_s^\ell|^2} \left| \frac{V_{td}}{V_{ts}} \right|^2. \quad (4.39)$$

As seen explicitly, the branching ratios are defined to include all three light neutrinos in the final state. The index SM3 reminds us that the extracted $|V_{td}|$ and $|V_{ts}|$ in the presence of 4G quarks can differ from those in the SM. We note also that for $X_d^\ell \neq X_s^\ell$, the relation of the last ratio to $|V_{td}/V_{ts}|$ is modified with respect to MFV models. In the absence of right-handed current contributions in the SM4, the formula for the ratio in (4.37) applies also to the branching ratios for $B \rightarrow K^*\nu\bar{\nu}$ and $B \rightarrow K\nu\bar{\nu}$ as well as to various distributions discussed in [74, 75]. Therefore we will not present them here.

4.7 $K^+ \rightarrow \pi^+\nu\bar{\nu}$ and $K_L \rightarrow \pi^0\nu\bar{\nu}$

The SM3 expressions for the specific light neutrino mass eigenstate can be easily generalised to the SM4 with the result

$$\text{Br}(K^+ \rightarrow \pi^+\nu_\ell\bar{\nu}_\ell) = \frac{\kappa_+}{3} \left[\left(\frac{\text{Im}(\lambda_t^{(K)} X_K^\ell)}{|V_{us}|^5} \right)^2 + \left(\frac{\text{Re}\lambda_c^{(K)}}{|V_{us}|} P_c^\ell(X) + \frac{\text{Re}(\lambda_t^{(K)} X_K^\ell)}{|V_{us}|^5} \right)^2 \right], \quad (4.40)$$

$$\text{Br}(K_L \rightarrow \pi^0\nu_\ell\bar{\nu}_\ell) = \frac{\kappa_L}{3} \left(\frac{\text{Im}(\lambda_t^{(K)} X_K^\ell)}{|V_{us}|^5} \right)^2. \quad (4.41)$$

Summing over three light neutrinos in the final state we simply have

$$\text{Br}(K^+ \rightarrow \pi^+ \nu \bar{\nu}) = \sum_{\ell=1,2,3} \text{Br}(K^+ \rightarrow \pi^+ \nu_\ell \bar{\nu}_\ell), \quad (4.42)$$

$$\text{Br}(K_L \rightarrow \pi^0 \nu \bar{\nu}) = \sum_{\ell=1,2,3} \text{Br}(K_L \rightarrow \pi^0 \nu_\ell \bar{\nu}_\ell). \quad (4.43)$$

In the case of small mixing of light leptons with heavy leptons, there is no ℓ -dependence and the factors "3" in the denominator in (4.40) and (4.41) drop out.

In the presence of substantial mixing with the 4G leptons, also the charm contribution will be affected by this mixing. The inclusion of this effect would require the reconsideration of QCD corrections and electroweak corrections in the charm sector. As the charm contribution is subleading, we do not think that this is required before the discovery of a 4G. Therefore we will simply set

$$P_c^\ell(X) = P_c(X) = 0.42 \pm 0.03, \quad (4.44)$$

with $P_c(X)$ calculated in the SM3 and including the NNLO QCD corrections [78], electroweak corrections [79] and LD contributions [80]. In reducing the parametric uncertainties in $P_c(X)$, the improved value of the charm quark mass $m_c(m_c)$ [62, 81, 82] played an important role.

Next, the determination of the relevant hadronic matrix elements from tree-level leading K decays, for $\lambda = 0.226$, gives [83]

$$\kappa_+ = (5.36 \pm 0.026) \cdot 10^{-11}, \quad \kappa_L = (2.31 \pm 0.01) \cdot 10^{-10}. \quad (4.45)$$

The most recent predictions in the SM3 read [78, 79]

$$\text{Br}(K^+ \rightarrow \pi^+ \nu \bar{\nu})_{\text{SM}} = (8.5 \pm 0.7) \cdot 10^{-11}, \quad \text{Br}(K_L \rightarrow \pi^0 \nu \bar{\nu})_{\text{SM}} = (2.8 \pm 0.6) \cdot 10^{-11}, \quad (4.46)$$

where the errors are dominated by parametrical uncertainties, in particular by the CKM parameters. The corresponding experimental data read [84, 85]

$$\text{Br}(K^+ \rightarrow \pi^+ \nu \bar{\nu}) = (17.3_{-10.5}^{+11.5}) \cdot 10^{-11}, \quad \text{Br}(K_L \rightarrow \pi^0 \nu \bar{\nu}) \leq 6.7 \cdot 10^{-8}. \quad (4.47)$$

The experimental upper bound on $\text{Br}(K_L \rightarrow \pi^0 \nu \bar{\nu})$ is still by more than three orders of magnitude above the SM3 value, but the present upper bound from E391a at KEK should be significantly improved in the coming decade. We will see in Section 7 that in the SM4 both branching ratios can be spectacularly enhanced over the SM3 expectations.

4.8 The $B \rightarrow X_s \gamma$ Decay

One of the most popular decays, used to constrain NP contributions, is the $B \rightarrow X_s \gamma$ decay, for which the measured branching ratio [66]

$$\text{Br}(B \rightarrow X_s \gamma)_{\text{exp}} = (3.52 \pm 0.30) \cdot 10^{-4} \quad (4.48)$$

agrees well with the NNLO prediction in the SM3 [86],

$$\text{Br}(B \rightarrow X_s \gamma)_{\text{SM}} = (3.15 \pm 0.23) \cdot 10^{-4}. \quad (4.49)$$

The effective Hamiltonian, relevant for this decay within the SM3, is given as follows,

$$\mathcal{H}_{\text{eff}}^{\text{SM}}(\bar{b} \rightarrow \bar{s} \gamma) = -\frac{G_F}{\sqrt{2}} \lambda_t^{(s)} \left[\sum_{i=1}^6 C_i(\mu_b) Q_i + C_{7\gamma}(\mu_b) Q_{7\gamma} + C_{8G}(\mu_b) Q_{8G} \right], \quad (4.50)$$

where Q_i are four-quark operators, $Q_{7\gamma}$ is the magnetic photon penguin operator and Q_{8G} the magnetic gluon penguin operator, contributing to $\bar{b} \rightarrow \bar{s} \gamma$ transitions. The explicit expression for the branching ratio $\text{Br}(B \rightarrow X_s \gamma)$, resulting from (4.50), is very complicated and we will not be presented here (see [86] and references therein).

For our purposes, it is sufficient to know that in the LO approximation, the Wilson coefficients $C_{7\gamma}$ and C_{8G} at the renormalisation scale $\mu_W = \mathcal{O}(M_W)$ are given as follows,

$$C_{7\gamma}^{(0)}(\mu_W) = -\frac{1}{2} D'_s, \quad C_{8G}^{(0)}(\mu_W) = -\frac{1}{2} E'_s, \quad (4.51)$$

with the explicit expressions for D'_s and E'_s given in Subsection 4.2.

In view of the importance of QCD corrections in this decay, we will make sure that in the limit of neglecting 4G contributions, we reproduce the NNLO result in the SM3 given in (4.49). To this end, we will use the known LO expressions for the relevant Wilson coefficients evaluated at an appropriately chosen renormalisation scale, μ_{eff} , which turns out to equal 3.22 GeV. The fact that this scale is somewhat lower than the bottom-quark mass, expresses the important role of QCD corrections, leading to an enhancement of the branching ratio. The 4G effects will then be included through the modification of the SM3 Wilson coefficients at $\mu = M_W$ without the inclusion of additional QCD corrections. As the dominant QCD corrections to $\text{Br}(B \rightarrow X_s \gamma)$ come anyway from the renormalisation group evolution from M_W down to μ_{eff} , and from the matrix elements of the operators Q_2 and $Q_{7\gamma}$ at μ_{eff} , these dominant corrections are common to the SM3 and the SM4. While not exact, this treatment of QCD corrections in the SM4 should be sufficient for our purposes.

Thus, in this approximate treatment, the SM4 formulae for $B \rightarrow X_s \gamma$ are obtained by making the following replacements in the master functions,

$$\lambda_t^{(s)} D'_0(x_t) \rightarrow \lambda_t^{(s)} D'_s, \quad \lambda_t^{(s)} E'_0(x_t) \rightarrow \lambda_t^{(s)} E'_s \quad (4.52)$$

and choosing $\mu_{\text{eff}} = 3.22 \text{ GeV}$. The Wilson coefficients $C_{7\gamma}(\mu_{\text{eff}})$ and $C_{8G}(\mu_{\text{eff}})$ are given in the SM4 as follows:

$$C_{7\gamma}(\mu_{\text{eff}}) = -(0.208 + 0.305D'_s + 0.052E'_s), \quad C_{8G}(\mu_{\text{eff}}) = -(0.095 + 0.325E'_s). \quad (4.53)$$

Consequently, the ratio of SM4 to SM3 branching ratios is given within our approximations by

$$\frac{\text{Br}(B \rightarrow X_s \gamma)}{\text{Br}(B \rightarrow X_s \gamma)_{\text{SM}}} = r_{bs\gamma}^2 \left| \frac{0.208 + 0.305D'_s + 0.052E'_s}{0.208 + 0.305D'_0(x_t) + 0.052E'_0(x_t)} \right|^2, \quad (4.54)$$

with $r_{bs\gamma}$ defined as

$$r_{bs\gamma} = \left(\frac{|V_{ts}^* V_{tb}|}{|V_{cb}|} \right) / \left(\frac{|V_{ts}^* V_{tb}|}{|V_{cb}|} \right)_{\text{SM}}. \quad (4.55)$$

4.9 Direct CP Violation in $B \rightarrow X_s \gamma$ and $S_{\phi K_S}$

4.9.1 Preliminaries

Of particular interest is the direct CP asymmetry $A_{\text{CP}}^{bs\gamma}$ [87–89] that, similar to $S_{\psi\phi}$, is predicted to be tiny (-0.5%) in the SM3 but could be much larger in some of its extensions, as analysed recently in detail in the context of the flavour-blind MSSM (FB-MSSM) [90] and supersymmetric flavour models [36]. In particular in the supersymmetric flavour models with exclusively left-handed currents, and also in the FBMSSM where these currents dominate, this asymmetry can be by one order of magnitude larger than in the SM3. This is in contrast to models with right-handed currents, where the $A_{\text{CP}}^{bs\gamma}$ asymmetry remains SM3-like [36].

As pointed out in [36, 90], it is interesting to consider the direct CP asymmetry in question together with the theoretically clean asymmetry $S_{\phi K_S}$ that is found to be significantly smaller than the expected value of approximately 0.70 [91–93]:

$$S_{\phi K_S} = 0.44 \pm 0.17, \quad S_{\eta' K_S} = 0.59 \pm 0.07, \quad (4.56)$$

while $S_{\eta' K_S}$ is fully consistent with the expectations although on the low side.

In supersymmetric models with exclusively left-handed currents and in the FBMSSM, the desire to explain the $S_{\phi K_S}$ anomaly automatically implies that $A_{\text{CP}}^{bs\gamma}$ is much larger in magnitude than its SM3 value [36, 90] and has opposite sign. Therefore, it is of interest to investigate whether in the SM4 the two CP asymmetries are large and correlated.

4.9.2 $A_{\text{CP}}^{bs\gamma}$ in the SM4

If NP effects dominate over the tiny SM3 contribution $A_{\text{CP}}^{\text{SM}}(b \rightarrow s\gamma) \simeq -0.5\%$, the following expression for $A_{\text{CP}}(b \rightarrow s\gamma)$ holds [88, 89],

$$\begin{aligned} A_{\text{CP}}(b \rightarrow s\gamma) &\equiv \frac{\Gamma(B \rightarrow X_{\bar{s}}\gamma) - \Gamma(\bar{B} \rightarrow X_s\gamma)}{\Gamma(B \rightarrow X_{\bar{s}}\gamma) + \Gamma(\bar{B} \rightarrow X_s\gamma)} \simeq \\ &\simeq -\frac{1}{|C_{7\gamma}|^2} (1.23 \text{ Im}[C_2 C_{7\gamma}] - 9.52 \text{ Im}[C_{8G}^* C_{7\gamma}] + 0.10 \text{ Im}[C_2 C_{8G}]) - 0.5 \quad (\text{in } \%), \end{aligned} \quad (4.57)$$

where we assumed a cut for the photon energy at $E_\gamma \simeq 1.8 \text{ GeV}$ (see [88, 89] for details). In (4.57), the Wilson coefficients C_i are evaluated at the scale μ_{eff} as given in (4.53). The Wilson coefficient C_2 is to a very good approximation independent of the 4G parameters and given by $C_2 \approx 1.14$. This treatment of QCD corrections is certainly an approximation and a full NNLO analysis would be much more involved. Yet, at present a NNLO analysis would clearly be premature.

We would like to note that our Wilson coefficients C_i correspond to the $\bar{b} \rightarrow \bar{s}$ transition and not to $b \rightarrow s$ used in [36, 88–90]. Consequently they are complex conjugates of the ones used in the latter papers. This explains the different placing of “*” in (4.57) relative to these papers.

4.9.3 Time-Dependent CP Asymmetries in $B_d \rightarrow \phi(\eta') K_S$

The time-dependent CP asymmetries in the decays of neutral B mesons into final CP eigenstates f can be written as

$$\mathcal{A}_f(t) = S_f \sin(\Delta M t) - C_f \cos(\Delta M t). \quad (4.58)$$

Our presentation follows closely [94]. Within the SM, it is predicted with good accuracy that the $|S_f|$ and C_f parameters are universal for all the transitions $\bar{b} \rightarrow \bar{q}' q' \bar{s}$ ($q' = c, s, d, u$). In particular, the SM3 predicts that $-\eta_f S_f \simeq \sin 2\beta$ and $C_f \simeq 0$ where $\eta_f = \pm 1$ is the CP eigenvalue of the final state f . NP effects can contribute to³

- (i) the B_d mixing amplitude [95],
- (ii) the decay amplitudes $\bar{b} \rightarrow \bar{q} q \bar{s}$ ($q = s, d, u$) [95–97].

³We assume that the asymmetry in the tree-level transition $\bar{b} \rightarrow \bar{c} c \bar{s}$ is not significantly affected by NP.

In case (i), the NP contribution shifts all S_f asymmetries away from $\sin 2\beta$ in a universal way, while the C_f asymmetries will still vanish. In case (ii), the various S_f and also the C_f asymmetries are, in general, different from their values in the SM3.

The CP asymmetries S_f and C_f in $B_d \rightarrow f$ decays are calculated as follows. One defines a complex quantity λ_f ,

$$\lambda_f = e^{-2i\varphi_{B_d}^{\text{tot}}}(\bar{A}_f/A_f), \quad (4.59)$$

where $\varphi_{B_d}^{\text{tot}}$ is the phase of the B_d -mixing amplitude, M_{12}^d , and A_f (\bar{A}_f) is the decay amplitude for $B_d(\bar{B}_d) \rightarrow f$. A_f and \bar{A}_f can be calculated from the effective Hamiltonian relevant for $\Delta B = 1$ decays [54] in the following way

$$A_f = \langle f | \mathcal{H}_{\text{eff}} | B_d \rangle, \quad \bar{A}_f = \langle f | \mathcal{H}_{\text{eff}} | \bar{B}_d \rangle, \quad (4.60)$$

where the Wilson coefficients of the effective Hamiltonian depend on the electroweak theory while the matrix elements $\langle f | O_i | B_d(\bar{B}_d) \rangle$ can be estimated, for instance, by means of QCD factorisation [94]. We then have

$$S_f = \frac{2\text{Im}(\lambda_f)}{1 + |\lambda_f|^2}, \quad C_f = \frac{1 - |\lambda_f|^2}{1 + |\lambda_f|^2}. \quad (4.61)$$

The SM3 contribution to the decay amplitudes, related to $\bar{b} \rightarrow \bar{q}' q' \bar{s}$ transitions, can always be written as a sum of two terms, $A_f^{\text{SM}} = A_f^c + A_f^u$, with $A_f^c \propto V_{cb}^* V_{cs}$ and $A_f^u \propto V_{ub}^* V_{us}$. Defining the ratio $a_f^u \equiv e^{-i\gamma}(A_f^u/A_f^c)$, we have

$$A_f^{\text{SM}} = A_f^c (1 + a_f^u e^{i\gamma}), \quad (4.62)$$

where the a_f^u parameters have been evaluated in the QCD factorisation approach⁴ [91, 94, 99]. Within the SM3, it turns out that $S_{\phi K_S} \simeq S_{\eta' K_S} \simeq S_{\psi K_S} \simeq \sin 2\beta$, with precise predictions given in Tables 1 and 6 of [36]. The term a_f^u provides only a negligible contribution to $B_d \rightarrow \psi K_S$, thus $\lambda_{\psi K_S}^{\text{SM3}} = -e^{-2i\beta}$. Also for charmless modes, the effects induced by a_f^u are small (at the percent level), being proportional to $|(V_{ub} V_{us}^*)/(V_{cb} V_{cs}^*)|$.

In the SM4, for simplicity, we follow the analysis in [94] which only takes into account the leading-order terms in α_s and neglects Λ/m_b corrections (except for so-called chirally enhanced terms). The modification of A_f in (4.62) due to 4G contributions can then be written as

$$A_f = A_f^c \left[1 + a_f^u e^{i\gamma} + \sum_i (b_{fi}^c + b_{fi}^u e^{i\gamma}) C_i^{\text{NP}}(M_W) \right], \quad (4.63)$$

⁴A critical discussion of the importance of power corrections and the potential size of long-distance final-state interactions in (4.62) can be found in [98]. As long as a model-independent prediction for these effects is lacking, we have to assign an irreducible theoretical error to the predictions for the a_f^u .

f	ϕK_s	$\eta' K_s$
b_{f3}^c	-46	-26
b_{f7}^c	22	3.8
b_{f9}^c	23	3.5
b_{f8G}^c	1.4	0.86

Table 2: Hadronic parameters at $\mu = m_b$ taken from [94]. The parameters b_{fi}^u can be obtained via $b_{fi}^u = (|V_{ub}V_{us}^*|/|V_{cb}V_{cs}^*|)b_{fi}^c$.

where $C_i^{\text{NP}}(M_W)$ are the NP contributions to the Wilson coefficients evaluated at the scale M_W . Defining the NP contributions to the master functions F_i given in (4.8)-(4.10) by ΔF_i with

$$F_i = F_0^{\text{SM}} + \Delta F_i, \quad (4.64)$$

the non-vanishing $C_i^{\text{NP}}(M_W)$ relevant for $\bar{b} \rightarrow \bar{s}$ transitions are given as follows:

$$C_3^{\text{NP}}(M_W) = \frac{\alpha}{6\pi} \frac{1}{\sin^2 \theta_W} (2\Delta Y_s - \Delta X_s), \quad (4.65)$$

$$C_7^{\text{NP}}(M_W) = \frac{\alpha}{6\pi} 4\Delta Z_s, \quad (4.66)$$

$$C_9^{\text{NP}}(M_W) = \frac{\alpha}{6\pi} \left[4\Delta Z_s - \frac{2}{\sin^2 \theta_W} (\Delta X_s + \Delta Y_s) \right], \quad (4.67)$$

$$C_{7\gamma}^{\text{NP}}(M_W) = -\frac{1}{2} \Delta D'_s, \quad (4.68)$$

$$C_{8G}^{\text{NP}}(M_W) = -\frac{1}{2} \Delta E'_s. \quad (4.69)$$

Here $\alpha = \alpha(M_W) = 1/127.9$ is the QED coupling constant and $\sin^2 \theta_W = 0.231$. The parameters b_{fi}^u and b_{fi}^c calculated in [94] are collected for the ϕK_S and $\eta' K_S$ channels in Table 2. As the effects in $B \rightarrow X_s \gamma$ are small, we follow [94] and neglect $C_{7\gamma}$.

The absence of complex conjugation on Wilson coefficients C_i in (4.63) as opposed to [36, 90] reflects the fact that our coefficients correspond to the $\bar{b} \rightarrow \bar{s}$ transition and not to $b \rightarrow s$ used in the latter papers.

We note that within a very good approximation

$$A_f \approx A_f^c \left[1 + \sum_i b_{fi}^c C_i^{\text{NP}}(M_W) \right] = A_f^c \left[1 + r_f \frac{\lambda_{t'}^{(s)}}{\lambda_t^{(s)}} \right], \quad (4.70)$$

where

$$r_{\phi K_S} = -0.248 Y_0(x_{t'}) + 0.004 X_0(x_{t'}) + 0.075 Z_0(x_{t'}) - 0.7 E'_0(x_{t'}), \quad (4.71)$$

$$r_{\eta' K_S} = -0.106 Y_0(x_{t'}) + 0.034 X_0(x_{t'}) + 0.012 Z_0(x_{t'}) - 0.43 E'_0(x_{t'}). \quad (4.72)$$

Thus, the departure of $S_{\phi K_S}$ and $S_{\eta' K_S}$ from $S_{\psi K_S}$ is governed by the common phase of $\lambda_{t'}^{(s)}/\lambda_t^{(s)}$ with the effect being larger in the case of $S_{\phi K_S}$. Denoting the final phase of A_f by φ_f , we find

$$S_f = -\eta_f \sin(2(\varphi_{B_d}^{\text{tot}} + \varphi_f)), \quad (4.73)$$

where η_f is the CP parity of the final state: $\eta_f = -1$ for both channels considered here. For $\varphi_f \neq 0$ the departure from $S_{\psi K_S}$ in (4.22) can be obtained.

It is known that going beyond leading order in the calculations of the b_f parameters, one would introduce a potentially sizable strong phase. We comment on this issue in Section 7.3.

4.10 $B \rightarrow X_s \ell^+ \ell^-$

No spectacular 4G effects are present in this decay, therefore we will only make sure that our numerical analysis is in accordance with the existing data on these decays. Basically, what one has to do is to replace in the known SM3 expressions for the branching ratios and the forward-backward asymmetry the SM3 master functions F_0 by the SM4 master functions of Section 4.2. In this context Section 5.5 of [100] illustrates explicitly this replacement, but the formulae are complicated and will not be repeated here. Alternatively, all the formulae can be found in [101]. The NNLO treatment can be found, for instance, in [102–105]. The functions that enter this analysis are Y_s , Z_s , E_s , E' and D' . Of particular interest is the forward-backward asymmetry in $b \rightarrow s\mu^+\mu^-$, in the inclusive and exclusive measurement, see also [100, 106–108].

The HFAG [66] group gives for $M(\ell^+\ell^-) > 0.2 \text{ GeV}$

$$\text{Br}(B \rightarrow X_s \ell^+ \ell^-) = 3.66_{-0.77}^{+0.76} \cdot 10^{-6}. \quad (4.74)$$

Due to the presence of resonances there is no rigorous theoretical prediction for the whole q^2 range. Instead, theory and experiment are compared for a high q^2 cut, $q^2 > 14.4 \text{ GeV}^2$, and a low q^2 range, $1 \text{ GeV}^2 < q^2 < 6 \text{ GeV}^2$. The BaBar [109] and Belle [110] collaboration published the following results for both ranges:

$$\text{Br}(B \rightarrow X_s \ell^+ \ell^-)_{\text{low}} = \begin{cases} (1.493 \pm 0.504_{-0.321}^{+0.411}) \cdot 10^{-6} & \text{Belle} \\ (1.8 \pm 0.7 \pm 0.5) \cdot 10^{-6} & \text{BaBar} \\ (1.6 \pm 0.5) \cdot 10^{-6} & \text{Average} \end{cases} \quad (4.75)$$

$$\text{Br}(B \rightarrow X_s \ell^+ \ell^-)_{q^2 > 14.4 \text{ GeV}^2} = \begin{cases} (0.418 \pm 0.117_{-0.068}^{+0.061}) \cdot 10^{-6} & \text{Belle} \\ (0.5 \pm 0.25_{-0.07}^{+0.08}) \cdot 10^{-6} & \text{BaBar} \\ (0.44 \pm 0.12) \cdot 10^{-6} & \text{Average} \end{cases} \quad (4.76)$$

We will use the averaged measurement for our numerical analysis. The NNLO prediction for the zero \hat{s}_0 of the forward-backward asymmetry A_{FB} in the SM3 is [103]

$$\hat{s}_0 = 0.162 \pm 0.008. \quad (4.77)$$

Note that according to [103], the NNLO contributions to $B \rightarrow X_s \ell^+ \ell^-$ are sizable and *negative*. To accommodate the NNLO effects we matched our NLO result to the NNLO result given in [103] for the low and high q^2 ranges independently.

4.11 $K_L \rightarrow \pi^0 \ell^+ \ell^-$

The rare decays $K_L \rightarrow \pi^0 e^+ e^-$ and $K_L \rightarrow \pi^0 \mu^+ \mu^-$ are dominated by CP-violating contributions. In the SM3, the main contribution comes from the indirect (mixing-induced) CP violation and its interference with the direct CP-violating contribution [111–114]. The direct CP-violating contribution to the branching ratio is in the ballpark of $4 \cdot 10^{-12}$, while the CP-conserving contribution is at most $3 \cdot 10^{-12}$. Among the rare K meson decays, the decays in question belong to the theoretically cleanest, but certainly cannot compete with $K \rightarrow \pi \nu \bar{\nu}$ decays. Moreover, the dominant indirect CP-violating contributions are practically determined by the measured decays $K_S \rightarrow \pi^0 \ell^+ \ell^-$ and the parameter ε_K . Consequently, the decays $K_L \rightarrow \pi^0 \ell^+ \ell^-$ are not as sensitive as the $K_L \rightarrow \pi^0 \nu \bar{\nu}$ decay to new physics contributions, present only in the subleading direct CP violation. However, as pointed out in [100], in the presence of large new CP-violating phases, the direct CP-violating contribution can become the dominant one, and the branching ratios for $K_L \rightarrow \pi^0 \ell^+ \ell^-$ can be significantly enhanced, with a stronger effect in the case of $K_L \rightarrow \pi^0 \mu^+ \mu^-$ [113, 114]. Most recent discussions can be found in [115, 116].

Adapting the formulae in [112–115] with the help of [100] to the SM4, we find

$$\text{Br}(K_L \rightarrow \pi^0 \ell^+ \ell^-) = (C_{\text{dir}}^\ell \pm C_{\text{int}}^\ell |a_s| + C_{\text{mix}}^\ell |a_s|^2 + C_{\text{CPC}}^\ell) \cdot 10^{-12}, \quad (4.78)$$

where

$$C_{\text{dir}}^e = (4.62 \pm 0.24)(\omega_{7V}^2 + \omega_{7A}^2), \quad C_{\text{dir}}^\mu = (1.09 \pm 0.05)(\omega_{7V}^2 + 2.32\omega_{7A}^2), \quad (4.79)$$

$$C_{\text{int}}^e = (11.3 \pm 0.3)\omega_{7V}, \quad C_{\text{int}}^\mu = (2.63 \pm 0.06)\omega_{7V}, \quad (4.80)$$

$$C_{\text{mix}}^e = 14.5 \pm 0.05, \quad C_{\text{mix}}^\mu = 3.36 \pm 0.20, \quad (4.81)$$

$$C_{\text{CPC}}^e \simeq 0, \quad C_{\text{CPC}}^\mu = 5.2 \pm 1.6, \quad (4.82)$$

$$|a_s| = 1.2 \pm 0.2 \quad (4.83)$$

with

$$\omega_{7V} = \frac{1}{2\pi} \left[P_0 + \frac{|Y_K|}{\sin^2 \theta_W} \frac{\sin \beta_Y^K}{\sin(\bar{\beta} - \bar{\beta}_s)} - 4|Z_K| \frac{\sin \beta_Z^K}{\sin(\bar{\beta} - \bar{\beta}_s)} \right] \left[\frac{\text{Im } \lambda_t^{(K)}}{1.4 \cdot 10^{-4}} \right], \quad (4.84)$$

$$\omega_{7A} = -\frac{1}{2\pi} \frac{|Y_K|}{\sin^2 \theta_W} \frac{\sin \beta_Y^K}{\sin(\bar{\beta} - \bar{\beta}_s)} \left[\frac{\text{Im } \lambda_t^{(K)}}{1.4 \cdot 10^{-4}} \right]. \quad (4.85)$$

Here $P_0 = 2.88 \pm 0.06$ [117] includes NLO QCD corrections and

$$\beta_Y^K = \bar{\beta} - \bar{\beta}_s - \theta_Y^K, \quad \beta_Z^K = \bar{\beta} - \bar{\beta}_s - \theta_Z^K \quad (4.86)$$

with Y_K and Z_K defined in (4.9) and (4.10). The phases $\bar{\beta}$ and $\bar{\beta}_s$ are defined in (4.24).

The effect of the new physics contributions is mainly felt in ω_{7A} , as the corresponding contributions in ω_{7V} cancel each other to a large extent.

The present experimental bounds [118, 119],

$$\text{Br}(K_L \rightarrow \pi^0 e^+ e^-) < 28 \cdot 10^{-11}, \quad \text{Br}(K_L \rightarrow \pi^0 \mu^+ \mu^-) < 38 \cdot 10^{-11}, \quad (4.87)$$

are still by one order of magnitude larger than the SM3 predictions, [115]

$$\text{Br}(K_L \rightarrow \pi^0 e^+ e^-)_{\text{SM}} = 3.54_{-0.85}^{+0.98} (1.56_{-0.49}^{+0.62}) \cdot 10^{-11}, \quad (4.88)$$

$$\text{Br}(K_L \rightarrow \pi^0 \mu^+ \mu^-)_{\text{SM}} = 1.41_{-0.26}^{+0.28} (0.95_{-0.21}^{+0.22}) \cdot 10^{-11}, \quad (4.89)$$

with the values in parentheses corresponding to the “−” sign in (4.78).

4.12 ε'/ε

An important observable is the ratio ε'/ε that measures the size of the direct CP violation in $K_L \rightarrow \pi\pi$ relative to the indirect CP violation described by ε_K . In the SM3 ε' is governed by QCD penguins but receives also an important destructively interfering contribution from electroweak penguins that is generally much more sensitive to NP than the QCD penguin contribution.

Now the electroweak penguin and box diagrams that enter the evaluation of the rare decay branching ratios, as $\text{Br}(K_L \rightarrow \pi^0 \nu \bar{\nu})$ and $\text{Br}(K^+ \rightarrow \pi^+ \nu \bar{\nu})$, have also a considerable impact on the electroweak component of ε'/ε so that in a given model specific correlations between ε'/ε and the branching ratios for rare K decays exist [120, 121]. Quite generally, the enhancement of rare decay branching ratios implies the suppression of ε'/ε although this correlation investigated first in [120, 121] contains some model dependence. Yet, as pointed out in [120] and analysed in more detail within the MSSM in [121], the enhancements of rare K decay branching ratios could be bounded in principle by ε'/ε . In fact, in [120] approximate bounds of $\text{Br}(K_L \rightarrow \pi^0 \nu \bar{\nu}) \lesssim 2 \cdot 10^{-10}$ and

$\text{Br}(K^+ \rightarrow \pi^+ \nu \bar{\nu}) \lesssim 2 \cdot 10^{-10}$ have been derived, where in the latter case the bound on $\text{Br}(K_L \rightarrow \mu^+ \mu^-)$ also played a role.

Unfortunately, the low precision on the relevant hadronic parameters B_6 and B_8 in the calculation of ε'/ε and the strong cancellation of QCD penguin and electroweak penguin contributions to this ratio, introduce significant uncertainties in the correlation in question.

It is hoped that lattice calculations will provide these elements in this decade [122].

Yet, the present experimental world average from NA48 [123] and KTeV [124, 125],

$$\varepsilon'/\varepsilon = (16.8 \pm 1.4) \cdot 10^{-4} , \quad (4.90)$$

could have an important impact on several extensions of the SM3 if B_6 and B_8 were known. An analysis of ε'/ε in the LHT model demonstrates this problem in explicit terms [126]. If one uses $B_6 = B_8 = 1$ as obtained in the large N approach [127], $(\varepsilon'/\varepsilon)_{\text{SM}}$ is in the ballpark of the experimental data, and sizable departures of $\text{Br}(K_L \rightarrow \pi^0 \nu \bar{\nu})$ from its SM3 value are not allowed. $K^+ \rightarrow \pi^+ \nu \bar{\nu}$, being CP conserving and consequently not as strongly correlated with ε'/ε as $K_L \rightarrow \pi^0 \nu \bar{\nu}$, could still be enhanced by 50%. On the other hand, if B_6 and B_8 are different from unity and $(\varepsilon'/\varepsilon)_{\text{SM}}$ disagrees with experiment, much more room for enhancements of rare K decay branching ratios through NP contributions is available. An analysis of ε'/ε in the context of the SM4 can be found in [13].

In the present paper, we will use the formulae given in Section 3 of [126] that are based on [128]. In order to use these formulae, one has to replace the complex master functions of the LHT model by the master functions of the SM4, relevant for the K system, that we have collected in Section 4.2. It is a good approximation to neglect the 4G effects on the flavour-conserving side of box diagrams contributing to X_K and Y_K , so that these functions together with Z_K are the same as in rare K decays considered above. E_K plays a subleading role in ε'/ε , but we include it in our numerical analysis which is presented in Section 7.

5 Constraints from Electroweak Precision Data

The electroweak precision observables (EPO), even if flavour conserving, have an impact on the allowed parameter space of the SM4. As the b' -quark does not enter our analysis of FCNC processes, we are first of all interested in the range of $m_{t'}$. From direct searches at the Tevatron, it follows that $m_{t'} > 256 \text{ GeV}$. Taking into account the EPO study in [5], together with the upper limit from perturbativity, a plausible range for $m_{t'}$ is given by

$$300 \text{ GeV} \leq m_{t'} \leq 600 \text{ GeV} . \quad (5.1)$$

Equally important are electroweak constraints on s_{34} [4, 6], as this mixing angle plays an important role in FCNC analyses [13–15, 26, 27].

As emphasised recently by Chanowitz [6], in the presence of $s_{34} \neq 0$, there are two non-decoupling radiative corrections to the EPO with quadratic sensitivity to $m_{t'}$: the T -parameter and $Zb\bar{b}$ vertex corrections. They are both proportional to $|V_{t'b}|^2 m_{t'}^2$, and in the case of the T -parameter there are also large corrections proportional to $|V_{tb'}|^2 m_{b'}^2$ if $m_{b'}^2 \gg m_t^2$. As seen in (2.29–2.32), for all relevant cases we have $|V_{t'b}| \approx |V_{tb'}| \approx s_{34}$. The results of a detailed analysis of Chanowitz can be summarised by an approximate upper bound on $|s_{34}|$ as a function of $m_{t'}$:

$$|s_{34}| \leq \frac{M_W}{m_{t'}}. \quad (5.2)$$

Together with the lower limit on $m_{t'}$, this leads to a more stringent upper bound on s_{34}

$$s_{34} \leq 0.27. \quad (5.3)$$

This bound eliminates examples of large s_{34} studied in [26, 27] and also has some impact on the FCNC analyses in [13–15]. Still, even for $m_{t'} \simeq 400 \text{ GeV}$, s_{34} can be as large as s_{12} , and in the full range of $m_{t'}$ considered by us it can be larger than $|V_{cb}| \simeq 0.04$, although smaller values are certainly allowed. We will incorporate (5.1) and (5.2) into our numerical analysis in Section 7.

6 Strategy for the Phenomenological Analysis

6.1 Part I: Global Analysis

In the first part of our numerical analysis, we will use the values for input parameters collected in Table 3. The values of non-perturbative parameters used in our analysis are taken from the unquenched lattice calculations summarised recently in [62]. They are compatible within the errors with the collection of Lubicz and Tarantino [129]. The references connected with other parameters are given in this table. The ranges used for the parameters $m_{t'}$ and s_{34} can be found in (5.1) and (5.2), respectively.

This analysis will give us the information on the presently allowed ranges for the NP parameters and the corresponding maximal departures from SM3 expectations for various observables that are consistent with the data on FCNC processes, EWPT and the unitarity of V_{SM4} . This will also give us a grand view of the patterns of flavour violation in the SM4, in particular about correlations between various observables that are less sensitive to the particular values of the parameters involved.

6.2 Part II: Anatomy

The goal of this part will be a detailed analysis of certain features of the SM4 that cannot be easily seen in a global analysis at present. This analysis consists of the following steps that we will outline in what follows.

Step 1: We will investigate how the SM4 addresses the present tensions in the unitarity triangle, in particular the tension between the values of $S_{\psi K_S}$ and $|\varepsilon_K|$ within the SM3. To this end, we will use the input parameters of Table 3, except that for $|V_{ub}|$ and δ_{13} , that are still not known with an accuracy better than 10% from tree level decays, we will choose three scenarios in which $|V_{ub}|$ and δ_{13} will take specific values with errors of 2 – 3%. In Table 7, we give three scenarios for $|V_{ub}|$ and δ_{13} , whose origin will be explained in Section 8.

Step 2: We will investigate how the future measurements of various branching ratios and CP asymmetries will have an impact on our analysis. The branching ratios for $B_s \rightarrow \mu^+ \mu^-$, $K^+ \rightarrow \pi^+ \nu \bar{\nu}$ and $K_L \rightarrow \pi^0 \nu \bar{\nu}$ and the CP asymmetry $S_{\psi\phi}$ will play important roles in this study, and various scenarios for future measurements of these observables will be analysed in Section 8.

6.3 Part III: Determination of the V_{SM4} matrix

In this part, we will outline and illustrate with examples how the new parameters of the SM4 can in principle be determined by using future data on FCNC processes. In this context, we pay particular attention to the different possible scenarios for the scaling of the 4G mixing angles. For each case, we will identify more or less pronounced correlations between the new CP-violating phases in the SM4 that allow us to define certain equivalence classes, which can clearly be distinguished by their predictions for rare decay flavour observables.

7 Global Numerical Analysis

7.1 Preliminaries

For our numerical analysis, we construct a large number of random points in parameter space that are evenly distributed in all the mixing angles and phases. We keep only those points that satisfy all tree level CKM constraints at 2σ (it is not possible to bring $|V_{cs}| = 1.04 \pm 0.06$ within 1σ of its central value) and the experimental constraints on

parameter	value	parameter	value
\hat{B}_K	0.725 ± 0.026 [62]	$ V_{ud} $	0.97418 ± 0.00027 [95]
F_{B_d}	(192.8 ± 9.9) MeV [62]	$ V_{us} $	0.2255 ± 0.0019 [95]
F_{B_s}	(238.8 ± 9.5) MeV [62]	$ V_{ub} $	$(3.93 \pm 0.36) \times 10^{-3}$ [95]
F_K	(155.8 ± 1.7) MeV [62]	$ V_{tb} $	$0.91 \pm 0.11 \pm 0.07$ [130]
\hat{B}_{B_d}	1.26 ± 0.11 [62]	$ V_{tb} $	> 0.71 at 95%CL [130]
\hat{B}_{B_s}	1.33 ± 0.06 [62]	$ V_{cd} $	0.230 ± 0.011 [95]
$\sqrt{\hat{B}_{B_d}} F_{B_d}$	(216 ± 15) MeV [62]	$ V_{cs} $	1.04 ± 0.06 [95]
$\sqrt{\hat{B}_{B_s}} F_{B_s}$	(275 ± 13) MeV [62]	$ V_{cb} $	$(41.2 \pm 1.1) \times 10^{-3}$ [95]
ξ	1.243 ± 0.028 [62]	κ_ε	0.92 ± 0.02 [61]
η_{cc}	1.51 ± 0.24 [131]	$ \varepsilon_K $	$(2.229 \pm 0.012) \cdot 10^{-3}$
η_{tt}	0.5765 ± 0.0065 [132]	$S_{\psi K_S}$	0.672 ± 0.024
η_{ct}	0.47 ± 0.04 [133]	$\tau(B_d)$	(1.525 ± 0.009) ps
η_B	0.551 ± 0.007 [132, 134]	$\tau(B_s)$	(1.425 ± 0.041) ps
$m_c(m_c)$	(1.268 ± 0.009) GeV [62, 82]	ΔM_d	(0.507 ± 0.005) ps $^{-1}$ [93]
$m_t(m_t)$	(163.5 ± 1.7) GeV [135]	ΔM_s	(17.77 ± 0.12) ps $^{-1}$ [93]

Table 3: Values of the input parameters used in our analysis.

the $\Delta F = 2$ observables,

$$\varepsilon_K, \quad \Delta M_K, \quad \Delta M_q, \quad \Delta M_d/\Delta M_s, \quad (7.1)$$

as well as the CP asymmetry $S_{\psi K_S}$ within 1σ and $\cos \varphi_{B_d}^{\text{tot}} > 0$.

In order to compare our results to the experimental values, we calculate the propagated error from the corresponding hadronic parameters using Gaussian error propagation. We accept a point if it is at 1σ within its theoretical uncertainty compatible with the experimental value and its respective uncertainty.

One exception is the mass difference ΔM_K : ΔM_K is very precisely measured, but it is subject to LD contributions that – in spite of many efforts – are not well understood at present. Several analyses indicate that these contributions are positive and in the ballpark of 30% of the measured value [136–138]. This is supported by the fact that, in the SM3, the value of the SD box-diagram contributions ΔM_K^{SD} to ΔM_K amounts to only $(70 \pm 10)\%$ of the measured value. Still, there is significant room in ΔM_K for NP contributions, and we demand $0.7 \leq \Delta M_K^{\text{SD}}/\Delta M_K^{\text{exp}} \leq 1.3$. Note that the contributions from the 4G quarks to the SD part of ΔM_K can exceed +30%. In this context we note that the SM3 value of $|\varepsilon_K|$ also appears to be lower than the data [61]. However, in this case, LD contributions are estimated to be small [61, 63], and the cure of this anomaly

can only come either from NP, or from significant changes in the input parameters like $|V_{cb}|$ and $|V_{ub}|$.

In addition to the $\Delta F = 2$ observables, we impose the following constraints from $\Delta F = 1$ observables:

$$\text{Br}(B \rightarrow X_s \ell^+ \ell^-)_{\text{low.}-\text{int.}}, \quad \text{Br}(B \rightarrow X_s \gamma), \quad \text{Br}(K^+ \rightarrow \pi^+ \nu \bar{\nu}), \quad (7.2)$$

each at 4σ , not taking into account the theoretical errors. We note that a constraint comes also from the upper bound on $\text{Br}(K_L \rightarrow \mu^+ \mu^-)_{\text{SD}}$ in (4.34).

Since ΔM_K poses no stringent bound on S_K , and S_K is correlated with X_K , Y_K etc., we chose to impose the experimental exclusion limits on various Kaon decays. For consistency reasons, as well as to eliminate highly tuned points, we also constrain $B_{s,d} \rightarrow \mu^+ \mu^-$.

Obviously, the chance of a point to fulfil all constraints is much larger for small mixing angles than for larger ones. We therefore have not plotted all the points that we found for small mixing angles, but rather tried to give a comparable number of parameter points over the full allowed range of mixing angles. We would like to stress that (even without this procedure) the point density in our plots must not be understood as a probability density. The main information of the various correlation plots is contained in the *enveloping curve* for these points, without any preference for different points within this region.

In presenting the results of the global analysis, it will be useful to use a special colour coding, in order to emphasise some aspects of the anatomy presented in the next section and to stress certain points that we found in the process of our numerical analysis:

- The large black point represents the SM3.
- Light blue and dark blue points stand for the results of our global analysis of the SM4 with the following distinction: light blue stands for $\text{Br}(K_L \rightarrow \pi^0 \nu \bar{\nu}) > 2 \cdot 10^{-10}$ and dark blue for $\text{Br}(K_L \rightarrow \pi^0 \nu \bar{\nu}) \leq 2 \cdot 10^{-10}$. Note that the regions with light and dark blue points are not always exclusive but that the dark blue points are plotted above the light blue ones.
- The yellow, green and red colours represent the three scenarios for $S_{\psi\phi}$ and $\text{Br}(B_s \rightarrow \mu^+ \mu^-)$ that are shown in Table 4 and related to Step 2 of the anatomy.

7.2 Violation of Universality

Imposing the existing constraints from tree level determinations of the CKM matrix, electroweak precision observables and the existing data on the FCNC and CP-violating

	BS1 (yellow)	BS2 (green)	BS3 (red)
$S_{\psi\phi}$	0.04 ± 0.01	0.04 ± 0.01	≥ 0.4
$\text{Br}(B_s \rightarrow \mu^+ \mu^-)$	$(2 \pm 0.2) \cdot 10^{-9}$	$(3.2 \pm 0.2) \cdot 10^{-9}$	$\geq 6 \cdot 10^{-9}$

Table 4: Three scenarios for $S_{\psi\phi}$ and $\text{Br}(B_s \rightarrow \mu^+ \mu^-)$.

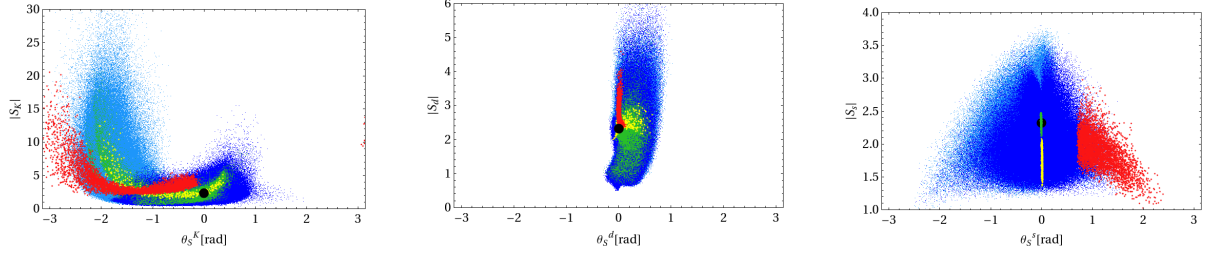


Figure 1: The arguments θ_S^i of the functions S_i plotted against the absolute values $|S_i|$ for $i = K$ (left panel), $i = d$ (centre panel) and $i = s$ (right panel).

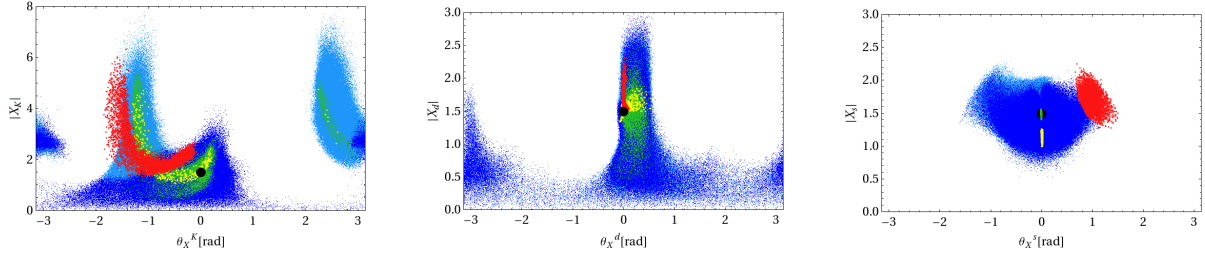


Figure 2: The arguments θ_X^i of the functions X_i plotted against the absolute values $|X_i|$ for $i = K$ (left panel), $i = d$ (centre panel) and $i = s$ (right panel).

observables, it is possible to significantly constrain the allowed ranges for the magnitudes and the phases of the master functions F_i introduced in Section 4. We recall that in the SM3, the master functions are real and independent of the meson system considered.

In Fig. 1 we show the allowed ranges in the planes $(\theta_S^i, |S_i|)$ for $i = K, d, s$. The flavour-universal SM3 value of $|S_i| = S_0(x_t)$ is indicated by a black dot. In Fig. 2, a similar analysis is done for the functions X_i . We observe that the flavour universality in question is significantly violated in a hierarchical manner:

- Concerning $|S_i|$, the largest effects are found for $|S_K|$, followed by $|S_d|$, and with the smallest effects found for $|S_s|$. This hierarchy is familiar from the LHT model and reflects the factor $1/\lambda_t^{(i)}$ in the definition of S_i with $|\lambda_t^{(K)}| \ll |\lambda_t^{(d)}| \leq |\lambda_t^{(s)}|$, as well as the fact that S_K is not as directly constrained through ε_K as S_d is through $S_{\psi K_s}$ and ΔM_d . In addition, as mentioned before, ΔM_K only poses a mild constraint.
- The departures of θ_S^i from zero are again largest in the K system. The strong

preference for $\theta_S^K < 0$ is related — as seen through (4.25) — to the ε_K -anomaly in the SM3 [61], whose solution favours $\varphi_K > \bar{\beta} - \bar{\beta}_s$.

- The phase θ_S^d is already rather constrained through $S_{\psi K_S}$, but a preference for $\theta_S^d > 0$ is clearly visible. This reflects the fact that for central values of $|V_{ub}|$, that are dominated by inclusive decays, the phase $\varphi_{B_d}^{\text{tot}}$ is required to be smaller than $\bar{\beta}$, in order to fit $S_{\psi K_S}$ (see (4.23)).
- θ_S^s is much less constrained than θ_S^d , as the CP violation in the B_s system is experimentally basically unknown. The $S_{\psi\phi}$ anomaly at Tevatron, corresponding to the red points in Fig. 1, requires $\theta_S^s > 0$, as explicitly seen in (4.23) and (4.22) [61, 139].
- Even for no effects in $S_{\psi\phi}$ and $Br(B_s \rightarrow \mu^+\mu^-)$ (green points) the SM4 still allows for large effects in the kaon system.

Similar hierarchies in the violation of universality are observed in the case of the functions X_i , with the effects in X_s being smallest, not only in the magnitude, but also in its phase.

7.3 $S_{\psi\phi}$ vs. $S_{\phi K_S}$ and $A_{\text{CP}}^{bs\gamma}$

As pointed out in [15], there is a strong correlation between the CP asymmetries $S_{\psi\phi}$ and $S_{\phi K_S}$ within the SM4. We show this correlation in the upper-left panel of Fig. 3. First of all, we observe that $S_{\psi\phi}$ can be as large as 0.8 although even larger values are possible. For $S_{\psi\phi} \approx 0.4$, the asymmetry $S_{\phi K_S}$ is strongly suppressed relative to $S_{\psi K_S}$ and in the ballpark of 0.4, close to its experimental central value represented by the horizontal dashed line. The analogous plot for $S_{\eta' K_S}$ is shown in the upper-right panel of Fig. 3. The suppression is now significantly weaker, and for $S_{\psi\phi} \approx 0.4$ one finds $S_{\eta' K_S} \approx 0.55$, in accordance with the data. The big black points represent the SM3 values of the asymmetries in question that are slightly above $S_{\psi K_S}$ [91–93].

Interestingly, for $S_{\psi\phi} \geq 0.6$ the values of $S_{\phi K_S}$ and $S_{\eta' K_S}$ predicted by the SM4 are below their central values indicated by data.

The correlation seen in the upper panels in Fig. 3 can easily be understood by noting that the ratio $\lambda_{t'}^{(s)}/\lambda_t^{(s)}$ and, in particular, its phase is responsible for departures of both, $S_{\psi\phi}$ and $S_{\phi K_S}$, from the SM3 predictions. A *positive* complex phase of this ratio implies the desired enhancement of $S_{\psi\phi}$ and, through (4.70) and (4.71), a *negative* phase $\varphi_{\phi K_S}$ of the decay amplitude $A_{\phi K_S}$. In turn, as seen in (4.73), $S_{\phi K_S}$ is suppressed relative to $S_{\psi K_S}$.

At this point some comments are in order

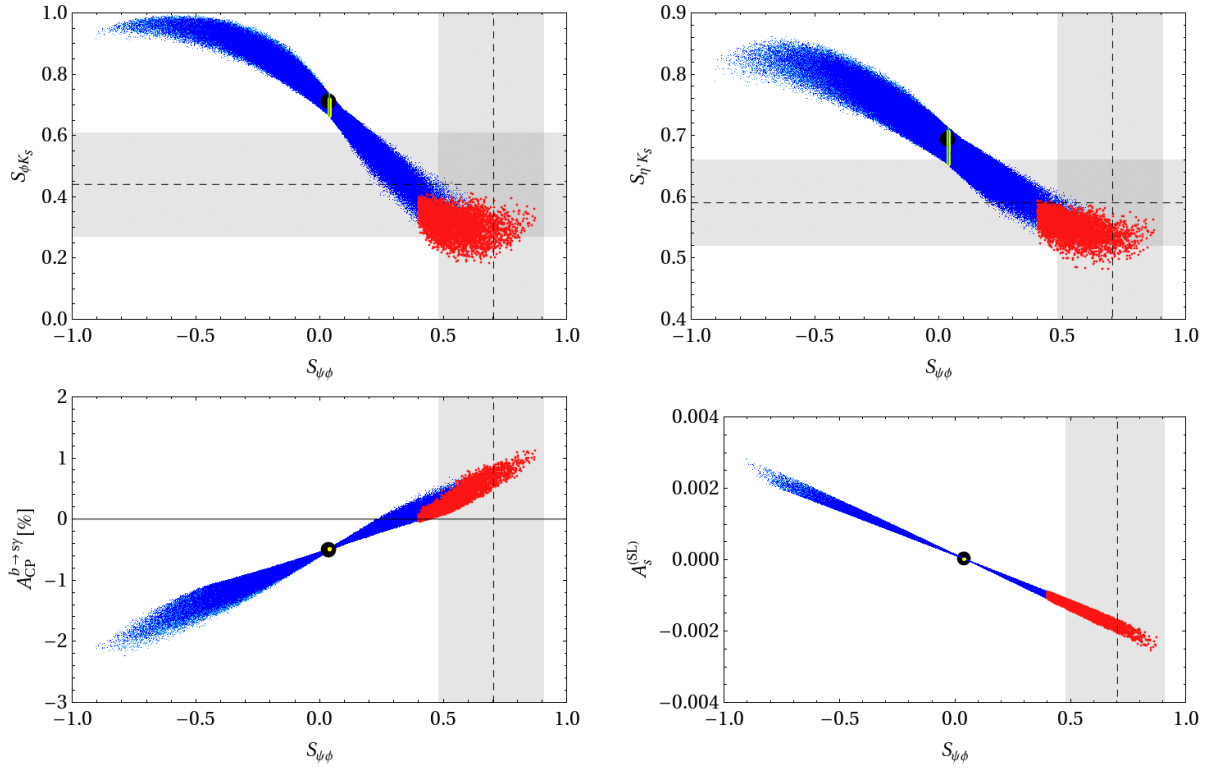


Figure 3: The CP asymmetries $S_{\phi K_S}$ (upper-left panel), $S_{\eta' K_S}$ (upper-right panel), $A_{CP}^{bs\gamma}$ (lower-left panel), A_{SL}^s (lower-right panel) shown as functions of $S_{\psi\phi}$.

- The theoretical errors on (the real part of) the b_f parameters in (4.63) are of minor importance. We checked numerically that varying the b_f parameters by 10% yields only small effects on the studied correlations.
- On the other hand, sizable strong phases from non-factorisable final-state interactions may alter the *slope* for the predicted correlation between $S_{\phi K_S}$ and $S_{\psi\phi}$. This effect explains the difference between our result and the analysis by Soni et al. [15, 140], where the non-perturbative parameters are taken from [141], which is based on a phenomenological optimisation of theory input in the context of the SM3.

The weaker suppression of $S_{\eta' K_S}$ originates in smaller values of non-perturbative parameters b_i as seen in Table 2. On the other hand, as pointed out in [36, 90] in the supersymmetric flavour models with exclusively left-handed currents and in the FBMSSM, the desire to explain the $S_{\phi K_S}$ anomaly implies automatically that $A_{\text{CP}}^{bs\gamma}$ is much larger in magnitude than its SM3 value and has opposite sign. A qualitatively similar behaviour is found in the SM4, but as $S_{\phi K_S}$ is strongly correlated with $S_{\psi\phi}$ and the latter asymmetry is theoretically cleaner, we prefer to show the correlation between $A_{\text{CP}}^{bs\gamma}$ and $S_{\psi\phi}$. As seen in the lower-left panel of Fig. 3, for $S_{\psi\phi} \approx 0.5$ the asymmetry $A_{\text{CP}}^{bs\gamma}$ reverses the sign but its magnitude is SM3-like. Larger effects are found for larger $|S_{\psi\phi}|$, in particular negative values of $S_{\psi\phi}$, which are however disfavoured by Tevatron data. We conclude that $A_{\text{CP}}^{bs\gamma}$ remains small also in the SM4, but the sign flip for large *positive* $S_{\psi\phi}$ could help to distinguish the SM4 from the SM3.

Finally, in the lower right panel of Fig. 3, we show the familiar correlation between A_{SL}^s and $S_{\psi\phi}$ [142]. The size of A_{SL}^s can be by an order of magnitude larger in the SM4 than in the SM3.

7.4 $B_{s,d} \rightarrow \mu^+ \mu^-$

In Fig. 4, we show $\text{Br}(B_d \rightarrow \mu^+ \mu^-)$ as a function of $\text{Br}(B_s \rightarrow \mu^+ \mu^-)$. The straight line in this plot represents the “Golden Relation” of CMFV models given in (4.31) with $r = 1$. We observe very strong departures from CMFV. We also observe that $\text{Br}(B_d \rightarrow \mu^+ \mu^-)$ can be as large as $8 \cdot 10^{-10}$ and $\text{Br}(B_s \rightarrow \mu^+ \mu^-)$ as large as $1 \cdot 10^{-8}$. The striking message from Fig. 4, reflecting the non-CMFV character of NP contributions, is that large enhancement of $\text{Br}(B_s \rightarrow \mu^+ \mu^-)$ implies SM3-like values of $\text{Br}(B_d \rightarrow \mu^+ \mu^-)$ and vice-versa.

In Fig. 5, we show $\text{Br}(B_d \rightarrow \mu^+ \mu^-)$ and $\text{Br}(B_s \rightarrow \mu^+ \mu^-)$ as functions of $S_{\psi\phi}$. The disparity between these plots shows the non-CMFV character of the NP contributions in the SM4. We observe a definite correlation between $\text{Br}(B_s \rightarrow \mu^+ \mu^-)$ and $S_{\psi\phi}$, thus, for a

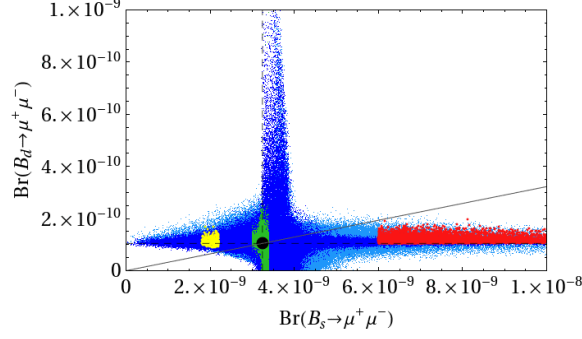


Figure 4: $\text{Br}(B_d \rightarrow \mu^+ \mu^-)$ as a function of $\text{Br}(B_s \rightarrow \mu^+ \mu^-)$.

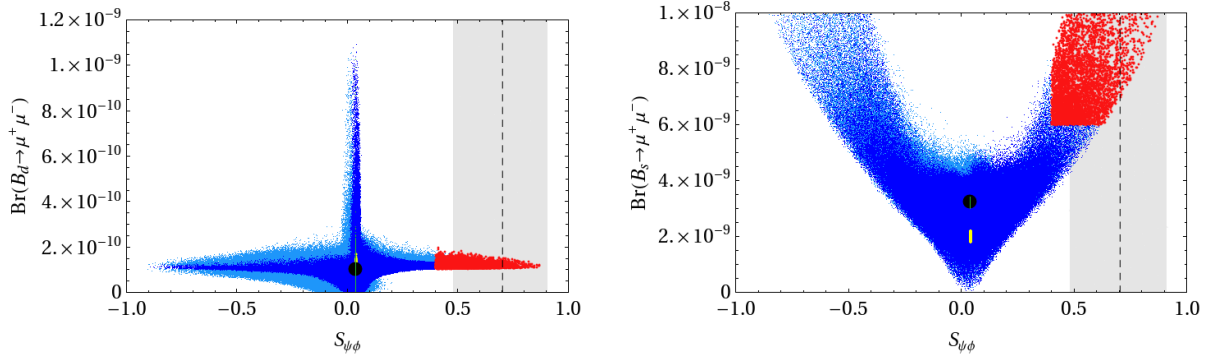


Figure 5: $\text{Br}(B_d \rightarrow \mu^+ \mu^-)$ (left panel) and $\text{Br}(B_s \rightarrow \mu^+ \mu^-)$ (right panel) each as a function of $S_{\psi\phi}$.

given value of $S_{\psi\phi}$, only a certain range for $\text{Br}(B_s \rightarrow \mu^+ \mu^-)$ is predicted. Moreover, with increasing $S_{\psi\phi}$ also $\text{Br}(B_s \rightarrow \mu^+ \mu^-)$ generally increases. In particular, for $S_{\psi\phi} > 0.4$, an enhancement of $\text{Br}(B_s \rightarrow \mu^+ \mu^-)$ is found. For $S_{\psi\phi} \approx 0.4$, we find that $\text{Br}(B_s \rightarrow \mu^+ \mu^-)$ can reach values as high as $7 \cdot 10^{-9}$. For larger values of $S_{\psi\phi}$, even higher values of $\text{Br}(B_s \rightarrow \mu^+ \mu^-)$ are possible. Interestingly, for SM3-like values of $S_{\psi\phi}$, the branching ratio $\text{Br}(B_s \rightarrow \mu^+ \mu^-)$ is more likely suppressed than enhanced. We conclude that a future measurement of $S_{\psi\phi}$ above 0.4 accompanied by $\text{Br}(B_s \rightarrow \mu^+ \mu^-)$ close to or below its SM3 value would put the SM4 into difficulties.

From the right panel in Fig. 5 we can infer the following *soft* bounds on $\text{Br}(B_s \rightarrow \mu^+ \mu^-)$ as a function of $S_{\psi\phi}$

$$\text{Br}(B_s \rightarrow \mu^+ \mu^-) \leq \left(6 + (4 \cdot (S_{\psi\phi} - (S_{\psi\phi})_{\text{SM}}))^4\right) \cdot 10^{-9}, \quad (7.3)$$

$$\text{Br}(B_s \rightarrow \mu^+ \mu^-) \geq \begin{cases} (-0.08 + S_{\psi\phi}) \cdot 10^{-8} & \text{for } S_{\psi\phi} > 0 \\ (-0.04 - S_{\psi\phi}) \cdot 10^{-8} & \text{for } S_{\psi\phi} < 0 \end{cases}. \quad (7.4)$$

In addition we find the global *soft* upper bound

$$\text{Br}(B_s \rightarrow \mu^+ \mu^-) \leq 1.3 \cdot 10^{-8}. \quad (7.5)$$

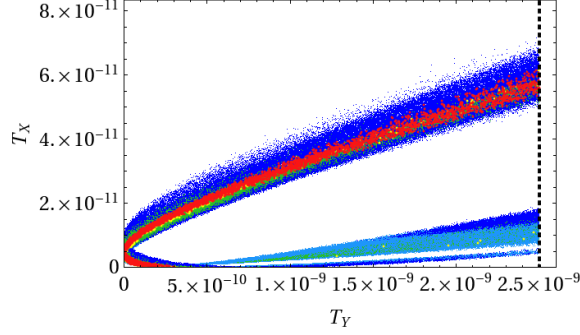


Figure 6: T_X as a function of T_Y , as defined in (7.6). The vertical dashed red line represents the bound (4.34).

7.5 $K_L \rightarrow \mu^+ \mu^-$

We begin our analysis of rare K decays with the SD contribution to $K_L \rightarrow \mu^+ \mu^-$, on which the bound is given in (4.34). It turns out that in the SM4 this bound can be strongly violated, and imposing it has an impact on the size of possible enhancements in other rare K decays. In order to see this transparently, let us define

$$T_Y \equiv \text{Br}(K_L \rightarrow \mu^+ \mu^-)_{\text{SD}}, \quad T_X \equiv \text{Br}(K^+ \rightarrow \pi^+ \nu \bar{\nu}) - \frac{\kappa^+}{\kappa_L} \text{Br}(K_L \rightarrow \pi^0 \nu \bar{\nu}), \quad (7.6)$$

with T_X entering the branching ratio $\text{Br}(K^+ \rightarrow \pi^+ \nu \bar{\nu})$ in (4.40). In Fig. 6, we show T_X as a function of T_Y and find a strong correlation between these two quantities which could be anticipated on the basis of the analytic expressions for T_X and T_Y . As T_Y is bounded from above directly through (4.34), we obtain also an upper bound on T_X . Throughout our numerical analysis, we impose the bound (4.34).

7.6 $K^+ \rightarrow \pi^+ \nu \bar{\nu}$ and $K_L \rightarrow \pi^0 \nu \bar{\nu}$

In Fig. 7, we show $\text{Br}(K_L \rightarrow \pi^0 \nu \bar{\nu})$ as a function of $\text{Br}(K^+ \rightarrow \pi^+ \nu \bar{\nu})$. The black point shows the central SM3 values of the branching ratios in question, and the shaded region corresponds to the experimental 1σ range for $\text{Br}(K^+ \rightarrow \pi^+ \nu \bar{\nu})$, with its central value given by the light vertical dashed line. Unless indicated otherwise, the meaning of dashed lines and shaded areas will be the same as described here throughout our analysis.

We observe that both branching ratios can be enhanced relative to the SM3 values in a spectacular manner. This is in particular the case for $\text{Br}(K_L \rightarrow \pi^0 \nu \bar{\nu})$, which can reach values as high as 10^{-9} , that is by a factor of 40 larger than found in the SM3. $\text{Br}(K^+ \rightarrow \pi^+ \nu \bar{\nu})$ can be by a factor of 4 larger than in the SM3. We note that the Grossman-Nir (GN) [143] bound on $\text{Br}(K_L \rightarrow \pi^0 \nu \bar{\nu})$ can be saturated for all values of $\text{Br}(K^+ \rightarrow \pi^+ \nu \bar{\nu})$ shown in the plot. We also observe that large enhancements of

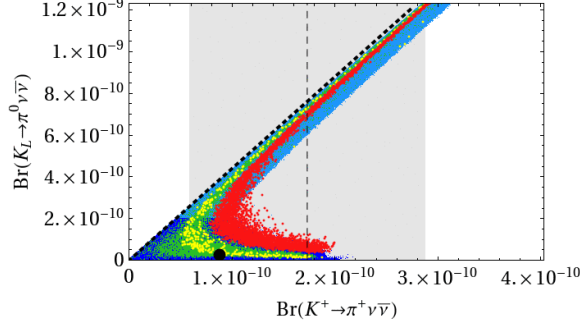


Figure 7: $\text{Br}(K_L \rightarrow \pi^0 \nu \bar{\nu})$ as a function of $\text{Br}(K^+ \rightarrow \pi^+ \nu \bar{\nu})$. The dotted line corresponds to the model-independent GN bound.

$\text{Br}(K_L \rightarrow \pi^0 \nu \bar{\nu})$ imply necessarily enhancements of $\text{Br}(K^+ \rightarrow \pi^+ \nu \bar{\nu})$. The converse is obviously not true, but for $\text{Br}(K^+ \rightarrow \pi^+ \nu \bar{\nu}) > 1.7 \cdot 10^{-10}$ the $\text{Br}(K_L \rightarrow \pi^0 \nu \bar{\nu})$ is either below 10^{-10} or close to the GN bound and larger than $6 \cdot 10^{-10}$. For an earlier analysis of $K \rightarrow \pi \nu \bar{\nu}$, where large effects of 4G quarks can be found, see [13].

The pattern seen in Fig. 7 can be understood as follows. The horizontal lower branch, on which $\text{Br}(K_L \rightarrow \pi^0 \nu \bar{\nu})$ does not depart by much from the SM3 values but $\text{Br}(K^+ \rightarrow \pi^+ \nu \bar{\nu})$ can be strongly enhanced, corresponds to the range of parameters for which the term T_X in (4.40) dominates $\text{Br}(K^+ \rightarrow \pi^+ \nu \bar{\nu})$. But as we have seen above, T_X is efficiently constrained by the bound on $\text{Br}(K_L \rightarrow \mu^+ \mu^-)_{\text{SD}}$, and consequently a stringent upper bound is put on $\text{Br}(K^+ \rightarrow \pi^+ \nu \bar{\nu})$ on this branch ⁵. The second branch, on which both $K \rightarrow \pi \nu \bar{\nu}$ branching ratios can be strongly enhanced, corresponds to the region of parameters for which T_X is subdominant and the first term in (4.40) dominates $\text{Br}(K^+ \rightarrow \pi^+ \nu \bar{\nu})$. Comparing (4.40) and (4.41), we observe in this case a very strong correlation between $\text{Br}(K_L \rightarrow \pi^0 \nu \bar{\nu})_{\text{SD}}$ and $\text{Br}(K^+ \rightarrow \pi^+ \nu \bar{\nu})$: their ratio is simply given by $\kappa_L/\kappa_+ \approx 4.3$ which is precisely the GN bound.

It is evident from this discussion that the upper branch, in contrast to the lower branch, is not affected by the bound on $\text{Br}(K_L \rightarrow \mu^+ \mu^-)$. In order to see how the latter bound affects other observables, we divide the points in Fig. 7 in two groups, with the ones corresponding to $\text{Br}(K_L \rightarrow \pi^0 \nu \bar{\nu}) > 2 \cdot 10^{-10}$ represented by *light blue* points.

In spite of the interesting pattern of deviations from the SM3 seen in Fig. 7, we conclude that on the basis of the present constraints the predictive power of the SM4 is limited, except that spectacular deviations from the SM3 are definitely possible, but suppressions cannot be excluded. We also note that even for large values of $S_{\psi\phi}$ and $\text{Br}(B_s \rightarrow \mu^+ \mu^-)$ that are represented by red points, large NP effects in both branching ratios are possible. In Fig. 8, we look closer at the latter feature. A large enhancement

⁵The fact that the bound on $\text{Br}(K_L \rightarrow \mu^+ \mu^-)_{\text{SD}}$ can have sizable impact on $\text{Br}(K^+ \rightarrow \pi^+ \nu \bar{\nu})$ has already been pointed out in [120]. See also [121].

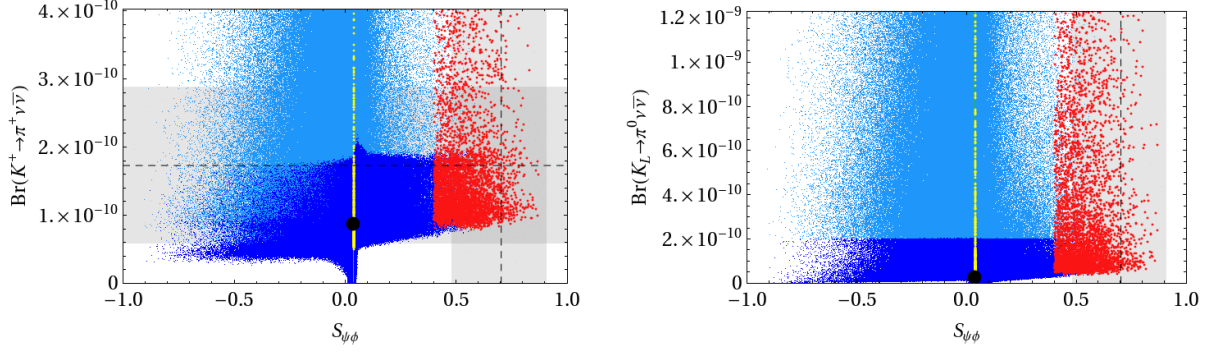


Figure 8: $\text{Br}(K^+ \rightarrow \pi^+ \nu \bar{\nu})$ (left panel) and $\text{Br}(K_L \rightarrow \pi^0 \nu \bar{\nu})$ (right panel) as functions of the CP asymmetry $S_{\psi\phi}$.

of both branching ratios is clearly possible as already seen in Fig. 7. Moreover, these plots look very different from those found in the LHT and RSc models [31–35].

In [144] the impact of ε_K on the correlation of $\text{Br}(K_L \rightarrow \pi^0 \nu \bar{\nu})$ and $\text{Br}(K^+ \rightarrow \pi^+ \nu \bar{\nu})$ was studied. It was argued that in the case of correlated phases in the NP contributions to $\Delta F = 2$ and $\Delta F = 1$ processes one naturally gets the observed two branched structure of the correlation. However even if this assumption is relaxed, the presence of additive NP contributions to ε_K implies

$$\theta_K^X \neq \bar{\beta} - \bar{\beta}_s \pm \frac{\pi}{2}, \quad (7.7)$$

and consequently the upper branch never reaches the GN bound. In the SM4 also $\text{Im}\lambda_c^{(K)}$ is affected and $|\text{Im}\lambda_c^{(K)}| \gg \left(|\text{Im}\lambda_c^{(K)}|\right)_{\text{SM}}$ can compensate for large effects introduced through changes in $\lambda_t^{(K)}$ and through $\lambda_{\nu}^{(K)}$. Effectively the SM4 is able to maximally violate the assumption of correlated new phases in ε_K and $K \rightarrow \pi \nu \bar{\nu}$ and the GN bound can be reached. The effects of $|\text{Im}\lambda_c^{(K)}| \gg \left(|\text{Im}\lambda_c^{(K)}|\right)_{\text{SM}}$ on $\text{Br}(K_L \rightarrow \pi^0 \nu \bar{\nu})$ can be neglected, which is evident from the structure of (4.40) and (4.41).

7.7 $K_L \rightarrow \mu^+ \mu^-$ and $K^+ \rightarrow \pi^+ \nu \bar{\nu}$

In order to understand still better the structure of NP effects in Fig. 7, we show in Fig. 9 the correlation between $\text{Br}(K_L \rightarrow \mu^+ \mu^-)_{\text{SD}}$ and $\text{Br}(K^+ \rightarrow \pi^+ \nu \bar{\nu})$. We observe that most points cluster around two branches corresponding to the two branches in Fig. 7. On one of them $\text{Br}(K_L \rightarrow \mu^+ \mu^-)_{\text{SD}}$ is suppressed relative to the SM3 value while $\text{Br}(K^+ \rightarrow \pi^+ \nu \bar{\nu})$ can be large. On the second branch $\text{Br}(K_L \rightarrow \mu^+ \mu^-)_{\text{SD}}$ can reach the upper limit at which point $\text{Br}(K^+ \rightarrow \pi^+ \nu \bar{\nu})$ is most likely in the ballpark of the central experimental value. Still, as seen in Fig. 9, other combinations of the values of both branching ratios cannot be excluded at present.

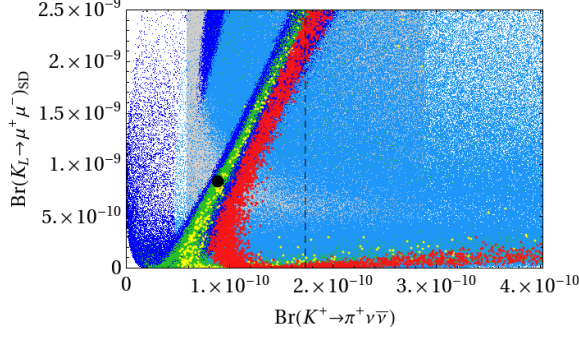


Figure 9: The SD contribution to $\text{Br}(K_L \rightarrow \mu^+ \mu^-)$ as a function of $\text{Br}(K^+ \rightarrow \pi^+ \nu \bar{\nu})$.

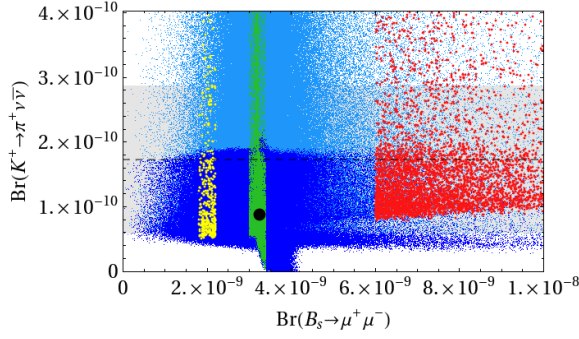


Figure 10: $\text{Br}(K^+ \rightarrow \pi^+ \nu \bar{\nu})$ as a function of $\text{Br}(B_s \rightarrow \mu^+ \mu^-)$.

7.8 $B_s \rightarrow \mu^+ \mu^-$ vs. $K^+ \rightarrow \pi^+ \nu \bar{\nu}$

In Fig. 10, we show $\text{Br}(K^+ \rightarrow \pi^+ \nu \bar{\nu})$ as a function of $\text{Br}(B_s \rightarrow \mu^+ \mu^-)$. The striking feature in this plot is the disparity of possible enhancements of both branching ratios relative to the SM3 values. While $\text{Br}(K^+ \rightarrow \pi^+ \nu \bar{\nu})$ can be strongly enhanced, as already seen in Figs. 7 and 8, the possible enhancement of $\text{Br}(B_s \rightarrow \mu^+ \mu^-)$ is more modest. We also conclude that there is no strong correlation between both branching ratios, so that they can be enhanced significantly at the same time, but this is not necessarily the case.

7.9 $B \rightarrow X_s \nu \bar{\nu}$, $K_L \rightarrow \pi^0 \nu \bar{\nu}$ and $B_s \rightarrow \mu^+ \mu^-$

In Fig. 11, we show $\text{Br}(K_L \rightarrow \pi^0 \nu \bar{\nu})$ as a function of $\text{Br}(B \rightarrow X_s \nu \bar{\nu})$. Similar to Fig. 10, the 4G effects can be much larger in $K_L \rightarrow \pi^0 \nu \bar{\nu}$ than in $B \rightarrow X_s \nu \bar{\nu}$. In fact, this plot is similar to the one in Fig. 10, except that the possible enhancement of $\text{Br}(B \rightarrow X_s \nu \bar{\nu})$ is more modest than the one of $\text{Br}(B_s \rightarrow \mu^+ \mu^-)$. While there is no visible correlation between the two branching ratios in Fig. 11, $\text{Br}(B \rightarrow X_s \nu \bar{\nu})$ is significantly correlated with $\text{Br}(B_s \rightarrow \mu^+ \mu^-)$ as seen in Fig. 12. In particular, both branching ratios are most likely either simultaneously enhanced or simultaneously suppressed with respect to their

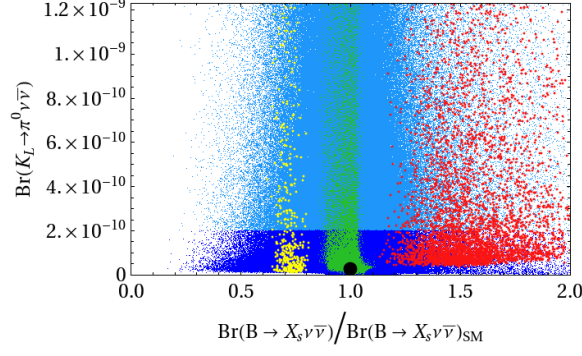


Figure 11: $\text{Br}(K_L \rightarrow \pi^0 \nu \bar{\nu})$ as a function of $\text{Br}(B \rightarrow X_s \nu \bar{\nu})$.

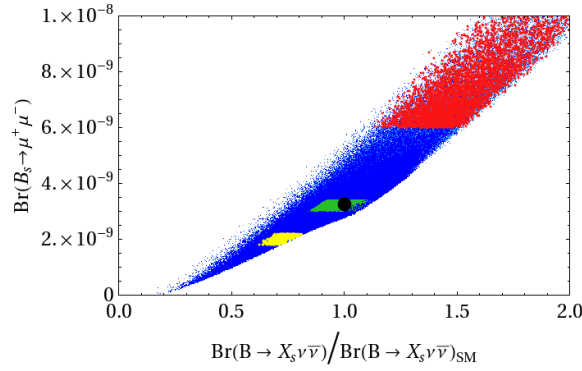


Figure 12: $\text{Br}(B_s \rightarrow \mu^+ \mu^-)$ as a function of $\text{Br}(B \rightarrow X_s \nu \bar{\nu})$.

SM3 values.

7.10 $K_L \rightarrow \pi^0 e^+ e^-$ vs. $K_L \rightarrow \pi^0 \mu^+ \mu^-$

In Fig. 13, we show the correlation between $\text{Br}(K_L \rightarrow \pi^0 e^+ e^-)$ and $\text{Br}(K_L \rightarrow \pi^0 \mu^+ \mu^-)$, also familiar from the LHT model [32]. We show only the “+” solution with the SM3 values given in (4.88) and (4.89). As expected, the allowed enhancements are not as pronounced as in the case of $K_L \rightarrow \pi^0 \nu \bar{\nu}$. However, they are still much larger than in the LHT model: one order of magnitude for both branching ratios with slightly larger effects for $K_L \rightarrow \pi^0 \mu^+ \mu^-$.

7.11 $K_L \rightarrow \pi^0 \ell^+ \ell^-$ vs. $K_L \rightarrow \pi^0 \nu \bar{\nu}$

In Fig. 14, we show a correlation between $\text{Br}(K_L \rightarrow \pi^0 \ell^+ \ell^-)$ and $\text{Br}(K_L \rightarrow \pi^0 \nu \bar{\nu})$ that has also been found in the LHT and RSc models [31–35]. The enhancement of one of the branching ratios implies automatically the enhancement of the other. We show only the results for $\text{Br}(K_L \rightarrow \pi^0 \nu \bar{\nu}) \leq 2 \cdot 10^{-10}$, as the extrapolation to higher values is straightforward. The main message from this plot is that the enhancement

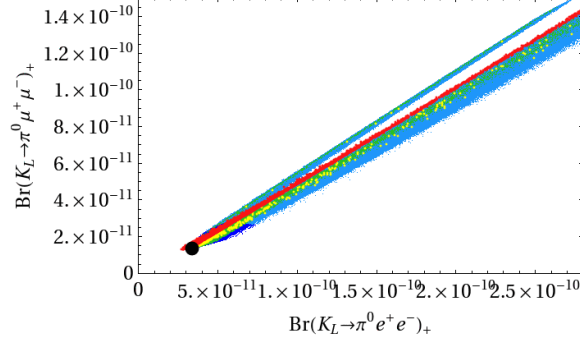


Figure 13: $\text{Br}(K_L \rightarrow \pi^0 e^+ e^-)$ as a function of $\text{Br}(K_L \rightarrow \pi^0 \mu^+ \mu^-)$.

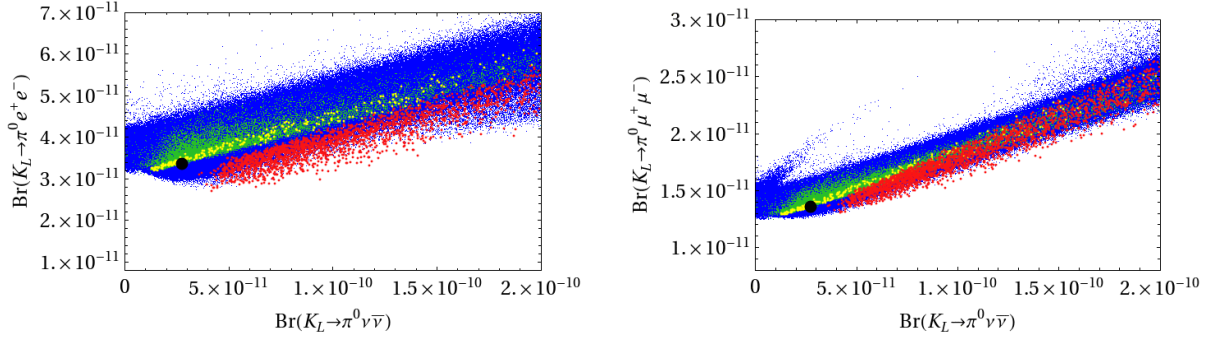


Figure 14: $\text{Br}(K_L \rightarrow \pi^0 e^+ e^-)_+$ as functions of $\text{Br}(K_L \rightarrow \pi^0 \nu \bar{\nu})$ (left panel), $\text{Br}(K_L \rightarrow \pi^0 \mu^+ \mu^-)_+$ as functions of $\text{Br}(K_L \rightarrow \pi^0 \nu \bar{\nu})$ (right panel).

of $\text{Br}(K_L \rightarrow \pi^0 \nu \bar{\nu})$ can be much larger than the one of $\text{Br}(K_L \rightarrow \pi^0 \ell^+ \ell^-)$, as already anticipated on the basis of analytic formulae.

7.12 The ratio ε'/ε

In Fig. 15, we show ε'/ε as a function of $S_{\psi\phi}$ for four different scenarios of the non-perturbative parameters R_6 and R_8 : $(R_6, R_8) = (1.0, 1.0)$ (upper left panel), $(1.5, 0.8)$ (upper right panel), $(2.0, 1.0)$ (lower left panel) and $(1.5, 0.5)$ (lower right panel). Each set of points has the SM3 value indicated by a black dot. $\Lambda_{\overline{\text{MS}}}$ has been set to 340 MeV. The non-perturbative parameters R_6 and R_8 are defined as

$$R_6 \equiv B_6^{(1/2)} \left[\frac{121 \text{ MeV}}{m_s(m_c) + m_d(m_c)} \right]^2, \quad R_8 \equiv B_8^{(3/2)} \left[\frac{121 \text{ MeV}}{m_s(m_c) + m_d(m_c)} \right]^2. \quad (7.8)$$

As a general feature the SM4 can fit ε'/ε for all sets of non-perturbative parameters considered by us. However, the striking feature of these plots is the difficulty in reproducing the experimental data for ε'/ε within the SM4 when $S_{\psi\phi}$ is large and positive (red points) as suggested by the Tevatron data. Thus if the latter data will be confirmed ε'/ε can put the SM4 under pressure, unless R_6 is significantly larger than unity and R_8

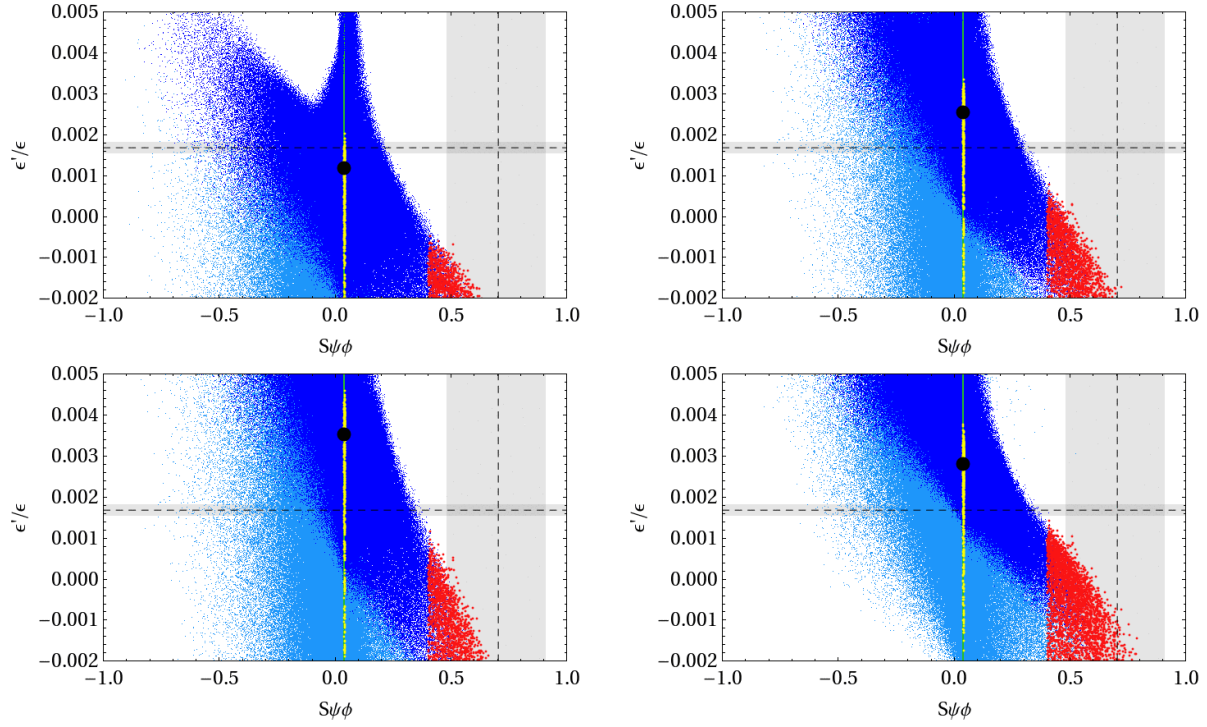


Figure 15: ε'/ε as a function of the CP asymmetry $S_{\psi\phi}$ for four different scenarios of the non-perturbative parameters. $(R_6, R_8) = (1.0, 1.0)$ (upper left panel), $(1.5, 0.8)$ (upper right panel), $(2.0, 1.0)$ (lower left panel) and $(1.5, 0.5)$ (lower right panel).

R_6	R_8	
1.0	1.0	dark blue
1.5	0.8	purple
2.0	1.0	green
1.5	0.5	orange

Table 5: Four scenarios for the parameters R_6 and R_8

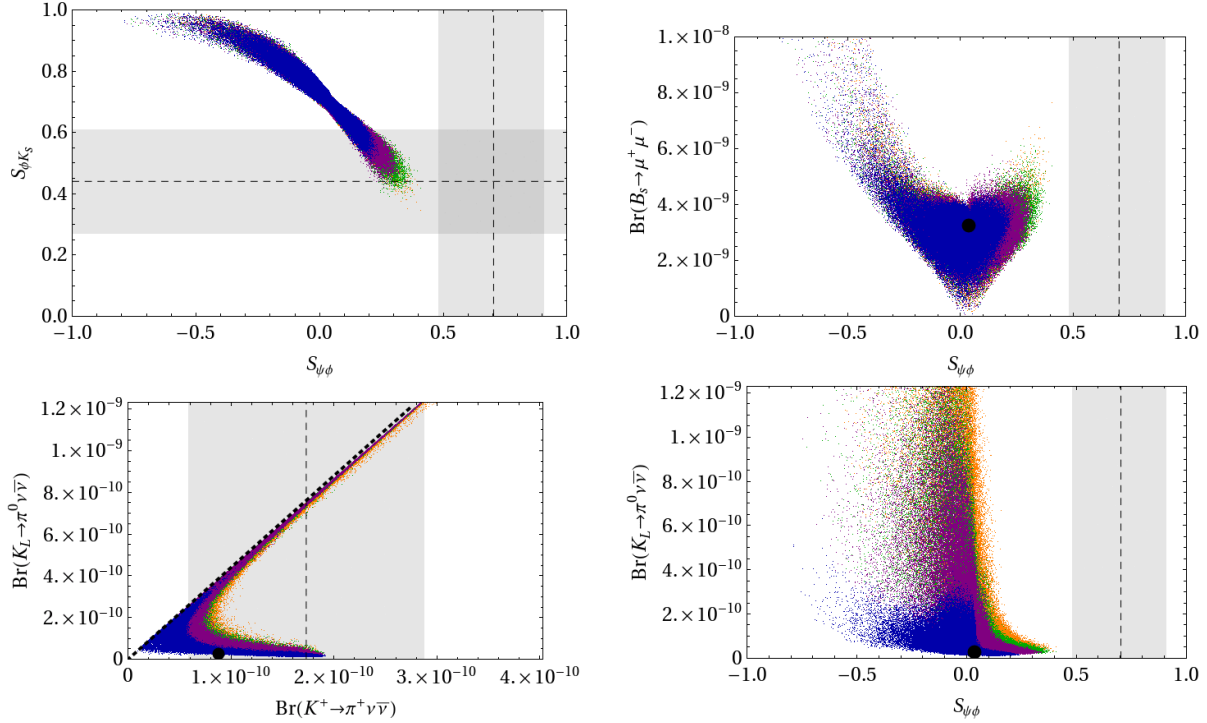


Figure 16: Correlations including the ε'/ε -constraint (colour-coding according to Table 5) .

sufficiently suppressed below one. This discussion demonstrates again that in order to use ε'/ε to constrain NP the knowledge of the parameters R_6 and R_8 has to be improved significantly. An analysis of ε'/ε in the 4G model has been presented in [13], where the hadronic uncertainties known from previous studies have been reemphasised. However, the direct impact of large $S_{\psi\phi}$ on ε'/ε has not been studied in details there as we do below.

It is then of interest to investigate what impact ε'/ε would have on our analysis when R_6 and R_8 were precisely known. To this end we introduce still another coding in Table 5, this time for different values of R_6 and R_8 . In Fig. 16 we show then the most interesting correlations, this time including also the ε'/ε -constraint. These are

$S_{\phi K_S}$ vs. $S_{\psi\phi}$, $\text{Br}(B_s \rightarrow \mu^+\mu^-)$ vs. $S_{\psi\phi}$, $\text{Br}(K_L \rightarrow \pi^0\nu\bar{\nu})$ vs. $\text{Br}(K^+ \rightarrow \pi^+\nu\bar{\nu})$ and $\text{Br}(K_L \rightarrow \pi^0\nu\bar{\nu})$ vs. $S_{\psi\phi}$. These plots should be compared to the plots in Figs. 3, 5, 7 and 8 respectively, where the ε'/ε constraint has not been taken into account.

We observe the following striking features already anticipated on the basis of Fig. 15:

- $S_{\psi\phi}$ can be at most 0.4 and this upper bound is only reached for the green and orange points where the ratio $R_6/R_8 \geq 2$
- For the large N case $R_6 = R_8 = 1$ represented by dark blue points, we identify the following rough absolute bounds

$$\begin{aligned} S_{\psi\phi} &\lesssim 0.25, & \text{Br}(K_L \rightarrow \pi^0\nu\bar{\nu}) &\lesssim 4 \cdot 10^{-10}, \\ \text{Br}(K^+ \rightarrow \pi^+\nu\bar{\nu}) &\lesssim 2 \cdot 10^{-10}, & \text{Br}(B_s \rightarrow \mu^+\mu^-) &\lesssim 4.9 \cdot 10^{-9}, \end{aligned}$$

where in the last case $S_{\psi\phi} > 0$ has been assumed in accordance with CDF and D0 data.

- Weaker bounds are found for purple and in particular green and orange points where the role of electroweak penguins relative to QCD penguins in ε'/ε is suppressed and it is easier to have larger 4G effects in rare K and B decays, while still satisfying the ε'/ε constraint.

Finally we would like to remark that the enhancements of rare K decay branching ratios found here are larger than the bounds in [120] would suggest. This is related to the fact that in the SM4 the NP effects in neutral meson mixing can be significantly larger than assumed in [120], implying that the range for $\text{Im}\lambda_t$ in the SM4 can be significantly larger than used in [120].

7.13 Violation of CKM Unitarity

From our discussion of unitarity of the matrix V_{4G} in Section 2, we see that the sub-matrix describing the 3G mixing, for non-vanishing mixing angles θ_{i4} , is necessarily non-unitary. A similar effect was observed also in the RS model with custodial protection [145]. In order to quantitatively describe the deviation from unitarity, we define

$$K^u \equiv V_{\text{CKM}3} V_{\text{CKM}3}^\dagger, \quad K^d \equiv V_{\text{CKM}3}^\dagger V_{\text{CKM}3} \quad (7.9)$$

which are generally different from the 3×3 unit matrix. In particular, we find

$$|K^u - \mathbb{1}|_{ij} = |V_{ib'} V_{jb'}^*|, \quad |K^d - \mathbb{1}|_{ij} = |V_{\ell'i} V_{\ell'j}^*|. \quad (7.10)$$

	$ \mathbb{1} - K _{ij}$	(a) 431	(b) 211	(c) 231	(d) 321
$ V_{ud} ^2 + V_{cd} ^2 + V_{td} ^2 = K_{11}^d$ $\quad 1 \quad \lambda^2 \quad \lambda^6$	$ V_{t'd} ^2 \sim \lambda^{2n_1}$	λ^8	λ^4	λ^4	λ^6
$ V_{us} ^2 + V_{cs} ^2 + V_{ts} ^2 = K_{22}^d$ $\quad \lambda^2 \quad 1 \quad \lambda^4$	$ V_{t's} ^2 \sim \lambda^{2n_2}$	λ^6	λ^2	λ^6	λ^4
$ V_{ub} ^2 + V_{cb} ^2 + V_{tb} ^2 = K_{33}^d$ $\quad \lambda^6 \quad \lambda^4 \quad 1$	$ V_{t'b} ^2 \sim \lambda^{2n_3}$	λ^2	λ^2	λ^2	λ^2
$ V_{ud} ^2 + V_{us} ^2 + V_{ub} ^2 = K_{11}^u$ $\quad 1 \quad \lambda^2 \quad \lambda^6$	$ V_{ub'} ^2 \sim \lambda^{2n_1}$	λ^8	λ^4	λ^4	λ^6
$ V_{cd} ^2 + V_{cs} ^2 + V_{cb} ^2 = K_{22}^u$ $\quad \lambda^2 \quad 1 \quad \lambda^4$	$ V_{cb'} ^2 \sim \lambda^{2n_2}$	λ^6	λ^2	λ^6	λ^4
$ V_{td} ^2 + V_{ts} ^2 + V_{tb} ^2 = K_{33}^u$ $\quad \lambda^6 \quad \lambda^4 \quad 1$	$ V_{tb'} ^2 \sim \lambda^{2n_3}$	λ^2	λ^2	λ^2	λ^2
$V_{ud}V_{us}^* + V_{cd}V_{cs}^* + V_{td}V_{ts}^* = K_{12}^d$ $\quad \lambda \quad \lambda \quad \lambda^5$	$ V_{t'd}V_{t's}^* \sim \lambda^{n_1+n_2}$	λ^7	λ^3	λ^5	λ^5
$V_{ud}V_{ub}^* + V_{cd}V_{cb}^* + V_{td}V_{tb}^* = K_{13}^d$ $\quad \lambda^3 \quad \lambda^3 \quad \lambda^3$	$ V_{t'd}V_{t'b}^* \sim \lambda^{n_1+n_3}$	λ^5	λ^3	λ^3	λ^4
$V_{us}V_{ub}^* + V_{cs}V_{cb}^* + V_{ts}V_{tb}^* = K_{23}^d$ $\quad \lambda^4 \quad \lambda^2 \quad \lambda^2$	$ V_{t's}V_{t'b}^* \sim \lambda^{n_2+n_3}$	λ^4	λ^2	λ^4	λ^3
$V_{ud}V_{cd}^* + V_{us}V_{cs}^* + V_{ub}V_{cb}^* = K_{12}^u$ $\quad \lambda \quad \lambda \quad \lambda^5$	$ V_{ub'}V_{cb'}^* \sim \lambda^{n_1+n_2}$	λ^7	λ^3	λ^5	λ^5
$V_{ud}V_{td}^* + V_{us}V_{ts}^* + V_{ub}V_{tb}^* = K_{13}^u$ $\quad \lambda^3 \quad \lambda^3 \quad \lambda^3$	$ V_{ub'}V_{tb'}^* \sim \lambda^{n_1+n_3}$	λ^5	λ^3	λ^3	λ^4
$V_{cd}V_{td}^* + V_{cs}V_{ts}^* + V_{cb}V_{tb}^* = K_{23}^u$ $\quad \lambda^4 \quad \lambda^2 \quad \lambda^2$	$ V_{cb'}V_{tb'}^* \sim \lambda^{n_2+n_3}$	λ^4	λ^2	λ^4	λ^3

Table 6: CKM unitarity relations and the amount by which they are broken in the SM4 in the four scaling scenarios introduced in Section 2. For comparison, in the first column we also give the scaling for the three individual terms on the l.h.s. of the relation.

In Table 6, we collect the entries of $K^{u,d}$ and give the deviations from 3G unitarity in terms of the scaling of the mixing angles θ_{i4} for the benchmark scenarios introduced in Section 2. We see that, for several unitarity relations, the violation in the SM3 can be of the same size as the largest individual contribution from 3G mixing angles.

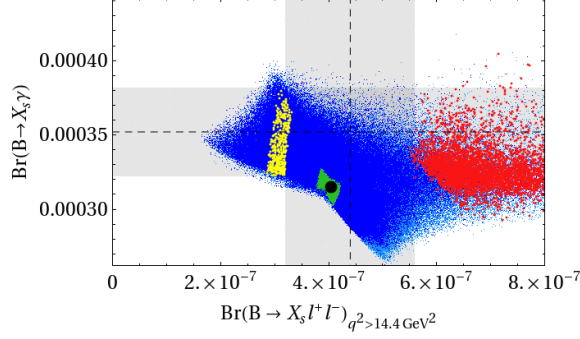


Figure 17: $\text{Br}(B \rightarrow X_s \gamma)$ as a function of $\text{Br}(B \rightarrow X_s \ell^+ \ell^-)_{q^2 > 14.4 \text{ GeV}^2}$.

7.14 $B \rightarrow X_s \gamma$ and $B \rightarrow X_s \ell^+ \ell^-$

In Fig. 17 we show $\text{Br}(B \rightarrow X_s \gamma)$ versus $\text{Br}(B \rightarrow X_s \ell^+ \ell^-)_{q^2 > 14.4 \text{ GeV}^2}$. This plot is self-explanatory and shows that enhancements of $S_{\psi\phi}$ and $\text{Br}(B_s \rightarrow \mu^+ \mu^-)$ (red points) are fully consistent with the experimental data for the two branching ratios shown in the plot. On the other hand the reduction of the experimental error on $\text{Br}(B \rightarrow X_s \ell^+ \ell^-)$ could have a significant impact on the red points. We confirmed that the zero s_0 of the forward-backward asymmetry remains SM3-like. Variations up to 10% are possible, but since this is comparable with the theoretical errors (NLO calculation) we do not further discuss this issue here. See Section 4.10 for details.

8 Anatomy

8.1 Step 1

We begin the anatomy of the SM4 by analysing the three scenarios for $|V_{ub}|$ and δ_{13} defined in Table 7. The three scenarios in question correspond to ones discussed in [36] and can be characterised as follows:

- S1:** $(\epsilon_K)_{\text{SM}}$ is lower than the data, while $S_{\Psi K_S}$ and $\Delta M_d/\Delta M_s$ are compatible with experiment. The *orange* points in Fig. 18-20 correspond to the removal of this anomaly within the SM4.
- S2:** $(S_{\psi K_S})_{\text{SM}}$ is above the data, while ϵ_K and $\Delta M_d/\Delta M_s$ are compatible with experiment. The *purple* points in Fig. 18-20 correspond to the removal of this anomaly within the SM4.
- S3:** $(\Delta M_d/\Delta M_s)_{\text{SM}}$ is much higher than the data, while ϵ_K and $S_{\Psi K_S}$ are compatible with experiment. The *green* points in Fig. 18-20 correspond to the removal of this anomaly within the SM4.

	S1 (orange)	S2 (purple)	S3 (green)
$ V_{ub} $	0.0034 ± 0.00015	0.0043 ± 0.0001	0.0037 ± 0.0001
δ_{13}	$(66 \pm 2)^\circ$	$(66 \pm 2)^\circ$	$(84 \pm 2)^\circ$

Table 7: Three scenarios for the parameters s_{13} and δ_{13}

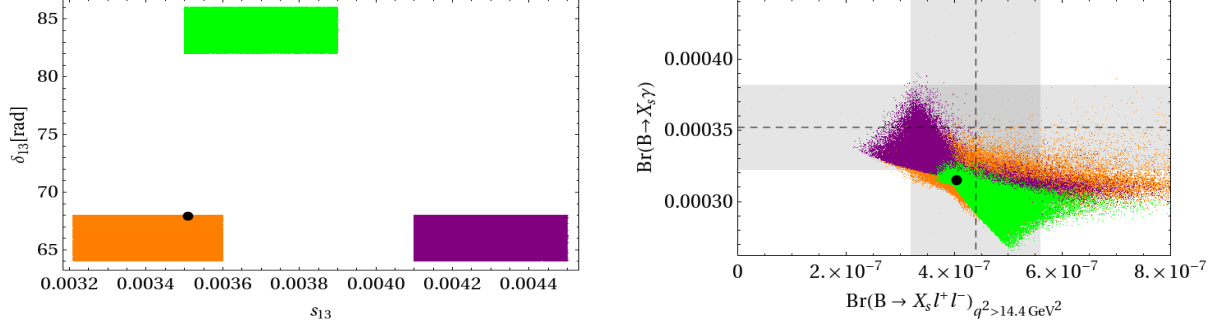


Figure 18: We show the colour coding of the tension scenarios (left panel) and $\text{Br}(B \rightarrow X_s \gamma)$ vs. $\text{Br}(B \rightarrow X_s \ell^+ \ell^-)_{q^2 > 14.4 \text{ GeV}^2}$ (right panel) for the tension scenarios defined in Tab. 7.

The clear lessons from this analysis are as follows:

- Due to the 4G contributions to ε_K and $S_{\psi K_S}$ in all scenarios simultaneous agreement with the data for these two observables can be achieved taking all existing constraints into account.
- However, only in scenario S1 values of $S_{\psi\phi}$ can be significantly enhanced and consequently $S_{\phi K_S}$ and $S_{\eta' K_S}$ significantly suppressed. As an example, we show in Fig. 19 (right panel) this situation by plotting $S_{\phi K_S}$ as a function of $S_{\psi\phi}$.
- As shown in Fig. 20, in all three scenarios significant enhancements of $\text{Br}(K^+ \rightarrow \pi^+ \nu \bar{\nu})$, $\text{Br}(K_L \rightarrow \pi^0 \nu \bar{\nu})$ and $\text{Br}(K_L \rightarrow \mu^+ \mu^-)$ are possible.
- On the other hand, as shown in the lower panel of Fig. 19 (right panel), the departure of $\text{Br}(B_s \rightarrow \mu^+ \mu^-)$ can be up to a factor of 4 for all three scenarios. However we found no points with large positive $S_{\psi\phi}$ for S2 and S3 which in turn puts a loose upper limit on $\text{Br}(B_s \rightarrow \mu^+ \mu^-)$ in these scenarios provided $S_{\psi\phi} > 0$.

8.2 Step 2

In the next three years, LHCb should be able to provide good data on $S_{\psi\phi}$ and $\text{Br}(B_s \rightarrow \mu^+ \mu^-)$. As we have seen in Fig. 5, a measurement of $S_{\psi\phi}$ above 0.5 accompanied by

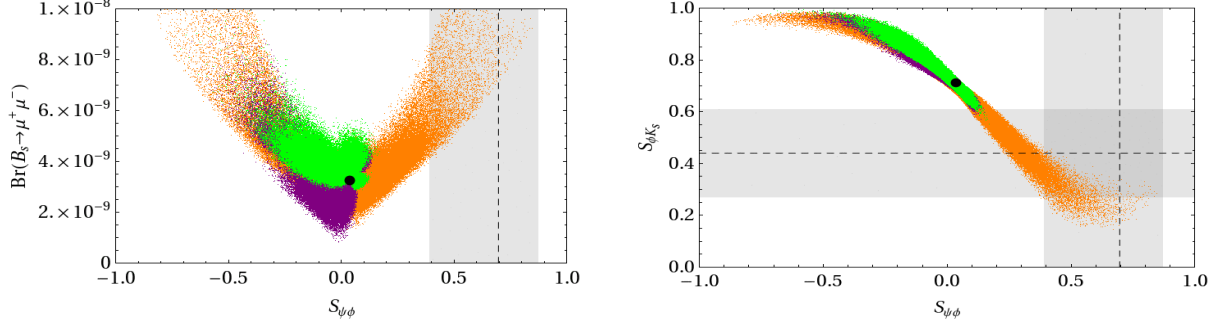


Figure 19: We show $\text{Br}(B_s \rightarrow \mu^+ \mu^-)$ vs. $S_{\psi\phi}$ (left panel) and $S_{\phi K_s}$ vs. $S_{\psi\phi}$ (right panel) for the tension scenarios defined in Tab. 7. The colour coding is defined in this table and can be read from the left panel of Fig. 18.

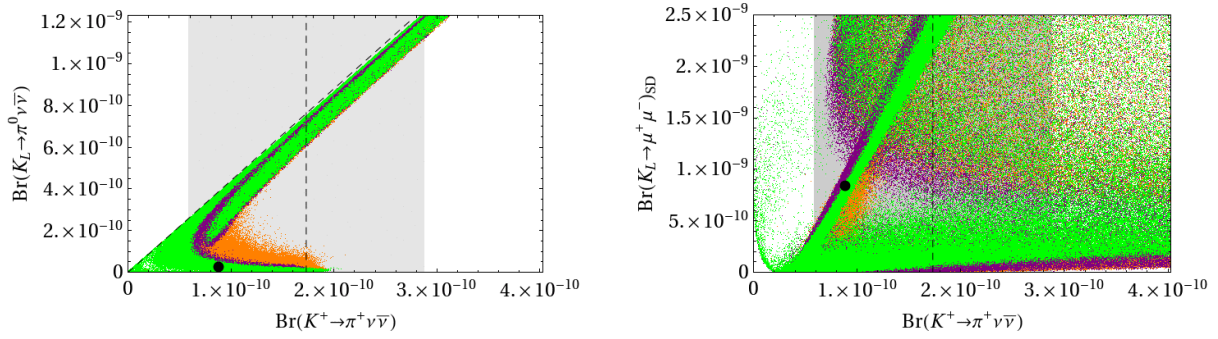


Figure 20: We show $\text{Br}(K_L \rightarrow \pi^0 \nu \bar{\nu})$ vs. $\text{Br}(K^+ \rightarrow \pi^+ \nu \bar{\nu})$ (left panel) and $\text{Br}(K_L \rightarrow \mu^+ \mu^-)_{\text{SD}}$ vs. $\text{Br}(K^+ \rightarrow \pi^+ \nu \bar{\nu})$ (right panel) for the tension scenarios defined in Tab. 7. The colour coding is defined in the table and can be read of Fig. 18 left panel.

$\text{Br}(B_s \rightarrow \mu^+ \mu^-)_{\text{exp}} \leq \text{Br}(B_s \rightarrow \mu^+ \mu^-)_{\text{SM}}$ would put the SM4 under pressure. Similarly for SM3-like values of $S_{\psi\phi}$, $\text{Br}(B_s \rightarrow \mu^+ \mu^-)$ can only be slightly enhanced over its SM3 value, and in fact a suppression of the latter branching ratio is more likely in this case.

In view of this pattern, we considered three scenarios shown in Table 4 and asked what they would imply for other decays. The result of this exercise is shown in all plots of Section 7 where the three scenarios of Table 4 are exhibited in three different colours indicated in this table. Alternatively, the colour coding can be conveniently inferred from Fig. 5. This results are self-explanatory and have been briefly discussed already in Section 7. Let us then only summarise our observations:

- As seen in Fig. 3, the $S_{\phi K_S}$ and $S_{\psi K_S}$ anomalies can only be explained in scenario BS3.
- As seen in Fig. 4, in the BS1 and BS3 scenarios the branching ratio $\text{Br}(B_d \rightarrow \mu^+ \mu^-)$ remains SM3-like, while in scenario BS2 it can be enhanced by a factor of two.
- As seen in Figs. 7 and 9 in all three scenarios large NP effects in $\text{Br}(K^+ \rightarrow \pi^+ \nu \bar{\nu})$, $\text{Br}(K_L \rightarrow \pi^0 \nu \bar{\nu})$ and $\text{Br}(K_L \rightarrow \mu^+ \mu^-)$ are possible. Moreover in scenario BS3 they are particularly strongly correlated with each other.
- For large positive values of $S_{\psi\phi}$ the predicted value of ε'/ε is significantly below the data, unless the hadronic matrix elements of the electroweak penguins are sufficiently suppressed with respect to the large N result and the ones of QCD penguins enhanced.

This analysis shows that we will learn a lot about the SM4 when $S_{\psi\phi}$, $\text{Br}(B_s \rightarrow \mu^+ \mu^-)$, $\text{Br}(K^+ \rightarrow \pi^+ \nu \bar{\nu})$ and $\text{Br}(K_L \rightarrow \pi^0 \nu \bar{\nu})$ will be precisely known.

9 Determining the V_{SM4} matrix

9.1 Preliminaries

As discussed in previous sections, the mixing between the third and fourth generation is bounded by the electroweak precision data and cannot be significantly larger than s_{12} . Similarly, s_{14} and s_{24} are bounded by (2.24). As a consequence, as can be explicitly seen by the generalised Wolfenstein expansion for our benchmark scenarios (2.29–2.32), the relation between CKM parameters and the matrix elements $V_{us}, V_{cd}, V_{ub}, V_{cb}$,

$$\begin{aligned} s_{12} &= \lambda \simeq |V_{us}| \simeq |V_{cd}|, & s_{23} &= A\lambda^2 \simeq |V_{cb}|, \\ s_{13} &= A\lambda^3 |z_\rho| \simeq |V_{ub}|, & \delta_{13} &= -\arg(z_\rho) \simeq -\arg(V_{ub}), \end{aligned} \quad (9.1)$$

are to a very good approximation unaffected by 4G contributions. Therefore the SM3 CKM parameters can be determined from the corresponding tree-level decays, practically without any NP pollution, with δ_{13} determined from $B \rightarrow DK$. In particular such a determination does not require the 3×3 CKM matrix to be unitary.⁶ In the present section we will further use (2.26) for the 4G mixing angles, in order to indicate how the V_{SM4} matrix can, in principle, be determined from future data.

A further comment on the determination of $\delta_{13} \approx \gamma$ is in order.

In the approximation of neglecting the phase of V_{cs} and V_{cb} , being real in the CKM convention, the $B_s \rightarrow D_s K$ complex in the SM3 measures directly a linear combination of the phase γ and the phase of B_s -mixing, where the latter can be extracted from $S_{\psi\phi}$. Analogous comments apply to $B_d \rightarrow D\pi$ decays. In the presence of 4G quarks, the phases in B_s and B_d mixing may change, but again they can be determined from the $S_{\psi\phi}$ and $S_{\psi K_S}$ asymmetries, respectively. The new feature, as seen in (2.19), are new phases of V_{cb} and V_{cs} induced by the presence of the 4G quarks. However, the imposition of tree-level and electroweak precision constraints implies that this NP pollution amounts to significantly less than 1° in the determination of δ_{13} and can be safely neglected. Analogous comments apply to other tree-level methods for the determination of δ_{13} .

The determination of the new parameters in the V_{SM4} matrix,

$$s_{14}, \quad s_{24}, \quad s_{34}, \quad \delta_{14}, \quad \delta_{24}, \quad (9.2)$$

is probably beyond the scope of flavour-violating high-energy processes explored at the LHC and will have to be made through FCNC processes that, as in the SM3, appear first at the one-loop level due to the GIM mechanism at work. The accuracy of this determination will depend on

- i) the precision of the relevant experimental data,
- ii) the theoretical cleanliness of the observables involved (i.e. observables with small hadronic uncertainties should be favoured),
- iii) the potential size of NP contributions to the considered observable.

Clearly, the room for NP contributions to observables that are known already precisely will depend on the values of the CKM parameters in (9.1). In this context, let us recall the existing tension between the experimental values of ε_K and $S_{\psi K_S}$ within the SM3 that has been extensively discussed in [61, 139, 146, 147]. Whether the SM3 has a problem

⁶Needless to say, $|V_{us}|, |V_{ub}|, |V_{cb}|$ and δ_{13} can be determined from tree-level decays even in the absence of this approximation, but the relation to the fundamental parameters is less transparent and involves the 4G parameters.

with ε_K , $S_{\psi K_S}$ or both observables depends on the values in (9.1). In turn, this will have an impact on the determination of the new parameters in (9.2). In what follows, we will first make a list of observables that could help us in the future to determine the parameters (9.2), subsequently illustrating such determinations on a few examples. A more extensive general numerical analysis appears to us to be premature at present. On the other hand, as we will see in Section 9.3, new insight can be gained by examining the anatomy of different scaling scenarios for the mixing angles and their implications for various flavour observables.

9.2 Basic Observables

Among the FCNC observables that have already been measured, the values for

$$\varepsilon_K, \quad \Delta M_d/\Delta M_s, \quad S_{\psi K_S}, \quad \text{Br}(B \rightarrow X_s \gamma) \quad (9.3)$$

have presently the dominant impact on the allowed structure of the V_{SM4} matrix. Indeed, $S_{\psi K_S}$ is theoretically very clean (see also the comment before Eq. (2.37)), and the hadronic uncertainties in ε_K and $\Delta M_d/\Delta M_s$ are below 5% already now and are expected to be decreased further in the coming years through improved lattice calculations.

Of particular interest in this decade will be the measurements of the branching ratios for

$$B_{s,d} \rightarrow \mu^+ \mu^-, \quad K^+ \rightarrow \pi^+ \nu \bar{\nu}, \quad K_L \rightarrow \pi^0 \nu \bar{\nu}, \quad B \rightarrow X_s \nu \bar{\nu}, \quad (9.4)$$

and, very importantly, of the CP-violating observables

$$S_{\psi\phi}, \quad S_{\phi K_S}, \quad A_{\text{CP}}(b \rightarrow s \gamma). \quad (9.5)$$

In particular, various correlations between all these observables will significantly constrain the allowed range of the SM4 parameters and even have the power to exclude this NP scenario. Assuming that the SM4 will survive these new tests and having at hand all these measurements, it will be possible to determine the matrix V_{SM4} . Indeed, let us note on the basis of the formulae of Section 4 that all these observables depend on six complex variables involving new parameters (see (2.33)),

$$\lambda_{t'}^{(K)}, \quad \lambda_{t'}^{(s)}, \quad \lambda_{t'}^{(d)}, \quad \lambda_t^{(K)}, \quad \lambda_t^{(s)}, \quad \lambda_t^{(d)}, \quad (9.6)$$

that are not fully independent as, with (9.1) being fixed, they depend on the five parameters in (9.2). It is instructive to write down the expressions for $\lambda_{t'}^{(i)}$ setting $c_{ij} = 1$ and

neglecting higher-order terms in the Wolfenstein expansion, leading to

$$\begin{aligned}
\lambda_{t'}^{(d)} &= V_{t'b}^* V_{t'd} \approx (s_{34} + s_{13}s_{14}e^{i(\delta_{13}-\delta_{14})} + s_{23}s_{24}e^{-i\delta_{24}}) \\
&\quad \times (e^{i\delta_{14}}s_{14} - e^{i\delta_{24}}s_{12}s_{24} - e^{i\delta_{13}}s_{13}s_{34} + s_{12}s_{23}s_{34}) \\
&\approx -e^{i\delta_{13}}s_{13}s_{34}^2 + s_{34}(s_{14}e^{i\delta_{14}} - s_{12}s_{24}e^{i\delta_{24}}) \\
&\quad + s_{14}s_{23}s_{24}e^{i(\delta_{1,4}-\delta_{24})} - s_{12}s_{23}(s_{24}^2 - s_{34}^2), \tag{9.7}
\end{aligned}$$

$$\begin{aligned}
\lambda_{t'}^{(s)} &= V_{t'b}^* V_{t's} \approx (s_{34} + s_{13}s_{14}e^{i(\delta_{13}-\delta_{14})} + s_{23}s_{24}e^{-i\delta_{24}}) \\
&\quad \times (e^{i\delta_{24}}s_{24} + e^{i\delta_{14}}s_{12}s_{14} - s_{23}s_{34}) \\
&\approx s_{12}s_{14}s_{34}e^{i\delta_{14}} + s_{24}s_{34}e^{i\delta_{24}} + s_{23}(s_{24}^2 - s_{34}^2), \tag{9.8}
\end{aligned}$$

$$\begin{aligned}
\lambda_{t'}^{(K)} &= V_{t's}^* V_{t'd} \approx (e^{-i\delta_{24}}s_{24} + e^{-i\delta_{14}}s_{12}s_{14} - s_{23}s_{34}) \\
&\quad \times (e^{i\delta_{14}}s_{14} - e^{i\delta_{24}}s_{12}s_{24} - e^{i\delta_{13}}s_{13}s_{34} + s_{12}s_{23}s_{34}) \\
&\approx s_{24}(-s_{12}s_{24} + s_{14}e^{i(\delta_{14}-\delta_{24})}) - s_{24}s_{34}e^{-i\delta_{24}}(-s_{12}s_{23} + s_{13}e^{i\delta_{13}}) \\
&\quad + (s_{12}s_{24}e^{i\delta_{24}} - s_{14}e^{i\delta_{14}})(s_{23}s_{34} - s_{12}s_{14}e^{-i\delta_{14}}) \\
&\approx \frac{\lambda_{t'}^{(s)*}\lambda_{t'}^{(d)}}{|V_{t'b}|^2}, \tag{9.9}
\end{aligned}$$

$$\begin{aligned}
\lambda_t^{(d)} &= V_{tb}^* V_{td} \approx -s_{13}e^{i\delta_{13}} - s_{14}s_{34}e^{i\delta_{14}} + s_{12}(s_{23} + s_{24}s_{34}e^{i\delta_{24}}) \\
&\approx -s_{13}e^{i\delta_{13}} + s_{12}s_{23} - \lambda_{t'}^{(d)}, \tag{9.10}
\end{aligned}$$

$$\begin{aligned}
\lambda_t^{(s)} &= V_{tb}^* V_{ts} \approx -s_{23} - s_{24}s_{34}e^{i\delta_{24}} \\
&\approx -s_{23} - \lambda_{t'}^{(s)}, \tag{9.11}
\end{aligned}$$

$$\begin{aligned}
\lambda_t^{(K)} &= V_{ts}^* V_{td} \approx (s_{23} + s_{24}s_{34}e^{-i\delta_{24}}) \\
&\quad \times (s_{13}e^{i\delta_{13}} + s_{14}s_{34}e^{i\delta_{14}} - s_{12}(s_{23} + s_{24}s_{34}e^{i\delta_{24}})) \\
&\approx \lambda_t^{(s)*}\lambda_t^{(d)}. \tag{9.12}
\end{aligned}$$

We observe that, in general, the variables $\lambda_{t'}^{(K,s,d)}$ involve all 5 mixing parameters associated with the 4G in a rather complicated way. Some simplification arises if we assume a certain scaling of the mixing angles θ_{i4} , for instance with one of our benchmark scenarios of Section 2. Let us, as an example, study the case (2.14), for which the above equations simplify as follows:

$$\begin{aligned}
\lambda_{t'}^{(s)} &\approx e^{i\delta_{24}}s_{24}s_{34} \equiv \sigma_{23}, \\
\lambda_{t'}^{(d)} &\approx s_{34}(s_{14}e^{i\delta_{14}} - s_{12}s_{24}e^{i\delta_{24}}) \equiv \sigma_{13} - s_{12}\sigma_{23}
\end{aligned}$$

$$\begin{aligned}
\lambda_{t'}^{(K)} &\approx s_{24} \left(-s_{12}s_{24} + s_{14}e^{i(\delta_{14}-\delta_{24})} \right) = \frac{1}{s_{34}^2} \sigma_{23}^* (\sigma_{13} - s_{12}\sigma_{23}) \quad \left[= \frac{1}{s_{34}^2} \lambda_{t'}^{(s)*} \lambda_{t'}^{(d)} \right], \\
\lambda_t^{(s)} &\approx -s_{23} - s_{24}s_{34}e^{i\delta_{24}} = -s_{23} - \lambda_{t'}^{(s)}, \\
\lambda_t^{(d)} &\approx -s_{13}e^{i\delta_{13}} - s_{14}s_{34}e^{i\delta_{14}} + s_{12} (s_{23} + s_{24}s_{34}e^{i\delta_{24}}) = -s_{13}e^{i\delta_{13}} + s_{12}s_{23} - \lambda_{t'}^{(d)}, \\
\lambda_t^{(K)} &\approx (s_{23} + s_{24}s_{34}e^{-i\delta_{24}}) (s_{13}e^{i\delta_{13}} + s_{14}s_{34}e^{i\delta_{14}} - s_{12} (s_{23} + s_{24}s_{34}e^{i\delta_{24}})) \\
&= \left(s_{23} + \lambda_{t'}^{(s)*} \right) \left(s_{13}e^{i\delta_{13}} - s_{12}s_{23} + \lambda_{t'}^{(d)} \right), \tag{9.13}
\end{aligned}$$

where the following two combinations of new parameters (9.2) have been introduced:

$$\sigma_{13} \equiv s_{14}s_{34}e^{i\delta_{14}}, \quad \sigma_{23} \equiv s_{24}s_{34}e^{i\delta_{24}}. \tag{9.14}$$

For this particular case, we observe that

- i) $\lambda_t^{(K)}$ and $\lambda_{t'}^{(K)}$ depend on σ_{13} , σ_{23} and s_{34} .
- ii) $\lambda_t^{(d)}$ and $\lambda_{t'}^{(d)}$ depend on σ_{13} and σ_{23} .
- iii) $\lambda_t^{(s)}$ and $\lambda_{t'}^{(s)}$ are sensitive to σ_{23} only. The determination of ΔM_s , $\text{Br}(B_s \rightarrow \mu^+ \mu^-)$ and $S_{\psi\phi}$ will thus play an important role in constraining these parameters. Moreover for $s_{24} \gtrsim s_{23}s_{34}$ and δ_{24} not too small, $S_{\psi\phi}$ should be much larger than its SM3 value $(S_{\psi\phi})_{SM} \approx 0.04$ as we have seen in Section 7.

In view of the many possibilities for theoretical parameters and phenomenological observables, we will in the following develop a general procedure that allows us to analyse future experimental data in a systematic manner. Let us first consider the plots in Fig. 21, which show correlations between various parameters of the SM4, on the basis of the three scenarios of Table 4. In particular,

- in the case of the scenario BS3 of Table 4, there is a strong correlation between s_{24} and s_{14} with $s_{24} \sim 4s_{14}$ and s_{24} in the range

$$0.046 \leq s_{24} \leq 0.17. \tag{9.15}$$

- δ_{14} and δ_{24} are also very strongly correlated in the BS3 scenario with $\delta_{14} \approx \delta_{24} \approx 270^\circ \pm 20^\circ$.
- in the lower left panel of Fig. 21 one can see the strong correlation (2.24) of s_{34} and $m_{t'}$. We checked numerically that treating the EWPT in this approximate manner indeed gives reasonable bounds on $m_{t'}$.

In the following section, we will analyse these correlations within specific scaling scenarios for the 4G mixing angles.

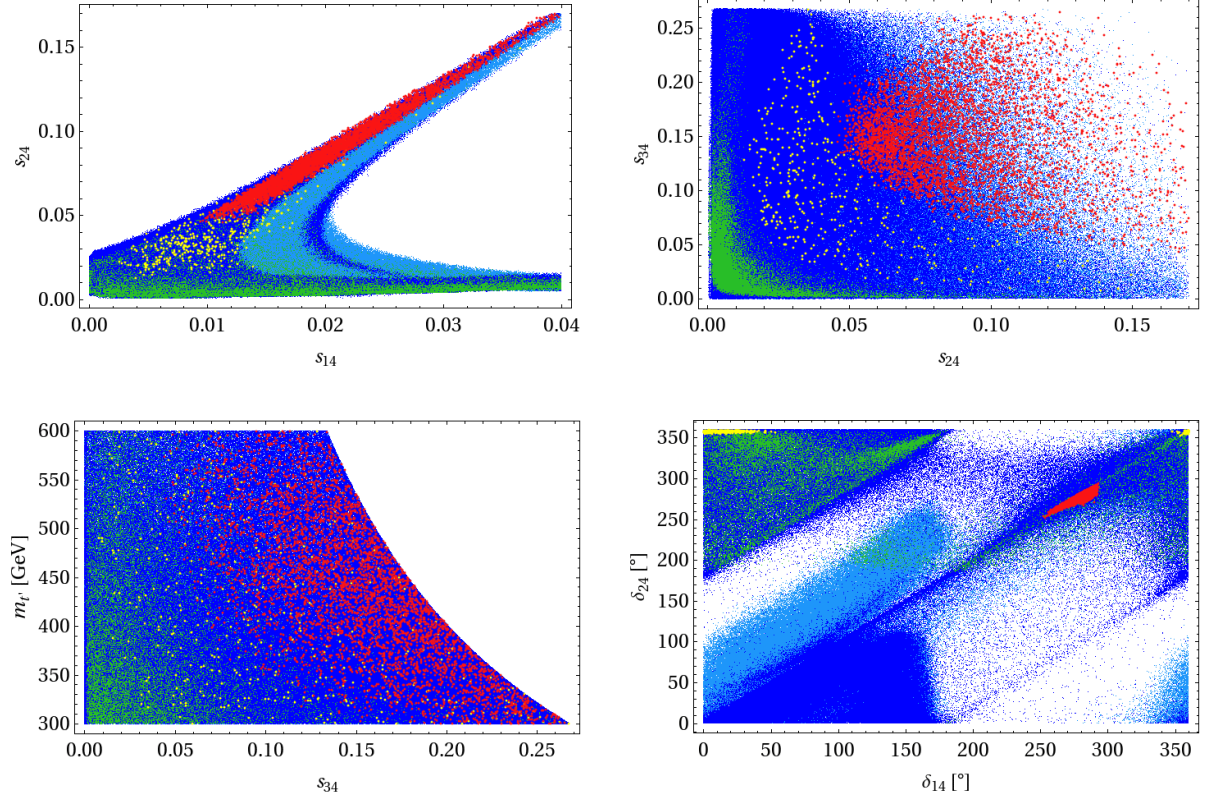


Figure 21: Correlations between the new parameters for the parameter points used in our global analysis. The mixing angle s_{24} as a function of s_{14} (upper left panel), s_{34} as a function of s_{24} (upper right panel), $m_{t'}$ as a function of s_{34} (lower left panel) and δ_{24} as a function of δ_{14} (lower right panel). The colour coding corresponds to scenarios of Table 4.

9.3 Anatomy of 4G mixing angles and CP phases

As explained in Section 2, the 4G mixing matrix allows for different scalings of the 4G mixing angles θ_{14} , θ_{24} and θ_{34} with the Wolfenstein parameter $\lambda \ll 1$. Among the set of parameters that fulfil the present constraints on flavour observables, we may thus classify different subsets by calculating the exponents

$$(n_1, n_2, n_3) = \text{round}(\log_\lambda [\theta_{14}, \theta_{24}, \theta_{34}]) , \quad (9.16)$$

in (2.28) for $\lambda = s_{12} \ll 1$. Furthermore (see also Fig. 21), for a given set (n_1, n_2, n_3) , the allowed values for the new CP phases δ_{14} and δ_{24} also exhibit a more or less strong correlation, which we will exploit to further distinguish different regions in the 4G parameter space. This enables us to identify a set of equivalence classes which – as we will illustrate – share certain characteristic features for the corresponding predictions for various flavour observables.

According to our discussion above, values (n_1, n_2, n_3) that do not fulfil the inequalities (2.9), from the theoretical point of view, should be considered as fine-tuned and will not be included in the subsequent discussion. (We convinced ourselves that we do not miss any of the observed phenomenological features by doing so.) For the remaining cases, we first identify – for a given scaling (n_1, n_2, n_3) – the allowed correlations between δ_{14} and δ_{24} , and then determine the assignment to one or the other equivalence class. Our procedure is summarised for the most prominent and representative examples in Table 8:

- Evidently, for small values of the n_i (i.e. large values of 4G mixing angles), one expects the largest deviations from the SM3 predictions. In fact, the most extreme case is characterised by example (2.14) from Section 2, with values $(n_1, n_2, n_3) = (2, 1, 1)$. As we already discussed, in this scenario the new 4G phases contribute at leading order to CP-violating observables, and therefore δ_{14} and δ_{24} are highly correlated and constrained. Separating the different relative and absolute signs of δ_{i4} enables us to classify the subsets 1a, 1b, 2a, 2b which show characteristic features in the selected set of observables shown in Tables 9+10. Similar correlations are found for the $(2, 2, 1)$ scenario.
- Decreasing the values of (some of) the mixing angles (i.e. increasing n_1, n_2, n_3), we observe that the correlations between the 4G phases become broader. Still, the values populate restricted areas in the δ_{24} – δ_{14} plane, which again allows to identify sub-classes with definite properties. A typical example is the case $(3, 2, 1)$ from our benchmark scenario (2.17). This scenario divides into two well-separated regions. Among one of them, we may (or may not) identify a subset of points as belonging to class 1a. This kind of arbitrariness is unavoidable (and expected), since the separation of points from scenario $(2, 2, 1)$ and $(3, 2, 1)$ is not clear-cut.

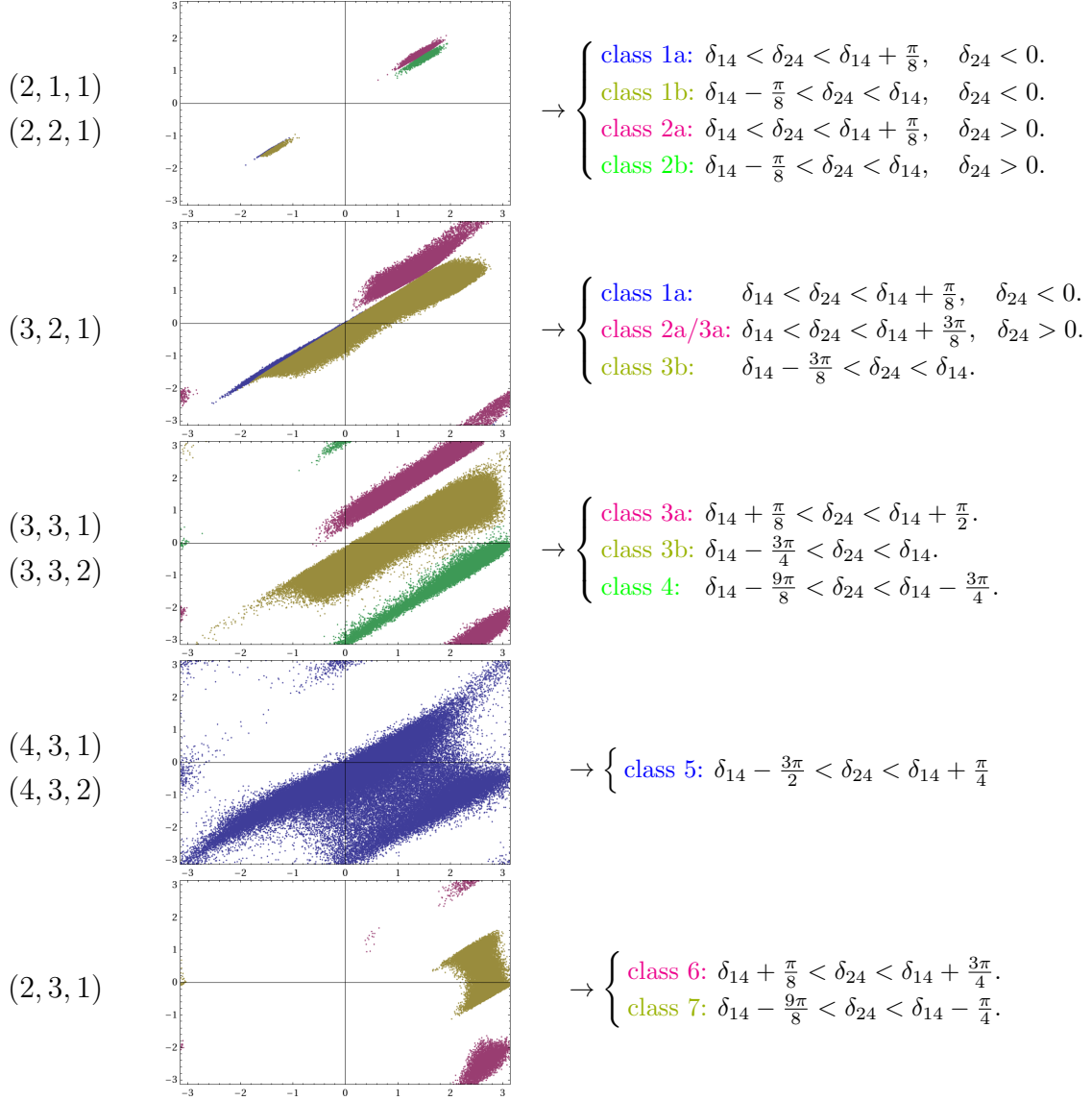


Table 8: Correlations between 4G phases for different scalings of 4G mixing angles (some selected examples). The constraints on the phases, of course, are understood to be periodic in units of 2π .

- For even smaller values of mixing angles, we observe for the cases (3, 3, 1) and (3, 3, 2) a separation into three sub-classes, where two classes (3a and 3b) can be considered as a continuation of those from the (3, 2, 1) scenario, and class 4 is new.
- Considering (4, 3, 1) (the benchmark scenario (2.12) discussed in Section 2) and (4, 3, 2), the former classes 3b and 4 merge into one class 5 which already covers around half of the δ_{24} - δ_{14} plane. Finally, for the scenario (2.16) with the scaling (2, 3, 1), the former class 3a continues into class 6, while 3b and 4 merge into class 7, where the parameter space in the δ_{24} - δ_{14} plane is again somewhat more constrained.

Having identified the different sub-classes, we investigate the characteristic features for certain phenomenological observables in Tables 9-12. We see that each class can be distinguished from the others by at least one of the shown correlations: $\text{Br}(B_s \rightarrow \mu^+ \mu^-)$ vs. $S_{\psi\phi}$, $S_{\phi K_S}$ vs. $S_{\psi\phi}$, $\text{Br}(b \rightarrow s\gamma)$ vs. $\text{Br}(B \rightarrow X_s \ell\ell)$, $\text{Br}(K_L \rightarrow \mu^+ \mu^-)_{\text{SD}}$ vs. $\text{Br}(K^+ \rightarrow \pi^+ \nu \bar{\nu})$ (The colour-coding is as defined in Table 4).

Turning the argument around, the observation of a combination of particular correlations in rare flavour processes can be translated into one or the other favoured scenario for 4G mixing angles and CP phases. Only after a particular scaling scenario has been identified, the formulae for $\lambda_{\ell'}^{(K,d,s)}$ in (9.9–9.11) can be simplified, and we may (more or less) unambiguously determine the 4G mixing parameters from the future experimental data. We emphasise that, quite generally, such a procedure should be applied to the analysis of flavour parameters in NP models without MFV. In particular, without a specific theory of flavour at hand, the fact that certain scaling scenarios – like (2.12) – are represented by only a small number of points in the overall scan of parameter space, should not be taken as a signal for a small probability to observe the associated correlations in flavour observables.

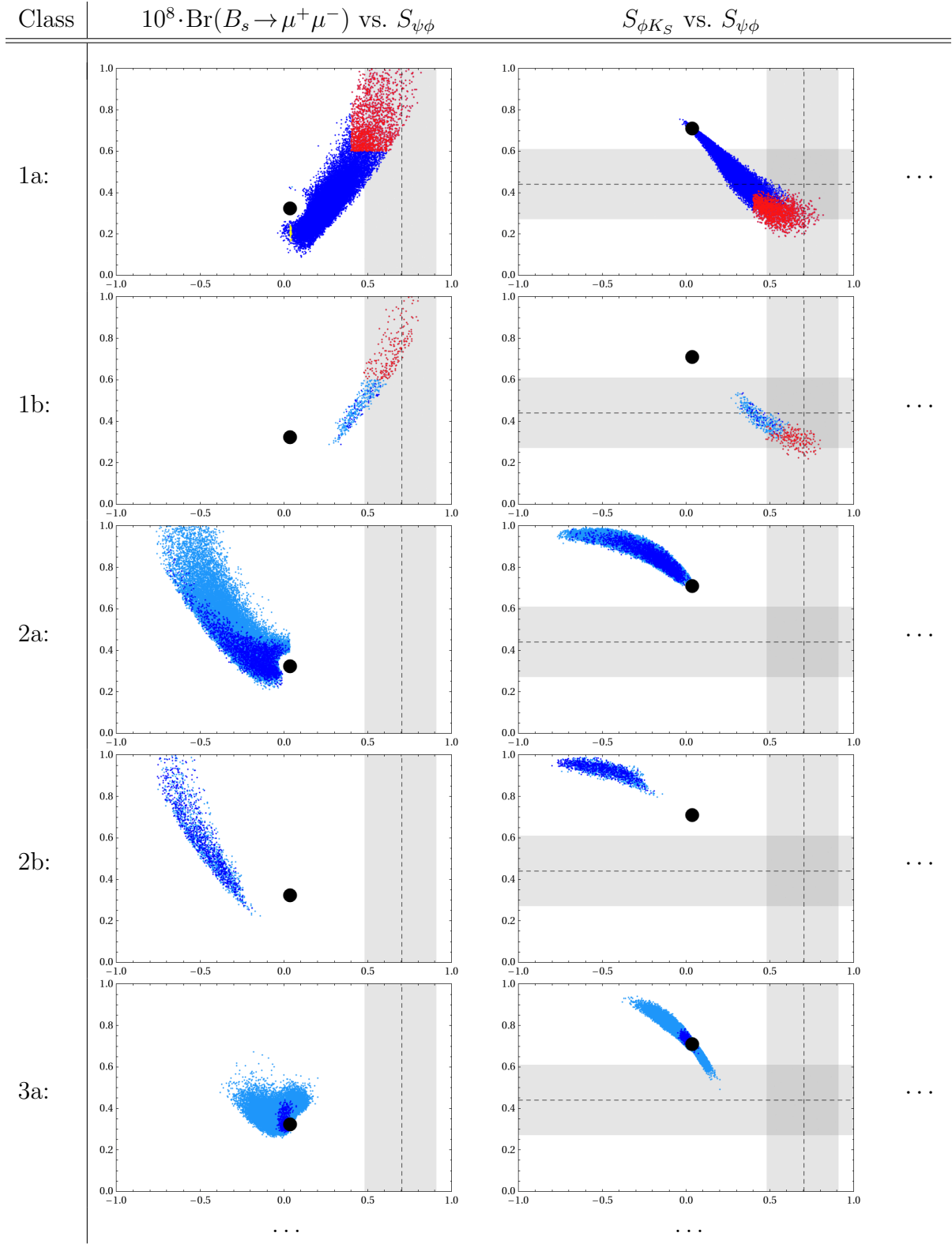


Table 9: Selected correlations for classes identified in Table 8 (part 1 of 4). (The colour-coding is as defined in Table 4).

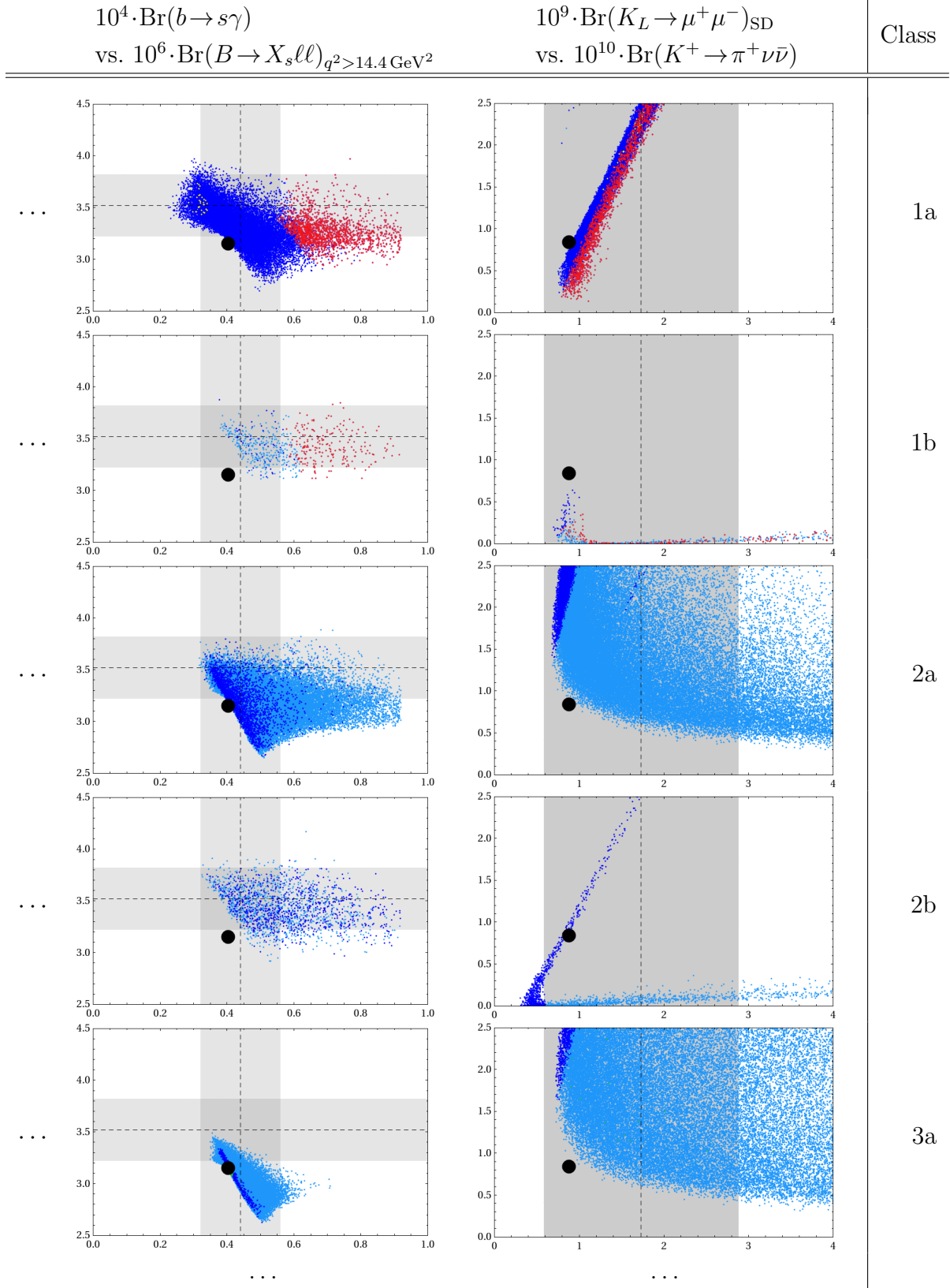


Table 10: Selected correlations for classes identified in Table 8 (part 2 of 4).

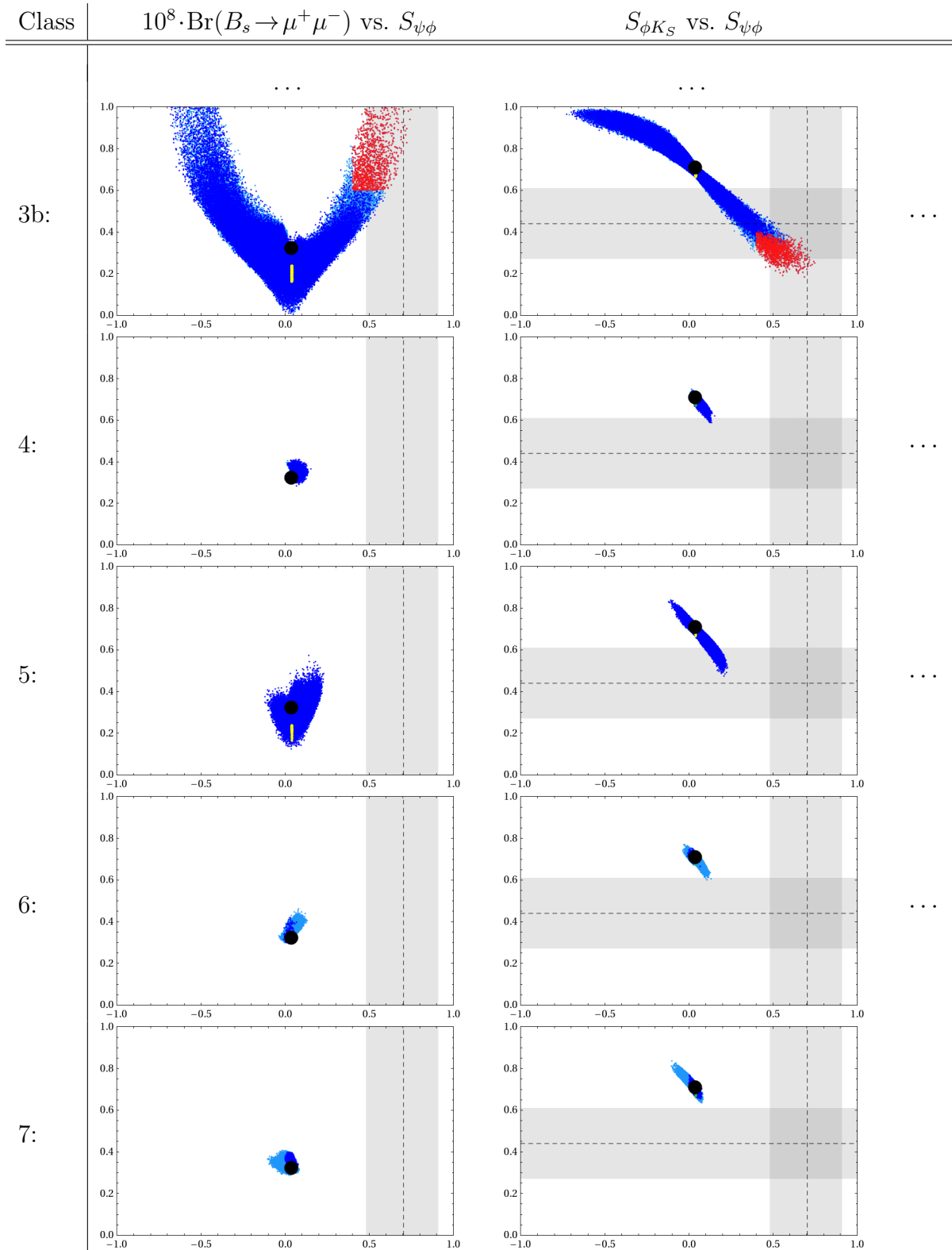


Table 11: Selected correlations for classes identified in Table 8 (part 3 of 4).

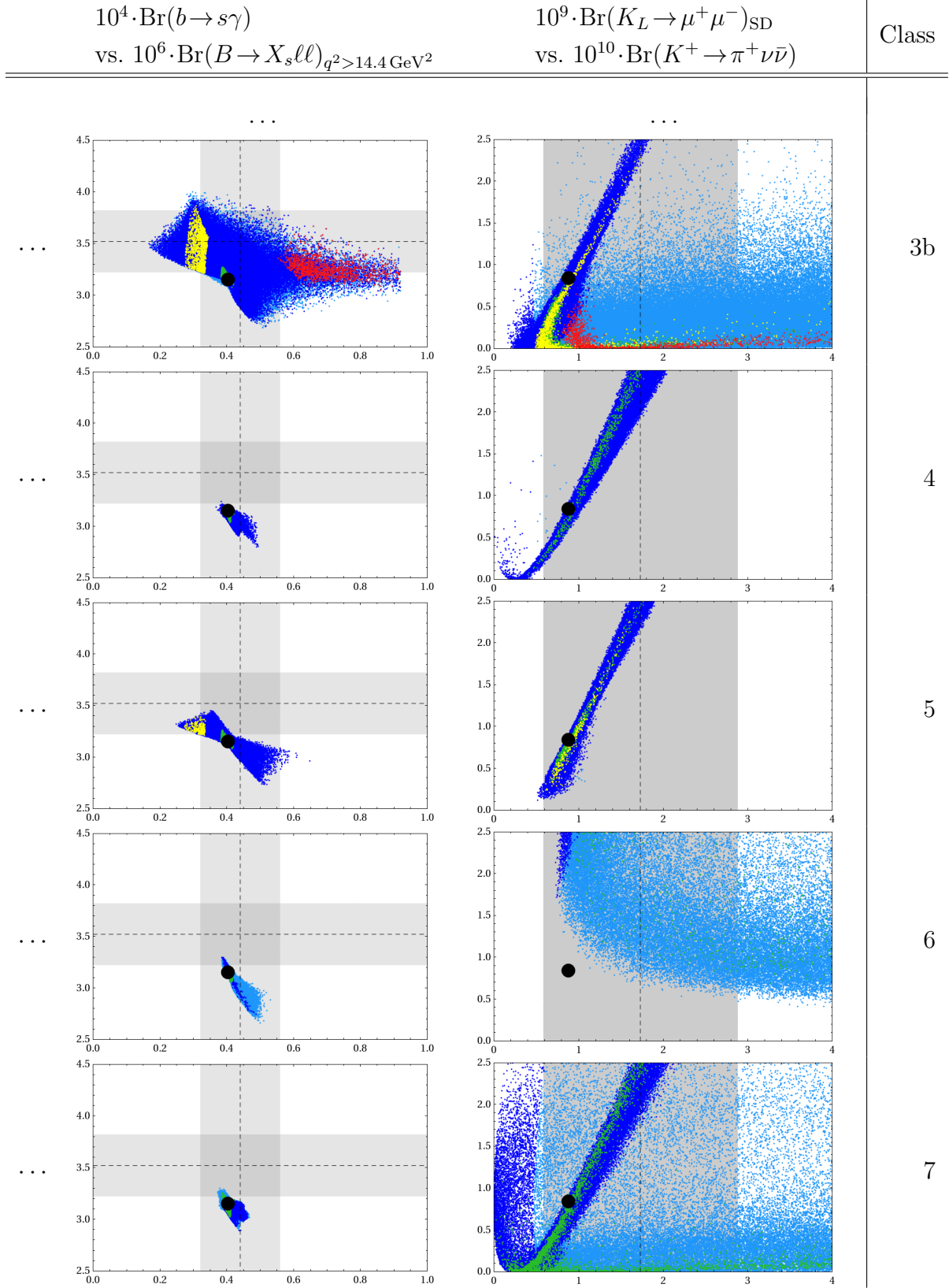


Table 12: Selected correlations for classes identified in Table 8 (part 4 of 4).

10 Summary and Conclusions

In the present paper we have performed a detailed analysis of non-MFV effects in the K , B_d and B_s systems in the SM4, paying particular attention to correlations between various flavour observables and addressing within this framework a number of anomalies present in the experimental data.

Similarly as in the LHT model, the RSc model and supersymmetric flavour models that have been analysed in [31–36], the correlations between various observables that are characteristic for models with MFV and in particular with CMFV can be strongly violated in the SM4 while still satisfying all existing data on flavour violating processes and electroweak precision observables.

Probably, the most striking signature of the SM4, compared to the LHT, RSc and SUSY flavour models, is the possibility of having simultaneously sizable NP effects in the K , B_d and B_s systems, even if truly spectacular effects are only possible in rare K decays with the prominent exception of $S_{\psi\phi}$ which can also be enhanced by an order of magnitude. This different pattern can be traced back to the fact that the mass scales involved in the SM4 are generally significantly lower than in the LHT and in particular in the RSc. Also the non-decoupling of the new heavy fermions t' and b' plays a role here, whereas an analogous effect does not occur in the LHT, RSc and SUSY.

We recall that in SUSY flavour models, NP effects in the K system are small but can be large in B physics observables to which dipole operators and scalar operators contribute. In models with right-handed currents also $S_{\psi\phi}$ can be large. In the LHT and RSc models, large effects are found predominantly in rare K decays, although $S_{\psi\phi}$ can also be sizable. These three different global patterns of flavour violation in the models in question could help one day to distinguish between these NP scenarios.

The most interesting patterns of flavour violation in the SM4 are the following ones.

- All existing tensions in the UT fits can be removed in this NP scenario.
- In particular the desire to explain the $S_{\psi\phi}$ anomaly implies, as seen in Fig. 3, uniquely the suppressions of the CP asymmetries $S_{\phi K_S}$ and $S_{\eta' K_S}$ in agreement with the data. This correlation has been pointed out in [15, 148, 149], and we confirm it here. However we observe that for $S_{\psi\phi}$ significantly larger than 0.6 the values of $S_{\phi K_S}$ and $S_{\eta' K_S}$ are below their central values indicated by the data.
- The same anomaly implies a sizable enhancement of $\text{Br}(B_s \rightarrow \mu^+ \mu^-)$ over the SM3 prediction although this effect is much more modest than in SUSY models where the Higgs penguin with large $\tan \beta$ is at work. Yet, values as high as $8 \cdot 10^{-9}$ are certainly possible in the SM4, which is well beyond those attainable in the LHT model and the RSc model.

- Possible enhancements of $\text{Br}(K^+ \rightarrow \pi^+\nu\bar{\nu})$ and $\text{Br}(K_L \rightarrow \pi^0\nu\bar{\nu})$ over the SM3 values are much larger than found in the LHT and RSc models and in particular in SUSY flavour models where they are SM3 like. Both branching ratios as high as several 10^{-10} are still possible in the SM4. Moreover, in this case, the two branching ratios are strongly correlated as seen in Fig. 7 and close to the GN bound. For an earlier analysis see [13].
- Interestingly, in contrast to the LHT and RSc models, a high value of $S_{\psi\phi}$ does not preclude a sizable enhancements of $\text{Br}(K^+ \rightarrow \pi^+\nu\bar{\nu})$, and $\text{Br}(K_L \rightarrow \pi^0\nu\bar{\nu})$.
- NP effects in $K_L \rightarrow \pi^0\ell^+\ell^-$ and $K_L \rightarrow \mu^+\mu^-$ can be visibly larger than in the LHT and RSc models. In particular $\text{Br}(K_L \rightarrow \mu^+\mu^-)_{\text{SD}}$ can easily violate the existing bound of $2.5 \cdot 10^{-9}$. Imposition of this bound on top of other constraints results in a characteristic shape of the correlation between $\text{Br}(K^+ \rightarrow \pi^+\nu\bar{\nu})$ and $\text{Br}(K_L \rightarrow \pi^0\nu\bar{\nu})$ shown in Fig. 7.
- The magnitude of the CP asymmetry $A_{\text{CP}}^{bs\gamma}$ remains small, but the desire to explain large values of $S_{\psi\phi}$ reverses its sign.
- Even in the presence of SM-like values for $S_{\psi\phi}$ and $\text{Br}(B_s \rightarrow \mu^+\mu^-)$, large effects in the K -system are possible as illustrated by green points in numerous plots.
- For large positive values of $S_{\psi\phi}$ the predicted value of ε'/ε is significantly below the data, unless the hadronic matrix elements of the electroweak penguins are sufficiently suppressed with respect to the large N result and the ones of QCD penguins enhanced.
- We have also reemphasised [120, 121] the important role ε'/ε will play in bounding rare K decay branching ratios once the relevant hadronic matrix elements in ε'/ε will be precisely known (see Sec. 7.12 for more details).

Other 4G effects in various observables and correlations between them can be found in numerous plots in Sections 7–9. In particular, in Section 9, we have addressed the question of the determination of the parameters of the SM4 with the help of future measurements employing various scenarios for the scalings of the 4G mixing matrix angles θ_{14}, θ_{24} and θ_{34} with the Wolfenstein parameter $\lambda \ll 1$.

In summary, the SM4 offers a very rich pattern of flavour violation which can be tested already in the coming years, in particular through precise measurements of $S_{\psi\phi}$, $\text{Br}(B_q \rightarrow \mu^+\mu^-)$, $\text{Br}(K^+ \rightarrow \pi^+\nu\bar{\nu})$ and, later, $S_{\phi K_s}$, $S_{\eta' K_s}$ and $\text{Br}(K_L \rightarrow \pi^0\nu\bar{\nu})$. Also, precise measurements of the phase $\gamma \approx \delta_{13}$ will be important for this investigation. We close our detailed analysis with the following important question: Can the SM4 be

excluded by precise measurements of FCNC processes? The answer is positive, provided large departures from the SM3 are observed with a different pattern of deviation from the SM3 predictions than found in our analysis. Let us just list three examples:

- Large values of $S_{\psi\phi} > 0.6$ accompanied with SM-like values of $\text{Br}(B_s \rightarrow \mu^+\mu^-)$ will clearly disfavour the SM4 as the explanation of the $S_{\psi\phi}$ anomaly.
- Similarly, such large values accompanied by the observation of $S_{\phi K_s} \approx S_{\eta' K_s} \approx S_{\psi K_s}$ would also put the SM4 into difficulties.
- Finally, $S_{\psi\phi} > 0.3$ accompanied by the ε'/ε relevant $R_6 \approx R_8 \approx 1$ from future lattice calculations will disfavour SM4 by means of the measured ε'/ε .

It is evident from our analysis and other analyses mentioned in the beginning of our paper that FCNC processes will contribute in a profound manner to the search for the 4G quarks and leptons and, in the case of direct discovery, to the exploration of the structure of their weak mixings. We hope that our numerous plots will help in monitoring the future data from LHC and high-intensity experiments, with the hope to firmly establish or firmly exclude the presence of the fourth sequential generation of quarks in nature.

Note added

Very recently, during the final stages of our work, a detailed study of rare K and B decays has been presented in [140], see also the discussion in Section 7.3.

Acknowledgements

We would like to thank Wolfgang Altmannshofer, Monika Blanke, Amarjit Soni and Soumitra Nandi for illuminating discussions. This research was partially supported by the Cluster of Excellence ‘Origin and Structure of the Universe’, the Graduiertenkolleg GRK 1054 of DFG and by the German ‘Bundesministerium für Bildung und Forschung’ under contract 05H09WOE.

A Relevant Functions

$$X_0(x_i) = \frac{x_i}{8} \left[\frac{x_i + 2}{x_i - 1} + \frac{3x_i - 6}{(x_i - 1)^2} \log x_i \right], \quad (\text{A.1})$$

$$Y_0(x_i) = \frac{x_i}{8} \left[\frac{x_i - 4}{x_i - 1} + \frac{3x_i}{(x_i - 1)^2} \log x_i \right], \quad (\text{A.2})$$

$$Z_0(x_i) = -\frac{1}{9} \log x_i + \frac{18x_i^4 - 163x_i^3 + 259x_i^2 - 108x_i}{144(x_i - 1)^3} + \frac{32x_i^4 - 38x_i^3 - 15x_i^2 + 18x_i}{72(x_i - 1)^4} \log x_i. \quad (\text{A.3})$$

$$C_0(x_i) = \frac{x_i}{8} \left[\frac{x_i - 6}{x_i - 1} + \frac{3x_i + 2}{(x_i - 1)^2} \log x_i \right], \quad (\text{A.4})$$

$$D_0(x_i) = -\frac{4}{9} \log x_i + \frac{-19x_i^3 + 25x_i^2}{36(x_i - 1)^3} + \frac{x_i^2(5x_i^2 - 2x_i - 6)}{18(x_i - 1)^4} \log x_i, \quad (\text{A.5})$$

$$E_0(x_i) = -\frac{2}{3} \log x_i + \frac{x_i^2(15 - 16x_i + 4x_i^2)}{6(x_i - 1)^4} \log x_i + \frac{x_i(18 - 11x_i - x_i^2)}{12(1 - x_i)^3}, \quad (\text{A.6})$$

$$D'_0(x_i) = -\frac{(3x_i^3 - 2x_i^2)}{2(x_i - 1)^4} \log x_i + \frac{(8x_i^3 + 5x_i^2 - 7x_i)}{12(x_i - 1)^3}, \quad (\text{A.7})$$

$$E'_0(x_i) = \frac{3x_i^2}{2(x_i - 1)^4} \log x_i + \frac{(x_i^3 - 5x_i^2 - 2x_i)}{4(x_i - 1)^3}. \quad (\text{A.8})$$

$$B^{\mu\bar{\mu}}(x_i, y_j) = \frac{1}{4} \left[U(x_i, y_j) + \frac{x_i y_j}{4} U(x_i, y_j) - 2x_i y_j \tilde{U}(x_i, y_j) \right], \quad (\text{A.9})$$

$$B^{\nu\bar{\nu}}(x_i, y_j) = \frac{1}{4} \left[U(x_i, y_j) + \frac{x_i y_j}{16} U(x_i, y_j) + \frac{x_i y_j}{2} \tilde{U}(x_i, y_j) \right], \quad (\text{A.10})$$

with

$$U(x_1, x_2) = \frac{x_1^2 \log x_1}{(x_1 - x_2)(1 - x_1)^2} + \frac{x_2^2 \log x_2}{(x_2 - x_1)(1 - x_2)^2} + \frac{1}{(1 - x_1)(1 - x_2)}, \quad (\text{A.11})$$

$$\tilde{U}(x_1, x_2) = \frac{x_1 \log x_1}{(x_1 - x_2)(1 - x_1)^2} + \frac{x_2 \log x_2}{(x_2 - x_1)(1 - x_2)^2} + \frac{1}{(1 - x_1)(1 - x_2)}. \quad (\text{A.12})$$

$S_0(x_i, x_j)$ for arbitrary x_i, x_j is given by [59]

$$S_0(x_i, x_j) = x_i x_j \left(\frac{(4 - 8x_j + x_j^2) \log x_j}{4(x_j - 1)^2(x_j - x_i)} + (i \leftrightarrow j) - \frac{3}{4(x_i - 1)(x_j - 1)} \right). \quad (\text{A.13})$$

In the limit of $\varepsilon \rightarrow 0$ in $S_0(x_i + \varepsilon, x_i - \varepsilon)$ one recovers the SM3 version of $S_0(x_i)$,

$$S_0(x_i) = \frac{x_i}{4} \frac{-4 + 15x_i - (12 - 6 \log x_i)x_i^2 + x_i^3}{(x_i - 1)^3}. \quad (\text{A.14})$$

References

- [1] P. H. Frampton, P. Q. Hung, and M. Sher, *Quarks and leptons beyond the third generation*, *Phys. Rept.* **330** (2000) 263, [hep-ph/9903387](#) .
- [2] M. Maltoni, V. A. Novikov, L. B. Okun, A. N. Rozanov, and M. I. Vysotsky, *Extra quark-lepton generations and precision measurements*, *Phys. Lett.* **B476** (2000) 107–115, [hep-ph/9911535](#) .
- [3] H.-J. He, N. Polonsky, and S. fang Su, *Extra families, Higgs spectrum and oblique corrections*, *Phys. Rev.* **D64** (2001) 053004, [hep-ph/0102144](#) .
- [4] J. Alwall *et al.*, *Is $V_{tb} \simeq 1$?*, *Eur. Phys. J.* **C49** (2007) 791–801, [hep-ph/0607115](#) .
- [5] G. D. Kribs, T. Plehn, M. Spannowsky, and T. M. P. Tait, *Four generations and Higgs physics*, *Phys. Rev.* **D76** (2007) 075016, [0706.3718](#) .
- [6] M. S. Chanowitz, *Bounding CKM Mixing with a Fourth Family*, *Phys. Rev.* **D79** (2009) 113008, [0904.3570](#) .
- [7] V. A. Novikov, A. N. Rozanov, and M. I. Vysotsky, *Once more on extra quark-lepton generations and precision measurements*, [0904.4570](#).
- [8] M. Hashimoto, *Constraints on Mass Spectrum of Fourth Generation Fermions and Higgs Bosons*, [1001.4335](#).
- [9] P. Q. Hung, *Minimal $SU(5)$ resuscitated by long-lived quarks and leptons*, *Phys. Rev. Lett.* **80** (1998) 3000–3003, [hep-ph/9712338](#) .
- [10] W.-S. Hou, *CP Violation and Baryogenesis from New Heavy Quarks*, *Chin. J. Phys.* **47** (2009) 134, [0803.1234](#) .
- [11] Y. Kikukawa, M. Kohda, and J. Yasuda, *The strongly coupled fourth family and a first-order electroweak phase transition (I) Quark sector*, *Prog. Theor. Phys.* **122** (2009) 401–426, [0901.1962](#) .
- [12] R. Fok and G. D. Kribs, *Four Generations, the Electroweak Phase Transition, and Supersymmetry*, *Phys. Rev.* **D78** (2008) 075023, [0803.4207](#) .
- [13] W.-S. Hou, M. Nagashima, and A. Soddu, *Enhanced $K_L \rightarrow \pi^0 \nu \bar{\nu}$ from direct CP violation in $B \rightarrow K\pi$ with four generations*, *Phys. Rev.* **D72** (2005) 115007, [hep-ph/0508237](#) .

- [14] W.-S. Hou, M. Nagashima, and A. Soddu, *Large time-dependent CP violation in B_s^0 system and finite $D^0 - \bar{D}^0$ mass difference in four generation standard model*, *Phys. Rev.* **D76** (2007) 016004, [hep-ph/0610385](#) .
- [15] A. Soni, A. K. Alok, A. Giri, R. Mohanta, and S. Nandi, *The Fourth family: A Natural explanation for the observed pattern of anomalies in B-CP asymmetries*, 0807.1971.
- [16] G. Burdman, L. Da Rold, and R. D. Matheus, *The Lepton Sector of a Fourth Generation*, 0912.5219.
- [17] B. Holdom, *Heavy quarks and electroweak symmetry breaking*, *Phys. Rev. Lett.* **57** (1986) 2496.
- [18] C. T. Hill, M. A. Luty, and E. A. Paschos, *Electroweak symmetry breaking by fourth generation condensates and the neutrino spectrum*, *Phys. Rev.* **D43** (1991) 3011–3025.
- [19] S. F. King, *Is electroweak symmetry broken by a fourth family of quarks?* , *Phys. Lett.* **B234** (1990) 108–112.
- [20] G. Burdman and L. Da Rold, *Electroweak Symmetry Breaking from a Holographic Fourth Generation*, *JHEP* **12** (2007) 086, [0710.0623](#) .
- [21] P. Q. Hung and C. Xiong, *Renormalization Group Fixed Point with a Fourth Generation: Higgs-induced Bound States and Condensates*, 0911.3890.
- [22] P. Q. Hung and C. Xiong, *Renormalization Group Fixed Point with a Fourth Generation: Solution to the hierarchy problem*, 0911.3892.
- [23] B. Holdom, *Approaching a strong fourth family*, *Phys. Lett.* **B686** (2010) 146–151, [1001.5321](#) .
- [24] B. Holdom *et al.*, *Four Statements about the Fourth Generation*, 0904.4698.
- [25] A. Arhrib and W.-S. Hou, *Effect of fourth generation CP phase on $b \rightarrow s$ transitions*, *Eur. Phys. J.* **C27** (2003) 555–561, [hep-ph/0211267](#) .
- [26] J. A. Herrera, R. H. Benavides, and W. A. Ponce, *Flavor changing neutral currents with a fourth family of quarks*, *Phys. Rev.* **D78** (2008) 073008, [0810.3871](#) .
- [27] M. Bobrowski, A. Lenz, J. Riedl, and J. Rohrwild, *How much space is left for a new family of fermions?*, *Phys. Rev.* **D79** (2009) 113006, [0902.4883](#) .

- [28] G. Eilam, B. Melic, and J. Trampetic, *CP violation and the 4th generation*, *Phys. Rev.* **D80** (2009) 116003, 0909.3227 .
- [29] Z. Murdock, S. Nandi, and Z. Tavartkiladze, *Perturbativity and a Fourth Generation in the MSSM*, *Phys. Lett.* **B668** (2008) 303–307, 0806.2064 .
- [30] R. M. Godbole, S. K. Vempati, and A. Wingerter, *Four Generations: SUSY and SUSY Breaking*, 0911.1882.
- [31] M. Blanke *et al.*, *Particle antiparticle mixing, ϵ_K , $\Delta(\Gamma(q))$, $A_{SL}(q)$, $A_{CP}(B_d \rightarrow \psi K_S)$, $A_{CP}(B_s \rightarrow \psi \phi)$ and $B \rightarrow X_{s,d} \gamma$ in the littlest Higgs model with T-parity*, *JHEP* **12** (2006) 003, hep-ph/0605214 .
- [32] M. Blanke *et al.*, *Rare and CP-Violating K and B Decays in the Littlest Higgs Model with T-Parity*, *JHEP* **01** (2007) 066, hep-ph/0610298 .
- [33] M. Blanke, A. J. Buras, B. Duling, S. Recksiegel, and C. Tarantino, *FCNC Processes in the Littlest Higgs Model with T-Parity: a 2009 Look*, *Acta Phys. Polon. B* **41** (2010) 657, 0906.5454 .
- [34] M. Blanke, A. J. Buras, B. Duling, S. Gori, and A. Weiler, *$\Delta F = 2$ Observables and Fine-Tuning in a Warped Extra Dimension with Custodial Protection*, *JHEP* **03** (2009) 001, 0809.1073 .
- [35] M. Blanke, A. J. Buras, B. Duling, K. Gemmler, and S. Gori, *Rare K and B Decays in a Warped Extra Dimension with Custodial Protection*, *JHEP* **03** (2009) 108, 0812.3803 .
- [36] W. Altmannshofer, A. J. Buras, S. Gori, P. Paradisi, and D. M. Straub, *Anatomy and Phenomenology of FCNC and CPV Effects in SUSY Theories*, *Nucl. Phys.* **B830** (2010) 17–94, 0909.1333 .
- [37] G. D’Ambrosio, G. F. Giudice, G. Isidori, and A. Strumia, *Minimal flavour violation: An effective field theory approach*, *Nucl. Phys.* **B645** (2002) 155–187, hep-ph/0207036 .
- [38] T. Feldmann, M. Jung, and T. Mannel, *Sequential Flavour Symmetry Breaking*, *Phys. Rev.* **D80** (2009) 033003, 0906.1523 .
- [39] A. Santamaria, *Masses, mixings, Yukawa couplings and their symmetries*, *Phys. Lett.* **B305** (1993) 90–97, hep-ph/9302301 .

- [40] J. Berger and Y. Grossman, *Parameter counting in models with global symmetries*, *Phys. Lett.* **B675** (2009) 365–370, 0811.1019 .
- [41] T. Feldmann and T. Mannel, *Minimal Flavour Violation and Beyond*, *JHEP* **02** (2007) 067, hep-ph/0611095 .
- [42] T. Feldmann and T. Mannel, *Large Top Mass and Non-Linear Representation of Flavour Symmetry*, *Phys. Rev. Lett.* **100** (2008) 171601, 0801.1802 .
- [43] A. L. Kagan, G. Perez, T. Volansky, and J. Zupan, *General Minimal Flavor Violation*, *Phys. Rev.* **D80** (2009) 076002, 0903.1794 .
- [44] C. D. Froggatt and H. B. Nielsen, *Hierarchy of Quark Masses, Cabibbo Angles and CP Violation*, *Nucl. Phys.* **B147** (1979) 277.
- [45] H. Fritzsch and J. Plankl, *The Mixing of Quark Flavors*, *Phys. Rev.* **D35** (1987) 1732.
- [46] H. Harari and M. Leurer, *Recommending a Standard Choice of Cabibbo Angles and KM Phases for Any Number of Generations*, *Phys. Lett.* **B181** (1986) 123.
- [47] A. A. Anselm, J. L. Chkareuli, N. G. Uraltsev, and T. A. Zhukovskaya, *On the Kobayashi-Maskawa model with four generations*, *Phys. Lett.* **B156** (1985) 102–108.
- [48] L. Wolfenstein, *Parametrization of the Kobayashi-Maskawa Matrix*, *Phys. Rev. Lett.* **51** (1983) 1945.
- [49] A. J. Buras, M. E. Lautenbacher, and G. Ostermaier, *Waiting for the top quark mass, $K^+ \rightarrow \pi^+ \nu \bar{\nu}$, $B_s^0 - \bar{B}_s^0$ mixing and CP asymmetries in B decays*, *Phys. Rev.* **D50** (1994) 3433–3446, hep-ph/9403384 .
- [50] W.-S. Hou, A. Soni, and H. Steger, *Effects of a Fourth Family on $b \rightarrow s\gamma$ and a Useful Parametrization of Quark Mixing for Rare B Decays*, *Phys. Lett.* **B192** (1987) 441.
- [51] C. Jarlskog, *Commutator of the Quark Mass Matrices in the Standard Electroweak Model and a Measure of Maximal CP Violation*, *Phys. Rev. Lett.* **55** (1985) 1039.
- [52] C. Jarlskog, *A Basis Independent Formulation of the Connection Between Quark Mass Matrices, CP Violation and Experiment*, *Z. Phys.* **C29** (1985) 491–497.

- [53] F. del Aguila and J. A. Aguilar-Saavedra, *Invariant formulation of CP violation for four quark families*, *Phys. Lett.* **B386** (1996) 241–246, [hep-ph/9605418](#) .
- [54] G. Buchalla, A. J. Buras, and M. E. Lautenbacher, *Weak Decays Beyond Leading Logarithms*, *Rev. Mod. Phys.* **68** (1996) 1125–1144, [hep-ph/9512380](#) .
- [55] G. Buchalla and A. J. Buras, *The rare decays $K \rightarrow \pi \nu \bar{\nu}$, $B \rightarrow X \nu \bar{\nu}$ and $B \rightarrow \ell^+ \ell^-$: An update*, *Nucl. Phys.* **B548** (1999) 309–327, [hep-ph/9901288](#) .
- [56] M. Misiak and J. Urban, *QCD corrections to FCNC decays mediated by Z-penguins and W-boxes*, *Phys. Lett.* **B451** (1999) 161–169, [hep-ph/9901278](#) .
- [57] M. Gorbahn and U. Haisch, *Charm quark contribution to $K_L \rightarrow \mu^+ \mu^-$ at next-to-next-to-leading order*, *Phys. Rev. Lett.* **97** (2006) 122002, [hep-ph/0605203](#) .
- [58] G. Buchalla, A. J. Buras, and M. K. Harlander, *Penguin box expansion: Flavor changing neutral current processes and a heavy top quark*, *Nucl. Phys.* **B349** (1991) 1–47.
- [59] A. J. Buras, W. Slominski, and H. Steger, *B Meson Decay, CP Violation, Mixing Angles and the Top Quark Mass*, *Nucl. Phys.* **B238** (1984) 529.
- [60] A. J. Buras, *Weak Hamiltonian, CP violation and rare decays*, [hep-ph/9806471](#).
- [61] A. J. Buras and D. Guadagnoli, *Correlations among new CP violating effects in $\Delta F = 2$ observables*, *Phys. Rev.* **D78** (2008) 033005, [0805.3887](#) .
- [62] J. Laiho, R. S. Van de Water, and E. Lunghi, *Lattice QCD inputs to the CKM unitarity triangle analysis*, [0910.2928](#).
- [63] A. J. Buras, D. Guadagnoli, and G. Isidori, *On ϵ_K beyond lowest order in the Operator Product Expansion*, [1002.3612](#).
- [64] **CDF Collaboration**, T. Aaltonen *et al.*, *First Flavor-Tagged Determination of Bounds on Mixing-Induced CP Violation in $B_s^0 \rightarrow J/\psi \phi$ Decays*, *Phys. Rev. Lett.* **100** (2008) 161802, [0712.2397](#) .
- [65] **D0 Collaboration**, V. M. Abazov *et al.*, *Measurement of B_s^0 mixing parameters from the flavor-tagged decay $B_s^0 \rightarrow J/\psi \phi$* , *Phys. Rev. Lett.* **101** (2008) 241801, [0802.2255](#) .
- [66] **Heavy Flavor Averaging Group Collaboration**, E. Barberio *et al.*, *Averages of b-hadron and c-hadron Properties at the End of 2007*, [0808.1297](#).

- [67] A. J. Buras, *Relations between $\Delta M_{s,d}$ and $B_{s,d} \rightarrow \mu\bar{\mu}$ in models with minimal flavour violation*, *Phys. Lett.* **B566** (2003) 115–119, hep-ph/0303060 .
- [68] J. Shigemitsu *et al.*, *Recent results on B mixing and decay constants from HPQCD*, 0910.4131.
- [69] CDF Collaboration, T. Aaltonen *et al.*, *Search for $B_s^0 \rightarrow \mu^+\mu^-$ and $B_d^0 \rightarrow \mu^+\mu^-$ decays with $2fb^{-1}$ of $p\bar{p}$ collisions*, *Phys. Rev. Lett.* **100** (2008) 101802, 0712.1708 .
- [70] D0 Collaboration, V. M. Abazov *et al.*, *Search for $B_s \rightarrow \mu^+\mu^-$ at D0*, *Phys. Rev.* **D76** (2007) 092001, 0707.3997 .
- [71] G. Punzi, *Flavour physics at the Tevatron*, 1001.4886.
- [72] G. Isidori and R. Unterdorfer, *On the short-distance constraints from $K_{L,S} \rightarrow \mu^+\mu^-$* , *JHEP* **01** (2004) 009, hep-ph/0311084 .
- [73] P. Colangelo, F. De Fazio, P. Santorelli, and E. Scrimieri, *Rare $B \rightarrow K^*\nu\bar{\nu}$ decays at B factories*, *Phys. Lett.* **B395** (1997) 339–344, hep-ph/9610297 .
- [74] G. Buchalla, G. Hiller, and G. Isidori, *Phenomenology of non-standard Z couplings in exclusive semileptonic $b \rightarrow s$ transitions*, *Phys. Rev.* **D63** (2001) 014015, hep-ph/0006136 .
- [75] W. Altmannshofer, A. J. Buras, D. M. Straub, and M. Wick, *New strategies for New Physics search in $B \rightarrow K^*\nu\bar{\nu}$, $B \rightarrow K\nu\bar{\nu}$ and $B \rightarrow X_s\nu\bar{\nu}$ decays*, *JHEP* **04** (2009) 022, 0902.0160 .
- [76] M. Bartsch, M. Beylich, G. Buchalla, and D. N. Gao, *Precision Flavour Physics with $B \rightarrow K\nu\bar{\nu}$ and $B \rightarrow K\ell^+\ell^-$* , *JHEP* **11** (2009) 011, 0909.1512 .
- [77] M. Bona *et al.*, *SuperB: A High-Luminosity Asymmetric e^+e^- Super Flavor Factory. Conceptual Design Report*, 0709.0451.
- [78] A. J. Buras, M. Gorbahn, U. Haisch, and U. Nierste, *Charm quark contribution to $K^+ \rightarrow \pi^+\nu\bar{\nu}$ at next-to-next-to-leading order*, *JHEP* **11** (2006) 002, hep-ph/0603079 .
- [79] J. Brod and M. Gorbahn, *Electroweak Corrections to the Charm Quark Contribution to $K^+ \rightarrow \pi^+\nu\bar{\nu}$* , *Phys. Rev.* **D78** (2008) 034006, 0805.4119 .
- [80] G. Isidori, F. Mescia, and C. Smith, *Light-quark loops in $K \rightarrow \pi\nu\bar{\nu}$* , *Nucl. Phys.* **B718** (2005) 319–338, hep-ph/0503107 .

- [81] K. G. Chetyrkin *et al.*, *Charm and Bottom Quark Masses: an Update*, *Phys. Rev.* **D80** (2009) 074010, 0907.2110 .
- [82] **HPQCD** Collaboration, I. Allison *et al.*, *High-Precision Charm-Quark Mass from Current-Current Correlators in Lattice and Continuum QCD*, *Phys. Rev.* **D78** (2008) 054513, 0805.2999 .
- [83] F. Mescia and C. Smith, *Improved estimates of rare K decay matrix-elements from K_{l3} decays*, *Phys. Rev.* **D76** (2007) 034017, 0705.2025 .
- [84] **E949** Collaboration, A. V. Artamonov *et al.*, *New measurement of the $K^+ \rightarrow \pi^+ \nu \bar{\nu}$ branching ratio*, *Phys. Rev. Lett.* **101** (2008) 191802, 0808.2459 .
- [85] **E391a** Collaboration, J. K. Ahn *et al.*, *Search for the Decay $K_L^0 \rightarrow \pi^0 \nu \bar{\nu}$* , *Phys. Rev. Lett.* **100** (2008) 201802, 0712.4164 .
- [86] M. Misiak *et al.*, *The first estimate of $B(\bar{B} \rightarrow X_s \gamma)$ at $O(\alpha_s^2)$* , *Phys. Rev. Lett.* **98** (2007) 022002, hep-ph/0609232 .
- [87] J. M. Soares, *CP violation in radiative b decays*, *Nucl. Phys.* **B367** (1991) 575–590.
- [88] A. L. Kagan and M. Neubert, *Direct CP violation in $B \rightarrow X_s \gamma$ decays as a signature of new physics*, *Phys. Rev.* **D58** (1998) 094012, hep-ph/9803368 .
- [89] A. L. Kagan and M. Neubert, *QCD anatomy of $B \rightarrow X_s \gamma$ decays*, *Eur. Phys. J.* **C7** (1999) 5–27, hep-ph/9805303 .
- [90] W. Altmannshofer, A. J. Buras, and P. Paradisi, *Low Energy Probes of CP Violation in a Flavor Blind MSSM*, *Phys. Lett.* **B669** (2008) 239–245, 0808.0707 .
- [91] M. Beneke, *Corrections to $\sin(2\beta)$ from CP asymmetries in $B^0 \rightarrow (\pi^0, \rho^0, \eta^0, \eta', \omega, \phi) K_S$ decays*, *Phys. Lett.* **B620** (2005) 143–150, hep-ph/0505075 .
- [92] M. Artuso *et al.*, *B , D and K decays*, *Eur. Phys. J.* **C57** (2008) 309–492, 0801.1833 .
- [93] **Heavy Flavor Averaging Group (HFAG)** Collaboration, E. Barberio *et al.*, *Averages of b -hadron properties at the end of 2006*, 0704.3575. Updates available on <http://www.slac.stanford.edu/xorg/hfag>.

- [94] G. Buchalla, G. Hiller, Y. Nir, and G. Raz, *The pattern of CP asymmetries in $b \rightarrow s$ transitions*, *JHEP* **09** (2005) 074, [hep-ph/0503151](#) .
- [95] **Particle Data Group** Collaboration, C. Amsler *et al.*, *Review of particle physics*, *Phys. Lett.* **B667** (2008) 1.
- [96] D. London and A. Soni, *Measuring the CP angle beta in hadronic $b \rightarrow s$ penguin decays*, *Phys. Lett.* **B407** (1997) 61–65, [hep-ph/9704277](#) .
- [97] Y. Grossman and M. P. Worah, *CP asymmetries in B decays with new physics in decay amplitudes*, *Phys. Lett.* **B395** (1997) 241–249, [hep-ph/9612269](#) .
- [98] H.-Y. Cheng, C.-K. Chua, and A. Soni, *Effects of Final-state Interactions on Mixing-induced CP Violation in Penguin-dominated B Decays*, *Phys. Rev.* **D72** (2005) 014006, [hep-ph/0502235](#) .
- [99] M. Beneke and M. Neubert, *Flavor-singlet B decay amplitudes in QCD factorization*, *Nucl. Phys.* **B651** (2003) 225–248, [hep-ph/0210085](#) .
- [100] A. J. Buras, R. Fleischer, S. Recksiegel, and F. Schwab, *Anatomy of prominent B and K decays and signatures of CP-violating new physics in the electroweak penguin sector*, *Nucl. Phys.* **B697** (2004) 133–206, [hep-ph/0402112](#) .
- [101] A. J. Buras and M. Münz, *Effective Hamiltonian for $B \rightarrow X_s e^+ e^-$ beyond leading logarithms in the NDR and HV schemes*, *Phys. Rev.* **D52** (1995) 186–195, [hep-ph/9501281](#) .
- [102] H. M. Asatrian, K. Bieri, C. Greub, and A. Hovhannisyan, *NNLL corrections to the angular distribution and to the forward-backward asymmetries in $b \rightarrow X_s \ell^+ \ell^-$* , *Phys. Rev.* **D66** (2002) 094013, [hep-ph/0209006](#) .
- [103] A. Ghinculov, T. Hurth, G. Isidori, and Y. P. Yao, *The rare decay $B \rightarrow X_s \ell^+ \ell^-$ to NNLL precision for arbitrary dilepton invariant mass*, *Nucl. Phys.* **B685** (2004) 351–392, [hep-ph/0312128](#) .
- [104] C. Bobeth, P. Gambino, M. Gorbahn, and U. Haisch, *Complete NNLO QCD analysis of $\bar{B} \rightarrow X_s \ell^+ \ell^-$ and higher order electroweak effects*, *JHEP* **04** (2004) 071, [hep-ph/0312090](#) .
- [105] T. Huber, T. Hurth, and E. Lunghi, *Logarithmically Enhanced Corrections to the Decay Rate and Forward Backward Asymmetry in $\bar{B} \rightarrow X_s \ell^+ \ell^-$* , *Nucl. Phys.* **B802** (2008) 40–62, [0712.3009](#) .

- [106] A. Ali, T. Mannel, and T. Morozumi, *Forward backward asymmetry of dilepton angular distribution in the decay $b \rightarrow s\ell^+\ell^-$* , *Phys. Lett.* **B273** (1991) 505–512.
- [107] G. Burdman, *Short distance coefficients and the vanishing of the lepton asymmetry in $B \rightarrow V\ell^+\ell^-$* , *Phys. Rev.* **D57** (1998) 4254–4257, [hep-ph/9710550](#) .
- [108] M. Beneke, T. Feldmann, and D. Seidel, *Systematic approach to exclusive $B \rightarrow V\ell^+\ell^-$, $V\gamma$ decays*, *Nucl. Phys.* **B612** (2001) 25–58, [hep-ph/0106067](#) .
- [109] **BABAR** Collaboration, B. Aubert *et al.*, *Measurement of the $B \rightarrow X_s\ell^+\ell^-$ branching fraction with a sum over exclusive modes*, *Phys. Rev. Lett.* **93** (2004) 081802, [hep-ex/0404006](#) .
- [110] **Belle** Collaboration, M. Iwasaki *et al.*, *Improved measurement of the electroweak penguin process $B \rightarrow X_s\ell^+\ell^-$* , *Phys. Rev.* **D72** (2005) 092005, [hep-ex/0503044](#) .
- [111] G. D’Ambrosio, G. Ecker, G. Isidori, and J. Portoles, *The decays $K \rightarrow \pi\ell^+\ell^-$ beyond leading order in the chiral expansion*, *JHEP* **08** (1998) 004, [hep-ph/9808289](#) .
- [112] G. Buchalla, G. D’Ambrosio, and G. Isidori, *Extracting short-distance physics from $K_{L,S} \rightarrow \pi^0 e^+ e^-$ decays*, *Nucl. Phys.* **B672** (2003) 387–408, [hep-ph/0308008](#) .
- [113] G. Isidori, C. Smith, and R. Unterdorfer, *The rare decay $K_L \rightarrow \pi^0 \mu^+ \mu^-$ within the SM*, *Eur. Phys. J.* **C36** (2004) 57–66, [hep-ph/0404127](#) .
- [114] S. Friot, D. Greynat, and E. De Rafael, *Rare kaon decays revisited*, *Phys. Lett.* **B595** (2004) 301–308, [hep-ph/0404136](#) .
- [115] F. Mescia, C. Smith, and S. Trine, *$K_L \rightarrow \pi^0 e^+ e^-$ and $K_L \rightarrow \pi^0 \mu^+ \mu^-$: A binary star on the stage of flavor physics*, *JHEP* **08** (2006) 088, [hep-ph/0606081](#) .
- [116] J. Prades, *ChPT Progress on Non-Leptonic and Radiative Kaon Decays*, *PoS KAON* (2008) 022, 0707.1789 .
- [117] A. J. Buras, M. E. Lautenbacher, M. Misiak, and M. Münz, *Direct CP violation in $K_L \rightarrow \pi^0 e^+ e^-$ beyond leading logarithms*, *Nucl. Phys.* **B423** (1994) 349–383, [hep-ph/9402347](#) .
- [118] **KTeV** Collaboration, A. Alavi-Harati *et al.*, *Search for the Rare Decay $K_L \rightarrow \pi^0 e^+ e^-$* , *Phys. Rev. Lett.* **93** (2004) 021805, [hep-ex/0309072](#) .

- [119] **KTEV** Collaboration, A. Alavi-Harati *et al.*, *Search for the Decay $K_L \rightarrow \pi^0 \mu^+ \mu^-$* , *Phys. Rev. Lett.* **84** (2000) 5279–5282, [hep-ex/0001006](#) .
- [120] A. J. Buras and L. Silvestrini, *Upper bounds on $K \rightarrow \pi \nu \bar{\nu}$ and $K_L \rightarrow \pi^0 e^+ e^-$ from ε'/ε and $K_L \rightarrow \mu^+ \mu^-$* , *Nucl. Phys.* **B546** (1999) 299–314, [hep-ph/9811471](#) .
- [121] A. J. Buras, G. Colangelo, G. Isidori, A. Romanino, and L. Silvestrini, *Connections between ε'/ε and rare kaon decays in supersymmetry*, *Nucl. Phys.* **B566** (2000) 3–32, [hep-ph/9908371](#) .
- [122] N. H. Christ, *Theoretical strategies for ε'/ε* , [0912.2917](#).
- [123] **NA48** Collaboration, J. R. Batley *et al.*, *A precision measurement of direct CP violation in the decay of neutral kaons into two pions*, *Phys. Lett.* **B544** (2002) 97–112, [hep-ex/0208009](#) .
- [124] **KTeV** Collaboration, A. Alavi-Harati *et al.*, *Measurements of Direct CP Violation, CPT Symmetry, and Other Parameters in the Neutral Kaon System*, *Phys. Rev.* **D67** (2003) 012005, [hep-ex/0208007](#) .
- [125] **KTeV** Collaboration, E. T. Worcester, *The Final Measurement of ε'/ε from KTeV*, [0909.2555](#).
- [126] M. Blanke, A. J. Buras, S. Recksiegel, C. Tarantino, and S. Uhlig, *Correlations between ε'/ε and rare K decays in the littlest Higgs model with T -parity*, *JHEP* **06** (2007) 082, [0704.3329](#) .
- [127] A. J. Buras and J. M. Gérard, *ε'/ε in the Standard Model*, *Phys. Lett.* **B203** (1988) 272.
- [128] A. J. Buras and M. Jamin, *ε'/ε at the NLO: 10 years later*, *JHEP* **01** (2004) 048, [hep-ph/0306217](#) .
- [129] V. Lubicz and C. Tarantino, *Flavour physics and Lattice QCD: averages of lattice inputs for the Unitarity Triangle Analysis*, *Nuovo Cim.* **123B** (2008) 674–688, [0807.4605](#) .
- [130] **CDF** Collaboration, T. Aaltonen *et al.*, *First Observation of Electroweak Single Top Quark Production*, *Phys. Rev. Lett.* **103** (2009) 092002, [0903.0885](#) .
- [131] S. Herrlich and U. Nierste, *Enhancement of the $K_L - K_S$ mass difference by short distance QCD corrections beyond leading logarithms*, *Nucl. Phys.* **B419** (1994) 292–322, [hep-ph/9310311](#) .

- [132] A. J. Buras, M. Jamin, and P. H. Weisz, *Leading and next-to-leading QCD corrections to ϵ parameter and $B^0 - \bar{B}^0$ mixing in the presence of a heavy quark*, *Nucl. Phys.* **B347** (1990) 491–536.
- [133] S. Herrlich and U. Nierste, *Indirect CP violation in the neutral kaon system beyond leading logarithms*, *Phys. Rev.* **D52** (1995) 6505–6518, [hep-ph/9507262](#) .
- [134] G. Buchalla, *Renormalization of $\Delta(B) = 2$ transitions in the static limit beyond leading logarithms*, *Phys. Lett.* **B395** (1997) 364–368, [hep-ph/9608232](#) .
- [135] **Tevatron Electroweak Working Group** Collaboration, *Combination of CDF and D0 Results on the Mass of the Top Quark*, 0903.2503.
- [136] A. J. Buras and J. M. Gérard, *1/N Expansion for Kaons*, *Nucl. Phys.* **B264** (1986) 371.
- [137] J. Bijnens, J. M. Gérard, and G. Klein, *The $K_L - K_S$ mass difference*, *Phys. Lett.* **B257** (1991) 191–195.
- [138] J.-M. Gerard, C. Smith, and S. Trine, *Radiative kaon decays and the penguin contribution to the Delta(I) = 1/2 rule*, *Nucl. Phys.* **B730** (2005) 1–36, [hep-ph/0508189](#) .
- [139] E. Lunghi and A. Soni, *Possible Indications of New Physics in B_d -mixing and in $\sin(2\beta)$ Determinations*, *Phys. Lett.* **B666** (2008) 162–165, [0803.4340](#) .
- [140] A. Soni, A. K. Alok, A. Giri, R. Mohanta, and S. Nandi, *SM with four generations: Selected implications for rare B and K decays*, [1002.0595](#).
- [141] M. Beneke and M. Neubert, *QCD factorization for $B \rightarrow PP$ and $B \rightarrow PV$ decays*, *Nucl. Phys.* **B675** (2003) 333–415, [hep-ph/0308039](#) .
- [142] Z. Ligeti, M. Papucci, and G. Perez, *Implications of the measurement of the $B_s^0 - \bar{B}_s^0$ mass difference*, *Phys. Rev. Lett* **97** (2006) 101801, [hep-ph/0604112](#) .
- [143] Y. Grossman and Y. Nir, *$K_L \rightarrow \pi^0 \nu \bar{\nu}$ beyond the Standard Model*, *Phys. Lett.* **B398** (1997) 163–168, [hep-ph/9701313](#) .
- [144] M. Blanke, *Insights from the Interplay of $K \rightarrow \pi \nu \bar{\nu}$ and ϵ_K on the New Physics Flavour Structure*, [0904.2528](#).
- [145] A. J. Buras, B. Duling, and S. Gori, *The Impact of Kaluza-Klein Fermions on Standard Model Fermion Couplings in a RS Model with Custodial Protection*, *JHEP* **09** (2009) 076, [0905.2318](#) .

- [146] A. J. Buras and D. Guadagnoli, *On the consistency between the observed amount of CP violation in the K and B_d systems within minimal flavor violation*, *Phys. Rev.* **D79** (2009) 053010, 0901.2056 .
- [147] E. Lunghi and A. Soni, *Hints for the scale of new CP-violating physics from B -CP anomalies*, *JHEP* **08** (2009) 051, 0903.5059 .
- [148] W.-S. Hou, H.-n. Li, S. Mishima, and M. Nagashima, *Fourth generation CP violation effect on $B \rightarrow K\pi$, ϕK and ρK in NLO PQCD*, *Phys. Rev. Lett.* **98** (2007) 131801, hep-ph/0611107 .
- [149] W.-S. Hou, M. Nagashima, G. Raz, and A. Soddu, *Four generation CP violation in $B \rightarrow \phi K^0, \pi^0 K^0, \eta' K^0$ and hadronic uncertainties*, *JHEP* **09** (2006) 012, hep-ph/0603097 .